Journal of South American Earth Sciences

Study on spatio-compositional variations and source facies for oils from the Central Wrench Corridor of the Oriente Basin (Ecuador)

--Manuscript Draft--

Manuscript Number:	SAMES-D-21-00414R2
Article Type:	Research Paper
Keywords:	oil-source correlation, oil groups, QEDA method, Sacha-Shushufindi Corridor, Ecuadorian Oriente Basin
Corresponding Author:	Gonzalo Marquez, PhD University of Huelva: Universidad de Huelva Huelva, Huelva SPAIN
First Author:	Gonzalo Marquez, PhD
Order of Authors:	Gonzalo Marquez, PhD
	Lenin González, MSc
	Albert Permanyer, PhD
	Carlos Boente, PhD
	Marco Guzmán, MSc
	Erica Lorenzo, PhD
Abstract:	This research paper contains an integration of classical biomarker work with higher diamondoid examination to better characterize the petroleum systems in the north-central portion of the Sacha-Shushufindi Corridor in the Ecuadorian Oriente Basin. A set of crude oils, cuttings, and outcrop rock samples were analysed to address aspects such as source-rock lithology, paleo-depositional conditions, migration distances, as well as oil-oil and oil-source correlations. For this, gas chromatography-mass spectrometry (GC-MS), GC-triple-quadrupole MS (GC-MS/MS), and carbon isotope ratio mass spectrometry (IRMS) were performed on maltene fractions both from oils and rock extracts. GC-MS/MS analyses of oil-derived asphalthene hydrous pyrolysates were also included on the study. Classical biomarker results suggest mixing of pulses from distant siliciclastic and carbonate-rich Napo source rocks, with former oil charges being slightly biodegraded during the Paleogene and fresher Neogene pulses. These two types of mid-Cretaceous source rocks were deposited in shallow marine to nearshore and low-oxygen inner to middle neritic environments, respectively, with considerable and scarce contribution of land-plant material in both cases. Such differentiation of the two source facies types of the Napo Group is supported by results from quantitative extended diamondoid analysis (QEDA).
Suggested Reviewers:	José Luis Rodríguez Gallego, PhD Full Professor, Universidad de Oviedo jgallego@uniovi.es He has notable experience in the subject matter object of this study
	Michael Krudge, PhD Full Professor, Montclair State University krugem@montclair.edu He is a prestigious specialist on petroleum geochemistry
	María Fernanda Fernanda Romero-Sarmiento, PhD Senior Researcher, IFPEN: IFP Energies nouvelles maria-fernanda.romero-sarmiento@ifpen.fr She is an experienced organic geochemist on the subject matter of this research work
	Manuel Martínez, PhD Emeritus Professor, Universidad Central de Venezuela manmarti@gmail.com He is a notable organic geochemist that has experience in the study of ecuadorian petroleum systems

Opposed Reviewers:	
Response to Reviewers:	

Dear Dr. Audemard:

I am submitting the last modified version of the manuscript (**SAMES-D-21-00414**) entitled "**Study on spatio-compositional variations and source facies for oils from the Central Wrench Corridor of the Oriente Basin (Ecuador)**" for your considerations in order to be published in Journal of South American Earth Sciences. The authors thank the two reviewers for their comments which have helped us to improve the original manuscript.

Attached you can find highlights, revised copies (clean and with track changes) and detail response to reviewers.

Yours sincerely,

Dr. Gonzalo Márquez

Dear Dr. Audemard:

All minor changes have been followed in the revised manuscript.

Please, be aware of changes (**in red**) in the text. Regarding the clean copy, references have been checked in the text and list.

Enclosed you will find the text, figures and tables.

Yours sincerely, Dr. Gonzalo Marquez

Highlights:

- Study on oils from the Central Wrench Corridor of the Ecuadorian Oriente Basin
- Evaluation of inter-field compositional changes in oil samples from north to south
- Identification of contributions of carbonate and clay-rich Napo source rock facies

Study on spatio-compositional variations and source facies for oils from the Central Wrench Corridor of the Oriente Basin (Ecuador)

G. MÁRQUEZ[a,*], L. GONZÁLEZ[b], A. PERMANYER[c], C. BOENTE[a], M.A. GUZMÁN[a] and E. LORENZO[d]

[a] Center for Research in Sustainable Chemistry (CIQSO), University of Huelva, 21006 Huelva, Spain

[b] School of Geology, Mines and Geophysics, Central University of Venezuela, Caracas, 3895/1010-A, Venezuela

[c] Departament of Mineralogy, Petrology and Applied Geology, University of Barcelona, 08028 Barcelona, Spain

[d] School of Engineering Sciences, State University Santa Elena Peninsula, 240204 La Libertad, Ecuador

Abstract: This research paper contains an integration of classical biomarker work with higher diamondoid examination to better characterize the petroleum systems in the north-central portion of the Sacha-Shushufindi Corridor in the Ecuadorian Oriente Basin. A set of crude oils, cuttings, and outcrop rock samples were analysed to address aspects such as source-rock lithology, paleo-depositional conditions, migration distances, as well as oil-oil and oil-source correlations. For this, gas chromatography-mass spectrometry (GC-MS), GC-triple-quadrupole MS (GC-MS/MS), and carbon isotope ratio mass spectrometry (IRMS) were performed on maltene fractions both from oils and rock extracts. GC-MS/MS analyses of oil-derived asphalthene hydrous pyrolysates were also included on the study. Classical biomarker results suggest mixing of pulses from distant siliciclastic and carbonate-rich Napo source rocks, with former oil charges being slightly biodegraded during the Paleogene and fresher Neogene pulses. These two types of Early-Late Cretaceous source rocks were deposited in shallow marine to nearshore and low-oxygen inner to middle neritic environments, respectively, with considerable and scarce contribution of land-plant material in both cases. Such differentiation of the two source facies types of the Napo Group is supported by results from quantitative extended diamondoid analysis (QEDA).

Keywords: oil-source correlation, oil groups, QEDA method, Sacha-Shushufindi Corridor, Ecuadorian Oriente Basin.

1. Introduction

The petroliferous East Ecuadorian or Oriente Basin is part of the large Amazonian retro-arc foreland basin system that was partially developed in the east of the northern Andean Mountains (Canfield et al., 1982; Estupiñán et al., 2010a; among others; see Fig. 1a). The Oriente Basin lies between the Pre-Cambrian Brazilian-Guyana basement shields to the east and the eastern Andes in Ecuador to the west, and is also geologically continuous to the Putumayo Basin (Colombia) and the Marañón Basin (Peru), northwards and southwards, respectively (Dashwood and Abbots, 1990;

*gonzalo.marquez@diq.uhu.es Tlfn./Fax: +34959217325

Marksteiner and Alemán, 1997; Bès de Berc et al., 2005; Xie et al., 2010). The asymmetric Oriente Basin occupies an area of approximately 100000 km^2 and lies across the shield and Subandean zones of Ecuador (Dashwood and Abbots, 1990). The Basin, underlined by Precambrian rocks from the Guyana shield, preserves a Paleozoic to Quaternary sedimentary sequence (Tschopp, 1953), and it can be divided into two geological and geomorphological zones separated by reverse faults: the Subandean Zone (an inverted sequence of sediments) to the west (adjacent to the Andes); and the Oriente Basin *sensu stricto* (a lowland region) to the east, which were formed during Andean orogenesis in the late Cenozoic (Baldock, 1985; Christophoul et al., 2002a).

Figure 1

Petroleum exploration in the Oriente Basin began in the 1920's (Tschopp, 1953) with the first commercial oilfield discovered by a subsidiary of Texaco at Lago Agrio in 1967. For the next 45 years, Texaco and other companies discovered around 150 oilfields including Shushufindi, Sacha, Auca, and Cononaco (Canfield el al., 1982; Higley, 2001; see Fig. 1), of which nearly 100 are currently active with a total production of half a million barrels per day (Yang et al., 2017). The discovered recoverable reserves in the Oriente Basin and Shushufindi-Aguarico area exceed 13000 and 2000 million barrels of oil (MMBO), respectively (Baby et al., 2014; Ma et al., 2017). Almost all of the East Ecuadorian Basin oil production comes from nearshore marine sandstones of the Hollín and Napo formations (Feininger, 1975).

Previous analyses of sampled oils and Napo rock samples over various tens of Oriente wells were carried out to elucidate oil-oil and oil-source rock correlations (Mello et al., 1995; Estupiñán, 2005; Yang et al., 2017). Although potential Santiago source rocks cannot be totally ruled out (Pindell and Tabbutt, 1995; Vallejo et al., 2002), organic-rich Napo/Chonta intervals appear to be the primary petroleum source rocks in the Oriente/Marañón province (e.g., Canfield et al., 1982). The Albian-Campanian Napo Group is a world-class source rock, equivalent to the Cretaceous La Luna, Gachetá, and Raya/Chonta formations of Venezuela, Colombia, and Peru, respectively (Estupiñán,

2005); and so Cretaceous oils from the Marañón Basin are similar to oils from Napo source rocks in the Oriente Basin (Mathalone and Montoya, 1995). Average total organic carbon (TOC) contents for Napo shales vary from over 4% (Type-II kerogen) in the west to around 1% (more terrigenous subfacies) in the east (Dashwood and Abbots, 1990; Xie et al., 2010). For instance, in the western part of the Oriente Basin, Cenomanian to early Turonian and mid-Coniacian sediments contain marine mature intervals with predominant amorphous organic matter and TOC values about 10% (Vallejo et al., 2002), whilst, to the east, in the segment denominated T block (see Fig. 1a; Hu et al., 2010), Albian to Cenomanian sediments depict organic-rich calcareous shales (TOC contents of 2 to 3%) with marginally mature marine organic matter (Yang et al., 2017). Also noteworthy is the huge absence of mature Napo source rocks in the Oriente Basin (Baby et al., 2013).

Biomarker and carbon isotope analyses of Oriente oils from Hollín, Napo, and Tena reservoirs indicate that they all are genetically correlated and appear to be derived from a common dominantly marine facies type (Mello et al., 1995; Estupiñán, 2005). The varying API gravities in these oils mainly suggest different alteration histories, although no or little in-reservoir oil maturation has occurred. In this regard, the mentioned-above reservoirs contain negligibly to severely altered oils and API gravity does not correlate with reservoir depth (Dashwood and Abbots, 1990). The main reservoirs contain low-sulfur light-to-medium oils in the north-central part of the Central Wrench or Sacha-Shushufindi Corridor (e.g., Lago Agrio), in contrast to sulfur-rich heavy oils on the eastern and western basin flanks (e.g., Tiputini and Pungarayacu, respectively; see Fig. 1a), with the exception of in situ mature light oils related to local volcanic activity at the Bermejo area (Lee et al., 2004). Moreover, medium oils can be found throughout the central-eastern Oriente Basin (e.g., Cuyabeno) while reservoirs also contain heavy oils in several southern locations (Oglan and Nishino, among others). In this sense, fresh water influx from the west resulted in biodegradation of oils in the shallow reservoirs and essentially water-washing in the deeper reservoirs (Smith, 1989);

in addition, re-migrating oils might have been biodegraded at Oglan and other areas (Dashwood and Abbots, 1990).

Given the above, the objectives of this research are: (i) to assess the origin, thermal maturity, and secondary processes of a set of Cretaceous oil samples from the north-central part of the Sacha-Shushufindi Corridor; (ii) to evaluate inter-field compositional changes in oil samples from north to south; (iii) to identify contributions of carbonate and siliciclastic Napo source rock facies; and (iv) to verify the migration model proposed for the Napo reservoirs (as in Dashwood and Abbots, 1990; Bernal, 1998). Such outcomes will improve the level of understanding achieved so far on the petroleum systems in the central-western part of the Ecuadorian Oriente Basin.

2. Geological background

2.1. Tectonic-structural framework

The tectonic and structural settings of the Oriente Basin have been described in numerous works (Tschopp, 1953; Dashwood and Abbots, 1990; Brookfield et al., 2009; among others). In the earliest Paleozoic, tectonic movements along the Ecuadorian margin of the oceanic proto-Pacific Plate led to structures involving Proterozoic metamorphic rocks and igneous cratons (Canfield et al., 1982; Balkwill et al., 1995); whilst in the Late Ordovician a passive margin had already developed after collision of plate boundaries (Mathalone and Montoya, 1995). A stage of mostly subduction-related deposition associated with transtension and transpression occurred during mid-Permian and Early Triassic times (Sempere, 1995). Starting in the Triassic, a period of rifting took place in the eastern Andean area along the proto-Pacific margin (Jaillard et al., 1990), and throughout the Jurassic, magmatic arcs developed (Mathalone and Montoya, 1995). The original Oriente Basin back-arc is the result of this post-rift subsidence (Jaillard et al., 1990; Dashwood and Abbots, 1990); whilst posterior tectonic activity (Late Jurassic to Early Cretaceous) led to a first stage of folding and uplifting of rift structures due to the accretion of allochthonous oceanic rocks onto the Ecuadorian margin (Aspden and Litherland, 1992). Another phase of convergence occurred in late Cretaceous-

Paleocene (Aspden and Litherland, 1992; Balkwill et al., 1995) linked to the Andean orogeny (Feininger and Bristow, 1980), and subsequent transpressive deformation created reverse faults and structural highs in the Oriente Basin (Balkwill et al., 1995). Lastly, transpression of the basin also occurred during the Pliocene-Quaternary (Baby et al., 1999).

The most important structures in the East Ecuadorian Basin comprise steeply dipping faults in en-echelon sets (Balkwill et al., 1995). These faults rose from basement into various stratigraphic horizons and their trends strike in approximately NNE-SSW directions. In general, oilfields are aligned along these structural trends and belong to inverted Pre-Cretaceous extensional systems and have deformed the foreland basin system since the Late Cretaceous (Baby et al., 2013). Main features can be defined as positive flower structures which developed along the three referred NNE-SSW transpressive zones (Christophoul et al., 2002a). From west to east, these tectonic domains are: (i) the Subandean Zone, which hosts two antiforms (the Napo Uplift to the north and the Cordillera of Cutucú to the south, separated by the Pastaza or Puyo Depression) that represent positive flower structures of Neogene age (Bès de Berc et al., 2005); (ii) the Central or Sacha-Shushufindi Corridor, developed in Late Cretaceous and Cenozoic times, resulting from the inversion of Late Triassic-Early Jurassic rift high-angle normal faults; (iii) the Eastern or Capirón-Tiputini Inverted System, generated by the inversion of Late Jurassic half-grabens (Christophoul, 1999). The central Corridor, the Eastern Inverted System, and the Subandean Zone formed, respectively, during Turonian-Maastrichtian, early Eocene, and Neogene ages (Baby et al., 2013).

According to Dashwood and Abbots (1990), the basin axis is distorted by low-relief (< 100 m) anticlinal folds that produce a 50 km-wide axial region and separate the softly dipping eastern flank from the more abrupt western flank. Late Cretaceous to Pliocene tectonic events created low-relief anticlines (Mathalone and Montoya, 1995). According to Dashwood and Abbots (1990), syn-sedimentary compressive deformation occurred throughout the Late Cretaceous on most of the pre-Cretaceous N-S trending normal faults and produced a first type of structures: footwall anticlines associated with normal faults (e.g., Auca and Cononaco oilfields). Subduction of the Nazca

(Pacific) Plate resulted in reverse movement on part of the early N-S faults, particularly on the western flank of the Oriente Basin during the Paleogene period. This led to another type of structures (hanging-wall anticlines over reverse faults; e.g., Lago Agrio and Shushufindi). Most of the productive structures in the area under study are NS-trending anticlines, generally faulted on one of the flanks, which belong to the two referred structural styles (Canfield et al., 1982).

2.2. Stratigraphy and sedimentology

As shown in Fig. 2, a typical stratigraphic section of the Central Wrench Corridor can be divided into a pre-Cretaceous series, a continental to shallow marine Cretaceous sedimentary cycle (White et al., 1995), and a Cenozoic foreland molassic and shallow marine cover (Baby et al., 1999). Stratigraphic nomenclature of the Ecuadorian Oriente Basin is taken from geologic studies by Shell (Faucher et al, 1971) and subsequent modifications (e.g., Jaillard, 1996). The pre-Cretaceous series comprises Paleozoic marine sediments, Triassic and Lower Jurassic marine to continental rift deposits, and Late Jurassic sediments related to the activity of the continental Misahualli volcanic arc (Aspden et al., 1987; Dashwood and Abbots, 1990). Though magmatic rocks have also been identified in the Oriente Basin (Barragán et al., 2005), the Cretaceous series essentially comprises Aptian to Coniacian transitional clastic-carbonate nonmarine-marine sediments (i.e. Hollín and Napo units) deposited in the retro-arc basin during periods of low tectonic activity (Baldock, 1985), which were controlled by marine transgressions and regressions on the continental shelf (Tschopp, 1953). In general, the Cenozoic series is comprised of sediments deposited after stable shelf-rise conditions abruptly ended during the Maastrichtian (Feininger and Bristow, 1980).

Figure 2

In more detail, the Silurian-Devonian Pumbuiza Formation is the most ancient unit and consists of mainly sandstones; while the pre-rift Late Carboniferous-Permian Macuma Formation comprises bedded carbonates and clastics (Ma et al., 2020). Stratigraphically upward, the Early Jurassic Santiago Formation comprises carbonates, shales, and evaporites (Gaibor et al., 2008). The Late Jurassic-Early Cretaceous Chapiza Formation is composed of conglomerates, sandstones, and siltstones (Pindell and Tabbutt, 1995). Above, lays unconformably, the Cretaceous sequence,

initiated with the Hollin unit (Daswhood and Abbots, 1990). The Hollín-Napo sequence is composed by cyclic sequences of sedimentary rocks, which have been historically interpreted as fluvio-deltaic to shallow marine tidal deposits passing westward (Canfield et al., 1982); although more recent interpretations by Shanmugam et al. (2000) and Higgs (2002) suggested a tide-dominated estuarine depositional environment and a tidal shelf model for Napo and Hollín sands. The sedimentation of Hollín (Aptian-Albian) Formation appears to be related to the Aguarico and Cononaco arches to the east (White et al., 1995) and was caused by an Early Cretaceous marine transgression from the western marginal sea, over the Guyana Shield, after which white quartz sandstones interbedded with carbonaceous mudstones were deposited under regressive conditions (De Righi and Bloomer, 1975). The sand-rich Hollín pericratonic Formation constitutes the main oil reservoir in the Ecuadorian Oriente Basin. Both the Hollín unit and Napo sandstone members can be divided into a lower or "main" sub-unit of more permeable quartzose sandstones and upper clay-containing glauconitic sandstones separated by thin shaly layers (Dashwood and Abbots, 1990).

The Napo Group, which rests conformably on Hollín Formation, progressively thins eastwards and was originally divided into three distinct sub-units (Tschopp, 1953). Subsequent studies during petroleum exploration led to a subdivision into Basal, Lower, Middle, and Upper Napo formations (Jaillard, et al., 1997). The Basal Napo Formation (late Albian) consists of a series of alternating sandstones, shales, limestones, and cherts (see Fig. 2). The Lower Napo unit (latest Albian-Cenomanian) consists of sandstones, shales and limestones. The Middle Napo Formation (middle Turonian-early Coniacian?) is dominated by biomicritic limestones with shale partings and subordinate sandstones. Finally, the Upper Napo unit (late Coniacian-Santonian) is dominated by shales with subordinate limestones and sandstones (Jaillard, 1996; Jaillard et al., 2005), and has been informally divided into M1 Limestone, M1 Shale, and M1 Sandstone or San Fernando members (Smith, 1989; Jaillard, 1996). The Basal to Middle Napo formations represent the more significant cycles of transgression and regression. In these units, transgressive packages in the Basal Napo (labelled Basal Shale, C Limestone, T Shale, and T Limestone members), Lower Napo (B Limestone and U Shale intervals), and Middle Napo Formation (A Limestone and M2 Limestone

members) alternate with regressive T, U, and M2 Sandstone members (Vallejo et al., 2002; Fig. 2). The transgressive sequences consist of marine bioclastic limestones and shales, while the regressive packages consist of tide-dominated estuary sandstones rather than fluvio-deltaic deposits (Shanmugam et al., 2000). The Napo sands (mainly the T and U sands) are important reservoirs with similar properties (Dashwood and Abbots, 1990); only slight differences arise between such lower and upper intervals: lower T and U reservoirs have porosity and permeability values ranging from 10 to 22% and up to 1500 mD, respectively, while upper T and U reservoirs exhibit values below 18% and 850 mD (Estupiñán, 2005).

The Maastrichtian-Cenozoic sedimentary cover was deposited after a major non-depositional hiatus at the base of the Maastrichtian-Paleocene Tena Formation (Lebras et al., 1987). This foreland unit comprises fluvial red-coloured claystones and siltstones with basal conglomeratic sandstones (Christophoul et al., 2002a). The Tena Formation ("basal Tena sand") is a secondary petroleum reservoir and gradually truncates the Upper Napo and even Middle Napo units westwards (Dashwood and Abbots, 1990). The Paleogene Tituyacu and Orteguaza formations comprise fluvial to marginal marine deposits composed of clastic sedimentary rocks (Christophoul, 1999). Finally, four diachronous Neogene mainly clastic rock units (Chalcana, Arajuno, Chambira, and Mesa/Mera; Fig. 2) have been also recognized in the Oriente Basin, east of the Pastaza depression (Baby et al., 1999). It has been reported that the late Miocene to Recent sedimentary infill of the Oriente Basin represents an alluvial fan system (Christophoul et al., 2002b).

3. Samples and methods

A set of 125 oil samples from wells in the Cretaceous Hollín, T and U sands of the Auca (19), Cononaco (13), Shushufindi (57), Guanta (14), Lago Agrio (10), Shushuqui (6), and Tetete (6) fields were analysed. Table 1 shows the list of oil samples from the Central Wrench Corridor at different latitudes, the respective reservoir intervals, and complementary data. Table 2 displays information on 6 selected cuttings from wells located in the central-western Oriente Basin, and 4 outcrop samples from the most organic-rich Napo sub-units (i.e. Basal Shale, B Limestone, U

Shale, and A Limestone; Bernal, 1998). These were taken for oil-source rock correlation purposes. Rock sampling sites are located in the Central Wrench Corridor/Subandean Zone from south to north (see cross section shown in Fig. 1b) to discard significant lateral changes in the organofacies of these Napo sub-units. One of the sampled Napo strata outcrops is located on the Namangoza River (4 km southwest of the city of Santiago de Méndez; Fig. 1a), and the rest of them are outcrop along the Misahualli River (Pungarayacu area) at the southern Napo Uplift (about 12 km east of the Tena city; Figs. 1a and 3). The latter location is accessible via a quarry road along the west side of the river.

Table 1

Table 2

Figure 3

Rock samples were disaggregated, air-dried for 24 h, and grounded manually at Barcelona University. A small aliquot was taken to perform Rock-Eval 2/TOC analysis using a Vinci Technologies instrument following the method established by Espitalié et al. (1977). Another aliquot was used for Soxhlet extraction of organic chemicals using a mixture of dichloromethane:methanol (3:1, v/v). These extracts were concentrated by rotary evaporation at 40°C, filtered (0.45 μm) and dissolved in dichloromethane. For some samples (immature Napo B limestones and U shales), another aliquot was taken to carry out artificial maturation for 3 days at 330 °C (Lijmbach et al., 1983). Vitrinite reflectance measurements were also performed in accordance with Escobar et al. (2016).

Oil samples and rock extracts were fractioned into saturates, aromatics, and polar compounds. For this, samples were firstly passed through a batch-type reactor in constant agitation for 1 h at 60 ºC, followed by a 12-h inactive period. Then, asphalthenes were obtained with *n*-heptane in a 1:40 v/v ratio using Whatman filters. Maltenes were fractionated into saturated hydrocarbons, aromatics, and resins by solid-liquid chromatography (De la Cruz et al., 1997). The aliphatic, aromatic, and resin

fractions were eluted with *n*-hexane, toluene, and toluene/methanol (70:30 v/v) using a silica-alumina column. Gas chromatography-mass spectrometry (GC-MS) analysis on saturated and aromatic fractions were performed using a HP 5890 Series II gas chromatograph and an Agilent 5973 N mass spectrometer, operating in "fullscan" mode and with an HP-5 column (60 m × 0.32 mm i.d., 0.5 μm μm film). Helium was used as carrier gas, and initial oven temperature was 50 ºC (held for 2 min), ramped at 2.5 ºC up to 300ºC (held for 70 min).

Whole oil gas chromatographic analyses were carried out using a J&W Agilent PONA GC column (50 m x 0.2 mm i.d.; film thickness 0.25 μm; helium was the carrier gas) in a Delta Chrom Series 9980 instrument with flame ionization detection. The operating conditions were: oven temperature at 35 °C for 15 min, increased from 35 to 320 °C at 2 °C/min, and finally maintained at 320 °C for 30 min. Data were acquired using the Agilent ChemStation program.

Carbon isotopic determination on saturate, aromatic, resin, and asphaltene (SARA) fractions was performed using a Thermo Finnigan 1112 elemental analyzer coupled to a Finnigan Mat Delta C mass spectrometer. USGS 24 graphite, IAEA-CH6 saccharose, IAEA-CH7 polyethylene, and NBS-22 oil were used as reference materials. V and Ni concentrations were determined by inductively coupled plasma atomic emission spectroscopy (ICP-AES) using a Perkin Elmer Optima 3000 sequential spectrometer according to ASTM D5708-05 (ASTM, 2005). Sulfur content in crude oils was determined following the ASTM D4294-10 method (ASTM, 2010) by an energy-dispersive X-ray Panalytical spectrometer (Axios model) with a digital signal processor and a dual multi-channel analyzer.

Quantitative extended diamondoid analysis (QEDA) was carried out on the saturated fractions (maltenes) from rock extracts and representative sampled oils (as in Moldowan et al., 2015). QEDA fingerprints were also observed in asphaltene fraction of these oils after hydrous pyrolysis treatment

(as in Summons et al., 2008). Gas chromatography-triple quadrupole mass spectrometry (GC-MS/MS) was used to determine the composition of higher diamondoids (Dahl et al., 1999; Pytlak et al., 2017). Four deuterated internal standards were used to quantify triamantane and extended diamondoids, namely, triamantane-d4 and cyclohexamantane-d8, as well as tetramantane-d6 and pentamantane-d6 for the four-cage (T1, T2, and T3) and five-cage (P1, P2, P3, and P4) non-enantiomorphic isomers (Moldowan et al., 2015).

4. Results

4.1. Source-rock samples

4.1.1. Rock-Eval results

Low PI values (< 0.1; Table 3) suggest that the studied rocks have been negligibly affected by weathering or contamination by well additives or migrated bitumen (Bissada, 1982). Rock-Eval T_{max} data for the Basal Shale, B Limestone, A Limestone, and U Shale samples lie in the 430-435 ºC, 427-439 ºC, 424-431 ºC, and 425-426 ºC ranges, respectively; these values correspond to calculated vitrinite reflectance (%Ro Calc) between 0.49 and 0.74% (Table 3), indicating immature and early mature organic material (Peters, 1986). Calculated %Ro values are similar to measured %Rr data (Table 3). These maturity data can be suggestive of the problems in unravelling the origin of the oil in the Sacha-Shushufindi Corridor (Dashwood and Abbots, 1990; Bernal, 1998): if the Napo reservoirs are in fact sourced from the same stratigraphic group (Mello et al., 1995), a long-distance migration has to be considered, since vitrinite reflectance data represent thermally immature or marginally mature conditions for oil generation in the north-central Oriente Basin according to Baby et al. (2013).

Table 3

Table 3 shows Rock-Eval 2/TOC data and vitrinite reflectance measurements. TOC values for the so-called B Limestone, Basal Shale, U Shale, and A Limestone samples range, respectively, 0.98 to 1.54 wt.%, 2.54 to 4.97 wt.%, 1.23 to 1.66 wt.%, and 2.12 to 3.09 wt.% (with a cut-off of 0.5%). As

for hydrogen index (HI) data (see Table 3), comparable A and B Limestone sub-units show similar values higher than 430 mg HC/g TOC, thus depicting good liquid hydrocarbon generation attributes; while the samples from the very similar U Shale (HI values of 315.1 and 328.8 mg HC/g TOC) and Basal Shale (HI: 340.1-358.7 mg HC/g TOC) facies also have adequate liquid hydrocarbon generation potential (Peters, 1986). This slight variation in HI values, given relatively similar Tmax values as previously discussed, would indicate a moderate heterogeneity in organic matter type in the carbonate-rich (A and B Limestones) versus shaly (U and Basal Shales) rock samples. PI values exceeding 0.1 for several rock samples from the Basal Shale and A Limestone sub-units (Table 3), would indicate that these samples had entered the oil window (Killops and Killops, 2005). In the pseudo-van Krevelen diagram (Fig. 4a), both A and B Limestone samples plot near the type II organic matter line, whereas the U and Basal Shale samples plot in the organic matter type II/III zonation, indicative of shallower marine settings with higher terrestrial contribution (Tissot and Welte, 1984). This differentiation between samples is also observed in the HI versus T_{max} plot (Fig. 4b), which avoids the uncertainty associated with the oxygen index (Peters, 1986; Cornford et al., 1998).

Figure 4

4.1.2. Carbon isotope signatures

The $\delta^{13}C$ values of the rock extracts from core and outcrop samples are within 2.5‰ of each other (see Table 3). $\delta^{13}C$ analyses of A Limestone and B Limestone rock extracts yield negative CV values, suggesting a predominantly marine source. However, in accordance with literature (Mello et al., 1995; Yang et al., 2017), the five remaining rock extracts have negligibly negative or slightly positive CV values, which might reflect a marine source with certain terrestrial contribution (Basal Shale and U Shale sub-units).

4.1.3. Biomarker-based approaches

Organic geochemical analyses of B Limestone, A Limestone, Basal Shale, and U Shale rock

extracts were conducted after artificial maturation (Lijmbach et al., 1983), as they showed low maturities which make oil-source correlation difficult. The *n*-alkane patterns in the extracted outcrop rock samples from the near-isopic B Limestone and A Limestone sub-units (marly intervals interbedded with calcareous shales and argillaceous limestones) are similar: unimodal type with maximum peaks between *n*-C_{16} and *n*-C_{19}, absence of odd-over-even carbon preference, as well as predominance of *n*-C_{17} over Pr and Pr/Ph < 1.1 (see Table 4, Fig. 5a). All this suggests marine precursor organic matter derived mostly from algae (Type II kerogen) deposited in mid-neritic environments under oxygen-depleted bottom water conditions (Hunt, 1996; Peters et al., 2005). By contrast, the U Shale and Basal Shale rock extracts show bimodal *n*-alkane distributions with maximum peaks at *n*-C_{15} to *n*-C_{17} and *n*-C_{27} to *n*-C_{29} with minor odd/even preference, together with Pr/Ph above 1, and predominance of Pr over *n*-C_{17} (Table 4; Fig. 5b). These features tend to occur in organic matter Type II-III or III (Tocco et al., 1995), and thus it can be inferred that U Shale and Basal Shale source rocks were deposited in shallow-water/nearshore settings with notable terrestrial input exposed during sedimentation to low-oxygen bottom water conditions (Hunt, 1996).

Table 4

Figure 5

The Basal Shale and U Shale extracts also present very similar triterpane and sterane distributions (see Table 4, Figs. 6a and 6c). These two rock extracts show biomarker characteristics typical of sedimentary rocks deposited under nearshore siliciclastic depositional paleo-environments: high abundance of diasteranes, regular sterane distribution dominated by C_{29} counterparts and $C_{28} \approx C_{27}$, stair-step progression of C_{31} to C_{35} homohopanes, 30-norhopane/hopane ratios below 0.7, C_{24}/C_{23} cheilanthane ratios above 0.8, and C_{26}/C_{25} cheilanthane ratios below 1 (Tissot and Welte, 1984; Peters et al., 2005; Huang et al., 2015). On the basis of these results, the environment of deposition for the Basal Shale and U Shale sub-units is inferred to be an inner shelf that experienced periodic influx of land-plant debris likely during times of high fresh water runoff (Mello et al., 1995; Yang et al., 2017). However, Basal Shale and U Shale source rocks have distinct triterpane and sterane

compositions compared with those of A Limestone and B Limestone rock samples (Table 4). These latter two subsets of rock samples have similar *m/z* 191 and 217 mass fragmentograms, which are indicative of marine carbonate-rich source facies (Figs. 6b and 6d). Source-based parameters such as C_{26}/C_{25} cheilanthane ratios below 1, abundance of tricyclopolyprenanes, prominence of C_{27} steranes with respect to their C_{28} and C_{29} counterparts, presence of gammacerane and C_{30} steranes, relatively low abundance of diasteranes, and 30-norhopane/hopane ratios around 1 suggest low-oxygen levels and marine moderately hypersaline depositional conditions with restricted water circulation for the last samples (Seifert and Moldowan, 1978; Cassani and Eglinton; 1986; Peters et al., 1995). As described in literature (Mello et al., 1995; Yang et al., 2017), maximum transgressions of the shoreline might indicate marly depositional regimes (i.e. B Limestone and A Limestone sub-units) in middle neritic environments with algal dominated input and a low influx of terrigenous material. The difference between a shaly source facies (Basal Shale and U Shale) versus a marly source facies (A and B Limestone) is also supported by dibenzothiophene-to-phenanthrene (DBT/P) values (clearly below and near one, respectively; Table 4) and methyl-dibenzothiophene patterns of 4 > 2+3 > 1 and 4 > 2+3 < 1, respectively (Hughes, 1984; Hughes et al., 1995).

Figure 6

4.2. Oil samples

4.2.1. Bulk oil geochemistry

The API gravity, total sulfur content, and SARA compositions of the sampled oils are shown in Table 1. An API map for T, U, and Hollín reservoirs is shown in Figure 7a. With the exception of Cononaco oils, where different API values are obtained in the Hollín (averaging 31º) and Napo reservoirs (20.2-21.3º), burial depth is not a control in oil gravity in any other of the study oilfields. Almost all the Lago Agrio, Guanta, Shushuqui, and Tetete oils from the Hollín, Napo, and basal Tena reservoirs exhibit API gravities (29º-31º) and similar compositions: saturate hydrocarbons (SAT) percentages range between 41% and 44%, aromatics (ARO) from 33% to 36%, and polar compounds (POL) from 22% to 24%.

Most oils from the mentioned-above Cretaceous reservoirs in the Shushufindi field exhibit API gravities in the 26-29º range, with SAT, ARO and POL percentages ranging from 38% to 41%, 33% to 36%, and 25% to 28%, respectively. Auca oils from the Napo and Hollín reservoirs have API gravities between 25º and 28º, as well as SAT, ARO and POL percentages of 36-38%, 34-36%, and 27-29%, respectively. As previously mentioned, Cononaco oils from the Hollín interval have API values around 31º and SARA contents comparable to those of the Shushufindi samples (see Table 1), whilst Cononaco oils produced from Napo reservoir have the lowest API gravities (<22º), ARO (< 35%), and SAT (≤ 36%) contents, as well as the highest POL proportions (> 30%) among all the oils under study. Relatively low total sulfur contents (St < 1%) were also found in oil samples from the Lago Agrio, Guanta, Shushuqui, Shushufindi, and Tetete oilfields, all from the northernmost part of the basin. Low-sulfur oils are characterized by St < 1% (Tissot and Welte, 1984). By contrast, oils from southernmost Auca and Cononaco fields show total sulfur contents exceeding 1%.

V/Ni ratios above 2 (see Table 4) suggest that the study oils originated from predominantly marine organic material deposited under oxygen-deprived conditions (Galarraga et al., 2008). When organic matter is deposited under reducing conditions, low concentrations of iron(II) ions lead to nickel(II) ions precipitating in metal sulphides rather than forming metal-organic compounds, and leading to high V/Ni ratios (Lewan, 1984). By contrast, during deposition of siliciclastic facies under more oxidizing conditions, abundantly available iron(II) ions react mainly with sulphide ions, thus forming pyrite, whereas nickel(II) ions form metal-organic compounds, leading to low V/Ni ratios. Despite the fact that V and Ni concentrations can be influenced by post-accumulation processes, it is reported that the V/Ni ratio tends to be unaltered due to the structural similarities of the metal-organic compounds which contain these two metals (Lewan and Maynard, 1982).

4.2.2. Carbon isotope data

Stable carbon isotope compositions of saturated and aromatic fractions of oil samples are compiled in Table 1. Among all the oils, the $\delta^{13}C$ values are very similar, with variations lower than 1.2‰ and standard deviations close to analytical error (0.5‰). Such similar isotopic compositions can indicate that they originated from the same source rock (Peters et al., 2005). As shown in the Sofer diagram (Sofer, 1984; Fig. 7b), all the sampled oils have negative or negligibly positive canonical variables (CV), suggesting a predominant marine input. However, these data must be interpreted with caution as several processes may alter the $\delta^{13}C$ signature (Peters et al., 2005).

Figure 7

4.2.3. Molecular characteristics

The *n*-alkane distributions for all the studied oils are quite similar and typical of predominantly marine precursor organic matter (Peters et al., 2005): *n*-C_{12} to *n*-C_{35} unimodal shaped, with maximum peaks between *n*-C_{17} and *n*-C_{19} (Fig. 8). Also, all of them have an odd over even carbon preference and pristane-to-phytane ratios (Pr/Ph) varying from 0.9 to 1.1 (Table 4), which is consistent with shaly source rocks deposited in a marine to transitional environment under oxygen-depleted conditions (Tissot and Welte, 1984). Although the relative proportions of pristane and phytane are said to be influenced by complex processes (e.g., Dzou et al., 1999), the Pr/Ph ratio is considered here to indicate the depositional environment. Pr/*n*-$C_{17} \geq 0.5$ (see Fig. 8) would suggest that all the oil samples originated from Type II/III kerogen and/or from multiple sources (Hunt, 1996). However, given that *n*-paraffins in early oil charge(s) could have been affected by paleo-biodegradation (Wenger et al., 2002), as discussed below, *n*-alkane-based parameters should be interpreted with caution in the case of these oils.

Figure 8

All the oil samples have similar *m/z* 191 (triterpanes) and *m/z* 217 (steranes) fragmentograms of the saturated fraction (Fig. 9; peak identifications in the Appendix), suggesting that they were generated from the same source(s). Several features common to all studied oils are: relatively abundant tricyclopolyprenanes, Pr/Ph values lower than 2, 18α(H)-22,29,30-trisnorneohopane to 17α(H)-

22,29,30-trisnorhopane ratios (Ts/Tm) lower than one, $C_{31}R/C_{30}$ hopane ratios exceeding 0.3, ratios between C_{26} and C_{25} tricyclopolyprenanes lower than unity, slightly dominance of C_{27} regular steranes over their C_{28} and C_{29} counterparts (see Table 4), and values above 0.5 (see Table 4) for the ratio of C_{29} regular steranes to C_{30} hopane, which can be indicative of predominantly marine algal precursor organic matter (Seifert and Moldowan, 1978; Seifert and Moldowan, 1981). Based on the significant proportion of C_{28} steranes, the age of the source of sampled oils may be post-Jurassic in age (Peters et al., 2005). As for clay versus carbonate saturated-based indicators, on one hand, pristane/phytane ratios around 1.1, C_{29}/C_{30} hopane values < 0.7, notable presence of diasteranes, low abundance of 18β(H)-des-E-hopane or C_{24}-17,21-secohopane, and carbon preference index values higher than unity may suggest that all the samples originated from clay-rich source rocks (Peters et al., 2005; Permanyer et al., 2013). Whilst on the other hand, significant presence of gammacerane and C_{30} steranes, Ph/*n*-C_{18} values > 0.3, similar abundance of pentahomohopanes with respect to their C_{34} homologues, and whole-oil $\delta^{13}C$ values higher than -28‰ (see Table 4 and Fig. 9) would be indicative of carbonate-rich source rocks (Seifert and Moldowan, 1981; Rullkötter et al., 1985; Chung et al., 1992).

Figure 9

When looking at aromatic-based source-related indicators, similar results are obtained: all oils analysed show the usual methylated dibenzothiophene V shape distribution pattern of carbonate-rich facies (Fig. 10a, peak identifications of aromatics are in the Appendix), with the co-eluting 2- and 3-methyl isomers having the lowest abundances (Hughes, 1984). Also, the higher relative abundance of dibenzothiophene and its alkylated homologues (c.a. 57%) compared to unsubstituted and alkyl-dibenzofurans (about 24%) and fluorenes (nearly 19%) supports carbonate facies (Li et al., 2013). By contrast, DBT/P and Pr/Ph ratios below and above 1 (Table 4), respectively, could suggest that the oil samples were derived from marine siliciclastic source rocks (Hughes et al., 1995). High abundance of 1,2,5-trimethylnaphthalene and 1,2,5,6-tetramethylnaphthalene over their respective counterparts in the oils (Figs. 10b and 11a) might be related to land-plant inputs (van

Aarsen and de Leeuw, 1992). Two representative samples from the Cononaco and Shuhufindi fields show differences in the relative abundances of dibenzothiophene and 1,2,5,6-tetramethyl-naphthalene (Figs. 11a and 11c), while they both show an appreciable presence of phenanthrene and similar methylphenanthrene distribution patterns (Figs. 11b and 11d). These can be interpreted as having distinct contributions of the aforementioned source facies types rather than being caused by different in-reservoir alteration processes (Thomson, 1987; Galarraga et al., 2010).

Figure 10

Figure 11

The mentioned-above results could be explained by a scenario requiring a mixture of charges which originated from two organic facies types: a first one reflecting a carbonate-rich deposition in inner to middle neritic environments under very low-oxygen conditions, and a second one representing siliciclastic source-rocks deposited in shallower water (paralic-neritic) settings.

5. Discussion

5.1. Oils from the north-central part of the Sacha-Shushufindi Corridor

5.1.1. Oil-oil and oil-source correlations

A hierarchical cluster analysis on the basis of 12 parameters (Pr/Ph, 29/30H, 31R/30H, diasterane ratio, sterane-to-hopane ratio, V/Ni, 24/23T, 26/25T, Ts/Tm, DBT/P, $\delta^{13}C_{SAT}$ and $\delta^{13}C_{ARO}$) was performed to classify the oil samples into groups. Multivariate statistical analysis was carried out through the centroid method (Márquez et al., 2016). The similarity percentage was used to quantify divergence after obtaining Euclidean distances. Figures 12 and 13 show dendrogram plots including and without Cononaco/Auca oils, respectively. This clustering was performed using the SPSS 22.0 package for Windows.

Figure 12

Figure 13

Oil samples have a notable degree of similarity between them, indicating that they all are genetically similar. Finally, in an attempt to establish the source rock facies of the study oils from the Hollín, Napo T and U intervals, classical biomarker evidence from the set of oil samples was compared to those from B Limestone/A Limestone and Basal Shale/U Shale rock extracts. Taking into account the distribution patterns of triterpanes, methyldibenzothiophenes (4 > 2+3 < 1), regular steranes ($C_{27} > C_{28} > C_{29}$), and *n*-paraffins (with maximum peaks below *n*-C_{20}), it is possible to state that the sampled oils from the northern-central Sacha-Shushufindi Corridor correlate well with carbonate-rich source-rock facies from the B Limestone and A Limestone intervals, rather than with facies from the Basal Shale and U Shale sub-units. These results are also in agreement with previous studies (Mello et al., 1995; Ma et al., 2020), suggesting A Limestone organic-rich layers of the Napo Group as the best horizons for hydrocarbon generation in the western Oriente Basin. Nevertheless, since analysed oils also show carbon preference indices above 1, DBT/P values below 1, and significant abundance of diasteranes, which are not typical from carbonate source rocks, all this makes plausible the scenario of mixed oils deriving from pulses originated from both post-Jurassic siliciclastic and carbonate-rich sources. In such sense, studied classical biomarker features would preclude the possibility that the studied oils have been appreciably sourced from Santiago organic-rich limestones contradicting previous literature (e.g., Dashwood and Abbots, 1990).

5.1.2. Contributions of carbonate and siliciclastic Napo source facies

Since classical biomarker techniques did not give an entirely unambiguous explanation on the precise origin of the petroleum hydrocarbon liquids from the Hollín, Napo T and U reservoirs in the north-central portion of the Sacha-Shushufindi Corridor, definitive identification of source facies types was conducted by higher diamondoid correlations (Moldowan et al., 2015). Extended diamondoid analysis of the two pairs of representative oils corroborated oil-oil correlations obtained from classical biomarker data (Fig. 14a). In order to further prove mixing processes, the asphaltene fractions from two of the characteristic oil samples from Shushufindi and Auca fields were also

subjected to QEDA analyses. QEDA fingerprint from each asphaltene hydrous pyrolysate is plotted together with that from the respective maltene fraction in Figure 14b. It should be noted that the concentrations of eight higher polymantanes relative to triamantane show significant differences between the maltene and asphaltene QEDA fingerprints. This suggests that these fractions are not fully related to each other and serves as a confirmation that the sampled oils have multiple sources.

Figure 14

QEDA fingerprints in maltenes from two representative oil samples (Shushufindi and Cononaco) were compared to rock extracts of B Limestone/A Limestone, Basal Shale/U Shale facies types, and two mixtures of the extracted A Limestone and Basal Shale rocks (the best potential source facies; see Table 3) with volume ratios 2:1 and 1:1, respectively, to simulate what the QEDA graphs of naturally occurring mixtures would look like (Fig. 14a). The B Limestone/A Limestone extracts show high relative abundances of all higher polymantanes when compared to those of U Shale/Basal Shale. This is in agreement with the fact that Type-II/III kerogens yield lower amounts of higher diamondoids than Type-II kerogens at similar maturities (Jiang et al., 2018). As analysed samples plot between 2:1 and 1:1 mixtures, it can be stated that QEDA provides evidence of oil mixing in the Cretaceous reservoirs of northern Oriente Basin, where significant contributions of various petroleum generation horizons (i.e. the carbonate-rich A Limestone and siliciclastic Basal Shale source facies types) form most of the oil samples. Among all the analysed samples, the Cononaco/Auca oils from the central part of the basin appear to have a similar charge history and are the ones depicting a greater contribution from the carbonate-rich source facies type.

5.1.3. Thermal maturation

The different levels of maturity of the study oils were evaluated using several molecular maturity parameters, such as triaromatic cracking and sterane isomerization ratios (Table 5). The sterane isomerization ratios (%20*S* and %ββ) are restricted to maturation levels from the immature stage to a maximum maturity of about 0.8% and peak oil generation (Fig. 15), respectively (Peters et al.,

2005). None of the oil samples reach the respective "equilibrium" values (55% and 70%) for %20*S* and %ββ: most of them (except for those from Cononaco and Auca fields) showed %20*S* and %ββ ratios close to 50% and 60%. This would denote a maturation level equivalent to the onset of the peak oil generation (%Rc_1≈0.75%). Cononaco and Auca oils showed lower %20*S* and %ββ values (45% and 55%, respectively), indicating maturities equivalent to ≈0.65% within the early oil window (Hunt, 1996).

Table 5

Figure 15

The characteristic triaromatic steroid peaks were identified in the *m/z* ion chromatograms for all the oil samples (Fig. 10c). The triaromatic steroid cracking ratio (TA) can be defined as the ratio of C_{20} triaromatic steroid relative abundance to the sum of the values for its C_{20} and C_{28} 20*R* counterparts (Peters et al., 2005). The sampled oils have similar TA values ranging between 0.32 and 0.35, also suggesting maturation levels in the early oil-generative zone (%Rc_2 about 0.66%). Table 5 shows the values for dimethylnaphthalene ratios (DNR-1; Radke et al., 1984). The oils presented DNR-1 values in the 1.8-2.0 range and DNR-1-based calculated vitrinite reflectance data (%Rc_3) below 0.7%, corroborating a maturity level equivalent to the beginning of the oil window. The predominance of 2-ethylnaphthalene over 1-ethylnaphthalene (Fig. 10d), together with the 4-/1-MDBT ratios slightly higher than one (Fig. 10a), would confirm that all the sampled oils have maturity levels near 0.7% at the early oil window (Radke, 1988; Peters et al., 2005).

Table 5 shows the methylphenanthrene index values (MPI-1; Radke et al., 1982; Radke and Welte, 1983) corresponding to all the oil samples. The studied oils showed MPI-1 values ranging from 0.6 to 0.7 and MPI-1-based calculated vitrinite reflectance data (%Rc_4) in the 0.76-0.81% range. These values suggest maturation levels near the peak of the oil-generative window and they are high when compared to the other calculated vitrinite reflectance data. This is in line with literature (Cassani et

al., 1988) indicating that the MPI-1 ratio is not a useful indicator of thermal maturity for oils predominantly derived from marine organic matter at vitrinite reflectance values lower than 0.9%.

5.1.4. Petroleum alteration processes

As it is well-known in literature (e.g., Philp and Mansuy, 1997), several indicators such as API gravity and total sulfur content of oils can be influenced by factors such as source facies type, migration history, and in-reservoir alteration processes. On the basis of SARA compositions (see Table 1), all the analysed oils have apparently undergone no or negligible biodegradation processes, as the ratio of SAT to ARO is always higher than one (Hakimi et al., 2011). Whole oil gas chromatograms of oil samples showed unaltered isoprenoids and comparable C_4-C_9 *n*-alkanes (Figs. 16a and 16b) with respect to C_{10}^+ *n*-paraffins. The notable presence of light hydrocarbons in the oils might denote refreshing of a biodegraded fluid. Toluene/*n*-C_7 and *n*-C_7/methylcyclohexane values in the 0.7-1.1 and 0.5-0.7 ranges for some representative oils suggest that initial stages of evaporative fractionation and negligible-to-slight biodegradation would not have an appreciable influence on observed specific gravities and total sulphur contents (Thomson, 1987). Furthermore, the *n*-C_6/*n*-C_7 and *i*-C_5/*n*-C_5 ratios are higher than unity for most oil samples, except for 20º API gravity Cononaco oils from the Napo T and U intervals which show values below 1 (Figs. 16a and 16b). In addition, the V contents of Cononaco oils from the T/U reservoirs (V> 21.2 ppm) are appreciably different from those from the Hollín unit (V<18.5 ppm). Such latter values are not what might be expected and can be indicative of variability in partial vaporization and subsequent API gravity variations (Welte et al., 1982; Mango, 1997). API values associated with Napo oils from the Cononaco field may be also partially explained by the role of local re-migration (Smith, 1989).

Figure 16

Total ion current (TIC) chromatograms of the saturated fraction of oil samples show non-depleted isoprenoids and a slight loss of C_{10} to C_{20} *n*-alkanes, suggesting the possibility of biodegradation processes despite the negligible or low presence of unresolved complex mixtures (see Fig. 8a). A lack of 25-norhopanes in the *m/z* 191 ion chromatograms (Figs. 9a and 9b; peak identifications are

in the Appendix) leads to discard severe biodegradation. Specific gravity values below 33º API could be explained by the mixture of biodegraded liquid with unaltered charges (Márquez et al., 2016). Given the Oriente Basin history (e.g., Baby et al., 2014), the most likely explanation consists of presuming the existence of different oil pulses: an early oil charge could have been paleo-biodegraded due to meteoric water influx when the reservoirs were shallow in the late Paleogene, and one or more later pulses could show no biodegradation as the reservoirs subsided in the Miocene and became too hot for microbial activity (Smith, 1989; Dashwood and Abbots, 1990). This hypothesis of crude oil mixtures is coherent with two reported event groups of oil generation and expulsion from the Napo/Chonta source rocks to the northwest (Bermejo area) and southwest ("Situche" and "Santiago" regions) of the basin (Bernal, 1998; Hu et al., 2010). This implies early charge(s) of oil that originated during "Early Andean" (latest Cretaceous-early Oligocene) compressional episodes and uplift of the Western Cordillera, whilst late charge(s) took place during "Late Andean" times when basin subsidence occurred in relation to the Neogene tectonic development of the Cordillera Real (Bernal, 1998), and reservoirs would have been buried again.

5.2. Inter-field compositional changes

Based on hierarchical clustering, we can establish two different sampled oil groups (Fig. 12): those from the southernmost Cononaco and Auca fields on one side, and the nearly identical remaining oils on the other. Some scatter occurs in the major oil group, but without enough differentiation to isolate additional subpopulations (Fig. 13). Sampled oils from the northernmost part of the Central Wrench Corridor showed total sulphur contents (St) lower than one, DBT/P < 1, C_{29}/C_{30} hopane values below 0.6, diasterane ratios exceeding 0.5, and Ts/Tm values near 0.5, which are typical of mostly shaly marine sources; while Cononaco/Auca oils can be characterized by DBT/P < 1, St > 1, C_{29}/C_{30} hopane values exceeding 0.6, diasterane ratios below 0.5, and Ts/Tm clearly below 0.5, indicating mixed carbonate-siliciclastic facies (Moldowan et al., 1994; Hughes et al., 1995). It can be also tentatively stated that there are notable similarities between Cononaco/Auca oils and the liquid hydrocarbons (of ~36 ºAPI) from the northern Peruvian Chonta-Vivian petroleum system

produced from the Piuntza-1X (4º6'52''S, 77º47'28''W) and Situche C-2X (3º8'53''S, 77º17'10''W) wells at depths of over 3 km: the latter show V contents about 30 ppm, as well as V/Ni, total sulfur contents and DBT/P values close to 2.9, 1.6% and 0.7, a slight predominance of C_{27} regular steranes, Pr/Ph ranging from 0.9 to 1.0, Ts/Tm below 0.4, Ph/*n*-C_{18} exceeding 0.3, significant presence of gammacerane and similar abundance of penta- and tetra-homohopanes, along with respective $\delta^{13}C$ values for the saturated and aromatic fractions from -27.7‰ to -27.3‰ and -26.8‰ to -26.3‰ (Navarro, 2005).

5.3. Petroleum migration and generation patterns

Analysed oil samples exhibit %20*S* and %ββ results plotting far off the maturation trendline, with %20*S* values around 50% and inferior to %ββ values. This is suggestive of long-range hydrocarbon migration through relatively permeable long distance carrier beds (Seifert and Moldowan, 1981). Very low ratios (< 0.25) of benzo[a]carbazole to benzo[c]carbazole isomers and low abundances of dibenzofurans corroborate long-range migration from oil kitchens to reservoirs (Terken and Frewin, 2000; Li et al., 2011). These features agree with the hypothesis that long-distance secondary hydrocarbon migrations of a few hundreds of kilometers occurred, particularly through the Hollín sandstones, and across the western Oriente Basin (Dashwood and Abbots, 1990; Baby et al., 2013).

Polar (POL), V and Ni contents are highly correlated among themselves (Pearson's coefficients of V-Ni, V-POL, and Ni-POL equal to 0.969, 0.874, and 0.85). This can reflect geochromatography in petroleum migration (Filby, 1994; Escobar et al., 2012) with hydrocarbon fractioning, where the polar fraction interacts with clay minerals (e.g., Waples, 1981). Particularly, the sampled oils from Cononaco and Auca fields showed the highest values of the three parameters (Table 1), which might indicate that these liquid hydrocarbons migrated from the Auca source kitchen area over shorter distances (Bernal, 1998). In general, it is observed that there is a decrease in POL, V and Ni contents from southwest to northeast: this agrees with northeasternward hydrocarbon migration in the central-western Ecuadorian Oriente Basin as described by several authors (e.g., Hu et al., 2010).

Previous 1D geochemical modeling data agree with the assertion of Napo source rocks across the Oriente Basin becoming thermally mature for oil generation during Cenozoic times (Dashwood and Abbots, 1990; Estupiñán et al., 2010a). In more detail, maturation and burial history suggest that in the Auca region, affected by intraplate magmatism (Barragan et al., 2005), i.e. the areas comprising the NW Oriente and SW Putumayo basins, as well as the Huasaga-Bobonaza Deep in the southwestern basin or further south, the Napo source rocks reached the onset of the oil window during pre-Miocene and mid-Miocene times (Bernal, 1998; Estupiñán et al., 2010b; Xie et al., 2010). Later subsidence in the southwest would have caused re-migration and another pulse of oil generation since the end of the Miocene (Hu et al., 2010). Hence "Situche" and "Santiago" regions located almost at the western Peruvian-Ecuadorian border or beyond and, to a much lesser extent, the "Auca" area linked to magmatic activity, were hypothetical source kitchens for oils in Hollin and Napo oilfields within the NNE-SSW corridor in the central part of the basin (Bernal, 1998; Baby et al., 2013), with carbonate-rich intervals as the major source rock. Particularly, the southernmost rock sample was taken from an outcrop near the Santiago Basin and the "Situche" area and has the highest carbonate character, comparable to that reported for the Chonta Formation in Peru (Pardo and Zúñiga, 1976). Lastly, clastic sediments located at the site of the present-time Andes ("Quito" kitchen) were proposed as alternative target source of the Ecuadorian Oriente oils (Feininger, 1975). This latter kitchen might explain in part the difference between oils from the Cononaco/Auca fields and all the other studied oils.

5. Conclusions

Our integrated geochemical study indicates a multiple petroleum charge of Cretaceous reservoirs in the Central Wrench Corridor of the Oriente Basin. Carbon isotopic signature of SARA fractions, biomarker ratios, along with maltene and asphaltene QEDA fingerprints for the sampled oils and distribution patterns of higher polymantanes at rock extracts point out that all the study oils

originated from the same stratigraphic sub-units of the Napo Group, particularly from the most organic-rich Limestone A and Basal Shale. Thus, Cretaceous-sourced oil samples are interpreted as deriving from at least two source facies types: marine carbonate-rich horizons deposited in inner to middle neritic settings with highly dominant algal input; and clay-rich source rock intervals deposited in a shallow to nearshore marine environment with appreciable terrigenous input.

The genetically related sampled oils can be divided into two slightly different subgroups. Classical biomarkers and QEDA suggest that mixed oils in Cretaceous reservoirs of the northern part of the Sacha-Shushufindi Corridor have higher contributions from the clay-rich source facies type in comparison to the Cononaco/Auca oils. More specifically, Cononaco oils from the T and U sandstone intervals might have experienced alteration processes such as partial vaporization and re-migration. This research work has contributed to adding evidence of the migration oil history within the study area. Petroleum accumulation in Cretaceous studied reservoirs might be explained by long-distance migration, in particular from southwestern source kitchen areas through the Hollín sandstones and across the western Oriente Basin.

Declaration of competing interest

The authors declare that they have no known competing financial interests or personal relationships that could have appeared to influence the work reported in this paper

Acknowledgments

Authors are grateful to Professors Galo Montenegro (ESPOL) and Marcos Escobar[†] (LUZ) for his scientific assistance and facilities to the samples. Carlos Boente obtained a post-doctoral contract within the program PAIDI 2020 (Ref 707 DOC 01097), co-financed by the Junta de Andalucía

(Andalusian Government) and the EU. We are also grateful to the two reviewers for their comments which helped to improve the original version of this manuscript.

References

Aspden, J.A., Litherland, M., 1992. The geology and Mesozoic collisional history of the Cordillera Real, Ecuador. Tectonophysics 205, 187–204. doi:10.1016/0040-1951(92)90426-7

Aspden, J.A., McCourt, W.J., Brook, M., 1987. Geometrical control of subduction-related magmatism: the Mesozoic and Cenozoic plutonic history of western Colombia. J. Geol. Soc. London. 144, 893–905. doi:10.1144/gsjgs.144.6.0893

ASTM, 2005. Standard Test Methods for Determination of Nickel, Vanadium, and Iron in Crude Oils and Residual Fuels by Inductively Coupled Plasma (ICP) Atomic Emission Spectrometry. Annual Book of the American Society For Testing Materials Standards, v. 05.03. West Conshohocken, Pennsylvania, ASTM International.

ASTM, 2010. Standard Test Method for Sulfur in Petroleum and Petroleum Products by Energy Dispersive X-ray Fluorescence Spectrometry. Annual Book of the American Society For Testing Materials Standards, v. 05.03. West Conshohocken, Pennsylvania, ASTM International.

Baby, P., Rivadeneira, M., Barragan, R., 2014. La Cuenca Oriente: geología y petróleo, Tercera edición. Institut Français d'Études Andines (IFEA), Petroamazonas EP, Lima, 414 p.

Baby, P., Rivadeneira, M., Barragan, R., Christophoul, F., 2013. Thick-skinned tectonics in the Oriente foreland basin of Ecuador. In: Nemcok, M., Mora, A., Cosgrove, J.W. (Eds.), Thick-skin-

dominated Orogens: from initial inversion to full accretion, vol. 377. Geol. Soc. Lond. Spec. Publ., 59–76.

Baby, P., Rivadeneira, M., Christophoul, F., Barragán, R., 1999. Style and timing of deformation in the Oriente Basin of Ecuador. 4th International Symposium on Andean Geodynamics, Extended Abstract, Gottingen, Germany, pp. 68–72.

Baldock, I.W., 1985. The Northern Andes: a review of the Ecuadorian Pacific Margin. In: Nairn, A.E.M., Stehli, H., Uyeda, E. (Eds.), The Ocean Basins and Margins. Plenum Press, NewYork, 181–218.

Balkwill, H., Rodriguez, G., Paredes, F., Almeida, J., 1995. Northern part of Oriente Basin, Ecuador: reflection seismic expression of structures. In: Tankard, A.J., Suárez, S.R., Welsink H.J. (Eds.), Petroleum Basins of South America, Am. Assoc. Pet. Geol. Memoir 62, 559–572.

Barragán, R., Baby, P., Duncan, R., 2005. Cretaceous alkaline intra-plate magmatism in the Ecuadorian Oriente Basin: Geochemical, geochronological and tectonic evidence. Earth Planet. Sci. Lett. 236, 670–690. doi:10.1016/j.epsl.2005.03.016

Bernal, C., 1998. Modelo teórico de generación y migración de hidrocarburos de la Formación Napo en la Cuenca Oriental del Ecuador. Thesis, Escuela Politécnica Nacional, Quito, 99 p.

Bès de Berc, S., Soula, J.C., Baby, P., Souris, M., Christophoul, F., Rosero, J., 2005. Geomorphic evidence of active deformation and uplift in a modern continental wedge-top-foredeep transition: Example of the eastern Ecuadorian Andes. Tectonophysics 399, 351–380. doi:10.1016/j.tecto.2004.12.030

Bissada, K.K., 1982. Geochemical constraints on petroleum generation and migration. In: Proceedings of the 2nd ASEAN Council on Petroleum (ASCOPE ‘81), Manila, Philippines, October 7-11, 1981, pp. 69–87.

Boreham, C.J., Crick, I.H., Powell, T.G., 1988. Alternative calibration of the Methylphenanthrene Index against vitrinite reflectance: Application to maturity measurements on oils and sediments. Org. Geochem. 12, 289–294. doi:10.1016/0146-6380(88)90266-5

Brookfield, M.E., Hemmings, D.P., Van Straaten, P., 2009. Paleoenvironments and origin of the sedimentary phosphorites of the Napo Formation (Late Cretaceous, Oriente Basin, Ecuador). J. South Am. Earth Sci. 28, 180–192. doi:10.1016/j.jsames.2009.02.004

Canfield, R.W., Bonilla, G., Robbins, R.K., 1982. Sacha oilfield of Ecuadorian Oriente. Am. Assoc. Pet. Geol. Bull. 66, 1076–1090.

Cassani, F., Eglinton, G., 1986. Organic geochemistry of Venezuelan extra-heavy oils. 1. Pyrolysis of asphaltenes: A technique for the correlation and maturity evaluation of crude oils. Chem. Geol. 56, 167–183. doi:10.1016/0009-2541(86)90001-X

Cassani, F., Gallango, O., Talukdar, S., Vallejos, C., Ehrmann, U., 1988. Methylphenanthrene maturity index of marine source rock extracts and crude oils from the Maracaibo Basin. Org. Geochem. 13, 73–80. doi:10.1016/0146-6380(88)90027-7

Christophoul, F., 1999. Discrimination des influences Tectoniques et Eustatiques dans les bassins liés a des zones de convergence: exemples du Bassin Subandin d’Équateur. Ph.D. thesis, Université Paul Sabatier-Toulouse III, 184 p.

Christophoul, F., Baby, P., Dávila, C., 2002a. Stratigraphic responses to a major tectonic event in a foreland basin: The Ecuadorian Oriente Basin from Eocene to Oligocene times. Tectonophysics 345, 281–298. doi:10.1016/S0040-1951(01)00217-7

Christophoul, F., Baby, P., Soula, J.-C., Rosero, M., Burgos, J., 2002b. Les ensembles fluviatiles néogènes du bassin subandin d'Équateur et implications dynamiques. Comptes Rendus Geosci. 334, 1029–1037. doi:10.1016/s1631-0713(02)01825-4

Chung, H.M., Rooney, M.A., Toon, M.B., Claypool, G.E., 1992. Carbon isotope composition of marine crude oils. Am. Assoc. Pet. Geol. Bull. 76, 1000–1007. doi:10.1306/bdff8952-1718-11d7-8645000102c1865d

Cornford, C., Gardner, P., Burgess, C., 1998. Geochemical truths in large data sets. I: Geochemical screening data. Org. Geochem. 29, 519–530. doi:10.1016/S0146-6380(98)00189-2

Dahl, J.E., Moldowan, J.M., Peters, K.E., Claypool, G.E., Rooney, M.A., Michael, G.E., Mello, M.R., Kohnen, M.L., 1999. Diamondoid hydrocarbons as indicators of natural oil cracking. Nature 399, 54–57. doi:10.1038/19953

Dashwood, M., Abbots, I., 1990. Aspects of the petroleum geology of the Oriente Basin, Ecuador. In: Brooks, J. (Ed.), Classic Petroleum Provinces, Special Publication-Geological Society of London, vol. 50, Blackwell, London, pp. 89–117.

De La Cruz, C., Márquez, N., Escobar, M., Segovia, S., 1997. An improved chromatographic method for the separation of saturated hydrocarbons, aromatic hydrocarbons, resins and asphaltenes

from heavy crude oils. 213th American Chemical Society National Meeting, San Francisco, April 13-17, pp. 416–418.

De Righi, M., Bloomer, G., 1975. Oil and gas developments in the Upper Amazon basin-Colombia, Ecuador and Peru. In: 9th World Petroleum Congress Proceedings, Tokyo, May 1-4, pp. 181–192.

Dzou, L.I., Holba, A.G., Ramón, J.C., Moldowan, J.M., Zinniker, D., 1999. Application of new diterpane biomarkers to source, biodegradation and mixing effects on Central Llanos Basin oils, Colombia. Org. Geochem. 30, 515–534. doi:10.1016/S0146-6380(99)00039-X

Escobar, M., Márquez, G., Azuaje, V., Da Silva, A., Tocco, R., 2012. Use of biomarkers, porphyrins, and trace elements to assess the origin, maturity, biodegradation, and migration of Alturitas oils in Venezuela. Fuel 97, 186–196. doi:10.1016/j.fuel.2012.03.002

Escobar, M., Márquez, G., Suárez-Ruiz, I., Juliao, T.M., Carruyo, G., Martínez, M., 2016. Source-rock potential of the lowest coal seams of the Marcelina Formation at the Paso Diablo mine in the Venezuelan Guasare Basin: Evidence for the correlation of Amana oils with these Paleocene coals. Int. J. Coal Geol. 163, 149–165. doi:10.1016/j.coal.2016.07.003

Espitalié, J., Laporte, J., Madec, M., Marquis, F., Leplat, P., Paulet, J., Boutefeu, A., 1977. Méthode rapide de caractérisation des roches mères, de leur potentiel pétrolier et de leur degré d'évolution. Revue Institut Francais du Pétrole 32, 23–42.

Estupiñán, J., 2005. Control diagenético sobre la calidad de los reservorios de las areniscas "U" y "T" de la Formación Napo del Cretácico de la Cuenca Oriente, Ecuador. Modelización térmica y su

relación con la generación de hidrocarburos. Tesis Doctoral, Universidad Complutense de Madrid, Madrid, 261 p.

Estupiñán, J., Marfil, R., Scherer, M., Permanyer, A., 2010a. Reservoir sandstones of the Cretaceous Napo Formation U and T members in the Oriente Basin, Ecuador: Links between diagenesis and sequence stratigraphy. J. Pet. Geol. 33, 221–245. doi:10.1111/j.1747-5457.2010.00475.x

Estupiñán, J., Permanyer, A., Marfil, R., Barbero, L., 2010b. Burial history and thermal evolution of the Cretaceous Napo Formation in the Oriente Basin of Ecuador. In: World Academy of Science, Engineering and Technology (WASET) Conference, Amsterdam, September 28-29, pp. 1299–1307.

Faucher, B., Vernet, R., Bizon, G., Bizon, J., Grekoff, N., Lys, M., Sigal, J., 1971. Sedimentary formations in Ecuador: A Stratigraphic and micropaleontological survey. Institut Francais du Pétrole, Paris, 220 pp.

Feininger, T., 1975. Origin of petroleum in the Oriente of Ecuador. American Association of Petroleum. Am. Assoc. Pet. Geol. Bull. 59, 1166–1175. doi:10.1306/83d91f4c-16c7-11d7-8645000102c1865d

Feininger, T., Bristow, C.R., 1980. Cretaceous and Paleocene geologic history of coastal Ecuador. Geologische Rundschau 69, 849–874.

Filby, R.H., 1994. Origin and nature of trace element species in crude oils, bitumens and kerogens: Implications for correlation and other geochemical studies.In: Parnell, J. (Ed.), Geofluids: Origin,

migration and evolution of fluids in sedimentary basins, Geological Society Special Publication No. 78, London, pp. 203-218.

Gaibor, J., Hochuli, J.P.A., Winkler, W., Toro, J., 2008. Hydrocarbon source potential of the Santiago Formation, Oriente Basin, SE of Ecuador. J. South Am. Earth Sci. 25, 145–156. doi:10.1016/j.jsames.2007.07.002

Galarraga, F., Reategui, K., Martïnez, A., Martínez, M., Llamas, J.F., Márquez, G., 2008. V/Ni ratio as a parameter in palaeoenvironmental characterisation of nonmature medium-crude oils from several Latin American basins. J. Pet. Sci. Eng. 61, 9–14. doi:10.1016/j.petrol.2007.10.001

Galarraga, F., Urbani, F., Escobar, M., Márquez, G., Martínez, M., Tocco, R., 2010. Main factors controlling the compositional variability of seepage oils from Trujillo State, Western Venezuela. J. Pet. Geol. 33, 255–267. doi:10.1111/j.1747-5457.2010.00477.x

Hakimi, M.H., Abdullah, W.H., Shalaby, M.R., 2011. Organic geochemical characteristics of crude oils from the Masila Basin, eastern Yemen. Org. Geochem. 42, 465–476. doi:10.1016/j.orggeochem.2011.03.015

Higgs, R., 2002. Tide-dominated estuarine facies in the Hollin and Napo (T and U) formations (Cretaceous), Sacha Field, Oriente Basin, Ecuador: Discussion. Am. Assoc. Pet. Geol. Bull. 86, 329–334. doi:10.1306/C9EBCE7D-1735-11D7-8645000102C1865D

Higley, D.K., 2001. The Putumayo-Oriente-Marañon Province of Colombia, Ecuador, and Peru—Mesozoic-Cenozoic and Paleozoic Petroleum Systems. USGS Digit. Data Ser., 40 p.

Hu, Y., Yin, J., Su, Y., Xin, Y., Wang, X., Xiao, G., Yu, Z., Wang, L., 2010. Geochemistry of heavy oil in the T Block, Oriente Basin and its origin mechanism. Acta Geol. Sin. 84, 406–414. doi:10.1111/j.1755-6724.2010.00143.x

Huang, H., Zhang, S., Su, J., 2015. Geochemistry of Tri- and Tetracyclic Terpanes in the Palaeozoic Oils from the Tarim Basin, Northwest China. Energy and Fuels 29, 7014–7025. doi:10.1021/acs.energyfuels.5b01613

Hughes, W.B., 1984. Use of thiophenic organosulphur compounds in characterizing of oils derived from carbonate versus siliciclastic sources. In: Palacas, G. (Ed.), Petroleum geochemistry and source rock potential of carbonate rocks. Am. Assoc. Pet. Geol. Studies in Geology No. 18, pp. 181–196.

Hughes, W.B., Holba, A.G., Dzou, L.I.P., 1995. The ratios of dibenzothiophene to phenanthrene and pristane to phytane as indicators of depositional environment and lithology of petroleum source rocks. Geochim. Cosmochim. Acta 59, 3581–3598. doi:10.1016/0016-7037(95)00225-O

Hunt, J.M., 1996. Petroleum Geochemistry and Geology, 2nd Edition. Freeman and Company, San Francisco, 743 p.

Jaillard, E., 1996. Sedimentary model for the Oriente Basin of Ecuador during the Cretaceous. In: Extended Abstracts of 3rd International Symposium on Andean Geodynamics (ISAG), Saint Malo, September 17-19, pp. 395–398.

Jaillard, E., Bengtson, P., Dhondt, A. V., 2005. Late Cretaceous marine transgressions in Ecuador and northern Peru: A refined stratigraphic framework. J. South Am. Earth Sci. 19, 307–323. doi:10.1016/j.jsames.2005.01.006

Jaillard, E., Soler, P., Carlier, G., Mourier, T., 1990. Geodynamic evolution of the northern and central Andes during early to middle Mesozoic times: A Tethyan model. J. Geol. Soc. London. 147, 1009–1022. doi:10.1144/gsjgs.147.6.1009

Jarvie, D.M., Claxton, B.L., Henk, B., Breyer, J., 2001. Oil and shale gas from the Barnett Shale, Fort Worth basin, Texas. Am. Assoc. Pet. Geol. Annual National Convention, Denver, June 3-6, p. A100.

Jiang, W., Li, Y., Xiong, Y., 2018. The effect of organic matter type on formation and evolution of diamondoids. Mar. Pet. Geol. 89, 714–720. doi:10.1016/j.marpetgeo.2017.11.003

Killops, S.D., Killops, V.J., 2005. Introduction to Organic Geochemistry, 2nd Edition. Wiley-Blackwell Publishing, Oxford, 393 p.

Lebras, M., Megard, F., Dupuy, C., Dostal, J., 1987. Geochemistry and tectonic setting of pre-collision Cretaceous and Paleogene volcanic rocks of Ecuador. Geol. Soc. Am. Bull. 99, 569–578. doi:10.1130/0016-7606(1987)99<569:GATSOP>2.0.CO;2

Lee, G.H., Eissa, M.A., Decker, C.L., Castagna, J.P., O'Meara, D.J., Marín, H.D., 2004. Aspects of the petroleum geology of the Bermejo field, Northwestern Oriente Basin, Ecuador. J. Pet. Geol. 27, 335–356. doi:10.1111/j.1747-5457.2004.tb00062.x

Lewan, M.D., 1984. Factors controlling the proportionality of vanadium to nickel in crude oils. Geochim. Cosmochim. Acta 48, 2231–2238. doi:10.1016/0016-7037(84)90219-9

Lewan, M.D., Maynard, J.B., 1982. Factors controlling enrichment of vanadium and nickel in the bitumen of organic sedimentary rocks. Geochim. Cosmochim. Acta 46, 2547–2560. doi:10.1016/0016-7037(82)90377-5

Li, M.J., Wang, T.G., Yang, F.L., Shi, Y., 2011. Molecular tracers for filling pathway in condensate pools: Alkyldibenzofuran. J. Oil Gas Technol. 33, 6–11.

Li, M., Wang, T., Zhong, N., Zhang, W., Sadik, A., Li, H., 2013. Ternary diagram of fluorenes, dibenzothiophenes and dibenzofurans: Indicating depositional environment of crude oil source rocks. Energy Explor. Exploit. 31, 569–588. doi:10.1260/0144-5987.31.4.569

Lijmbach, G.W.M., van der Veen, F.M., Englehardt, E D., 1983. Geochemical characterization of crude oils and source rocks using field ionization mass spectrometry. In: Bjorøy, M., Albrecht, C., Cornford, C. (Eds.), Advances in Organic Geochemistry, John Wiley and Sons, New York, pp. 788–798.

Ma, Z.Z., Chen, H., Xie, Y., Zhang, Z., Liu, Y., Yang, X., Zhou, Y., Wang, D., 2017. Division and resources evaluation of hydrocarbon plays in Putomayo-Oriente-Maranon Basin, South America. Pet. Explor. Dev. 44, 247–256. doi:10.1016/S1876-3804(17)30027-7

Ma, Z.Z., Tian, Z.T., Zhou, Y.B., Yang, X.F., Tian, Y., 2020. Geochemical characterization and origin of crude oils in the Oriente basin, Ecuador, South America. J. South Am. Earth Sci. 104, 102790. doi:10.1016/j.jsames.2020.102790

Mango, F.D., 1997. The light hydrocarbons in petroleum: A critical review. Org. Geochem. 26, 417–440. doi:10.1016/S0146-6380(97)00031-4

Marksteiner, R., Alemán, A., 1997. Petroleum systems along the fold belt associated to the Marañon-Oriente-Putumayo foreland basin. Memoirs of 6th Bolivarian Symposium: Petroleum Exploration in the Sub-Andean Basins, Cartagena, Colombia, September 14-17, pp. 63–74.

Márquez, G., Escobar, M., Lorenzo, E., Duno, L., Esquinas, N., Gallego, J.R., 2016. Intra- and inter-field compositional changes of oils from the Misoa B4 reservoir in the Ceuta Southeast Area (Lake Maracaibo, Venezuela). Fuel 167, 118–134. doi:10.1016/j.fuel.2015.11.046

Mathalone, J.M.P., Montoya R., M., 1995, Petroleum geology of the Sub-Andean basins of Peru. In: Tankard, A.J., Suárez, S.R., Welsink H.J. (Eds.), Petroleum Basins of South America, Am. Assoc. Pet. Geol. Memoir 62, pp. 423–444.

Mello, M.R., Koutsoukos, E.A.M., Erazo, W.Z., 1995. The Napo Formation, Oriente basin, Ecuador: hydrocarbon source potential and paleo environmental assessment. In: Katz, B.J. (Ed.), Petroleum source rocks, Springer-Verlag, Berlin, pp. 167–181.

Moldowan, J.M., Dahl, J., Zinniker, D., Barbanti, S.M., 2015. Underutilized advanced geochemical technologies for oil and gas exploration and production-1. The diamondoids. J. Pet. Sci. Eng. 126, 87–96. doi:10.1016/j.petrol.2014.11.010

Moldowan, J.M., Peters, K.E., Carlson, R.M.K., Schoell, M., Abu-Ali, M., 1994. Diverse applications of petroleum biomarker maturity parameters. Arab. J. Sci. Eng. 19, 273–298.

Navarro, L., 2005. The Santiago Basin: Structural style and petroleum systems. BSc thesis, San Agustín National University, Arequipa, Peru, 112 p.

Pardo A., Zúñiga F., 1976. Stratigraphy and tectonic evolution of the jungle region of Peru. In: Proceedings of the II Latin American Congress on Geology, Caracas, November 11-16, 1973, pp. 569–608.

Permanyer, A., Márquez, G., Gallego, J.R., 2013. Compositional variability in oils and formation waters from the Ayoluengo and Hontomín fields (Burgos, Spain). Implications for assessing biodegradation and reservoir compartmentalization. Org. Geochem. 54, 125–139. doi:10.1016/j.orggeochem.2012.10.007

Peters, K.E., 1986. Guidelines for evaluating petroleum source rocks using programmed pyrolysis. Am. Assoc. Pet. Geol. Bull. 70, 318–329.

Peters, K.E., Clark, M.E., das Gupta, U., McCaffrey, M.A., Lee, C.Y., 1995. Recognition of an Infracambrian source rock based on biomarkers in the Bagehwala-1 oil, India. Am. Assoc. Pet. Geol. Bull. 79, 1481–1494.

Peters, K., Walters, C.C., Moldowan, J.M., 2005. The Biomarker Guide: Biomarkers and Isotopes in Petroleum Systems and Earth history, 2nd Edition. Cambridge University Press, London, 1132 p.

Pindell, J., Tabbutt, K., 1995. Mesozoic–Cenozoic Andean paleogeography and regional controls on hydrocarbon systems. In: Tankard, A.J., Suárez, R., Welsink, H.J. (Eds.), Petroleum Basins of South America. Am. Assoc. Pet. Geol. Memoir 62, pp. 101–128.

Philp, R.P., Mansuy, L., 1997. Petroleum geochemistry: concepts, applications, and results. Energy and Fuels 11, 749–760. doi:10.1021/ef960174v

Pytlak L., Kowalski A., Gross D., Sachsenhofer R.F., 2017. Composition of diamondoids in oil samples from the alpine foreland basin, Austria: potential as indices of source rock facies, maturity and biodegradation. J. Pet. Geol. 40, 153–171. doi:10.1111/jpg.12670

Radke, M., 1988. Application of aromatic compounds as maturity indicators in source rocks and crude oils. Mar. Pet. Geol. 5, 224–236. doi:10.1016/0264-8172(88)90003-7

Radke, M., Welte, D. H., 1983. The methylphenantrene index (MPI): a maturity parameter based on aromatic hydrocarbons. In: Bjoroy, M., Albrecht, C., Cornford, C., de Groot, K., Eglinton, G., Galimov, E., Leythaeuser, D., Pelet, R., Rullkötter, J., Speers, G. (Eds.), Advances in Organic Geochemistry. John Wiley and Sons, New York, pp. 504-512.

Radke, M., Leythaeuser, D., Teichmüller, M., 1984. Relationship between rank and composition of aromatic hydrocarbons for coals of different origins. Org. Geochem. 6, 423–430. doi:10.1016/0146-6380(84)90065-2

Radke, M., Welte, D.H., Willsch, H., 1982. Geochemical study on a well in the Western Canada Basin: relation of the aromatic distribution pattern to maturity of organic matter. Geochim. Cosmochim. Acta 46, 1–10. doi:10.1016/0016-7037(82)90285-X

Rullkötter, J., Spiro, B., Nissenbaum, A., 1985. Biological marker characteristics of oils and asphalts from carbonate source rocks in a rapidly subsiding graben, Dead Sea, Israel. Geochim. Cosmochim. Acta 49, 1357–1370. doi:10.1016/0016-7037(85)90286-8

Seifert W.K., Moldowan, J.M., 1978. Application of steranes, terpanes and monoaromatic to the maturation, migration and source of crude oils. Geochim. Cosmochim. Acta 42, 77–95.

Seifert, W.K., Moldowan, J.M., 1981. Palaeoreconstruction by biological markers. Geochim. Cosmochim. Acta 45, 783–794.

Sempere, T., 1995. Phanerozoic evolution of Bolivia and adjacent regions. In: Tankard, A.J., Suarez S.R., Welsink, H.J. (Eds.). Petroleum Basins of South America, Am. Assoc. Pet. Geol. Memoir 62, pp. 207–230.

Shanmugam, G., Poffenberger, M., Toro Álava, J., 2000. Tide-dominated estuarine facies in the Hollin and Napo (’T’ and “U”) formations (Cretaceous), Sacha field, Oriente Basin, Ecuador. Am. Assoc. Pet. Geol. Bull. 84, 652–682. doi:10.1306/c9ebce7d-1735-11d7-8645000102c1865d

Smith, L.R., 1989. Regional variations in formation water salinity, Hollin and Napo Formations (Cretaceous), Oriente Basin, Ecuador. Am. Assoc. Pet. Geol. Bull. 73, 757–776. doi:10.1306/44b4a258-170a-11d7-8645000102c1865d

Sofer, Z., 1984. Stable Carbon Isotope composition of crude oils: application to source depositional environments and petroleum alteration. Am. Assoc. Pet. Geol. Bull. 68, 31–49. doi:10.1306/ad460963-16f7-11d7-8645000102c1865d

Summons, R.E., Hope, J.M., Swart, R., Walter, M.R., 2008. Origin of Nama Basin bitumen seeps: Petroleum derived from a Permian lacustrine source rock traversing southwestern Gondwana. Org. Geochem. 39, 589–607. doi:10.1016/j.orggeochem.2007.12.002

Terken, J.M.J., Frewin, N.L., 2000. The Dhahaban petroleum system of Oman. Am. Assoc. Pet. Geol. Bull. 84, 523–544. doi:10.1306/c9ebce41-1735-11d7-8645000102c1865d

Thompson, K.F.M., 1987. Fractionated aromatic petroleums and the generation of gas-condensates. Org. Geochem. 11, 573–590. doi:10.1016/0146-6380(87)90011-8

Tissot, B.P., Welte, D.H., 1984. Petroleum Formation and Occurrence, 2nd Edition. Springer-Verlag, New York, 699 p. doi:10.1007/978-3-642-87813-8

Tocco, R., Escobar, M., Ruggiero, A., Galarraga, F., 1995. Geochemistry of seep oils and rock samples of the early Tertiary section from the Northandean Flank of the Venezuelan Los Andes. Org. Geochem. 23, 311–327. doi:10.1016/0146-6380(95)00013-5

Tschopp, H.J., 1953. Oil explorations in the Oriente of Ecuador, 1938-50. Am. Assoc. Pet. Geol. Bull. 37, 2303–2347. doi:10.1306/5ceadd94-16bb-11d7-8645000102c1865d

Vallejo, C., Hochuli, P.A., Winkler, W., von Salis, K., 2002. Palynological and sequence stratigraphic analysis of the Napo Group in the Pungarayacu 30 well, Sub-Andean Zone, Ecuador. Cretac. Res. 23, 845–859. doi:10.1006/cres.2002.1028

van Aarssen, B.G.K., de Leeuw, J.W., 1992. High-molecular-mass substances in resinites as possible precursors of specific hydrocarbons in fossil fuels. Org. Geochem. 19, 315–326. doi:10.1016/0146-6380(92)90002-F

Waples, D.W., 1981. Organic geochemistry for exploration geologist. Burges Publishing Company, Minneapolis, 151 p.

Welte, D.H., Kratochvil, H., Rullkötter, J., Ladwein, H., Schaefer, R.G., 1982. Organic geochemistry of crude oils from the Vienna Basin and an assessment of their origin. Chem. Geol. 35, 33–68. doi:10.1016/0009-2541(82)90018-3

Wenger, L.M., Davis, C.L., Isaksen, G.H., 2002. Multiple controls on petroleum biodegradation and impact on oil quality. SPE Reserv. Eval. Eng. 5, 375–383. doi:10.2118/80168-PA

White, H., Skopec, R., Ramirez, F., Rodas, J., Bonilla, G., 1995. Reservoir characteristics of the Hollin and Napo formations, western Oriente Basin, Ecuador. In: Tankard, A.J., Suarez S.R., Welsink, H.J. (Eds.). Petroleum Basins of South America, Am. Assoc. Pet. Geol. Memoir 62, pp. 573–596.

Xie, Y., Cheng, J., Su, Y., Hu, Y., 2010. Petroleum geology and exploration potential of Oriente-Marañon Basin. Pet. Explor. Dev. 37, 51–56. doi:10.1016/S1876-3804(10)60014-6

Yang, X.F., Xie, Y.F., Zhang, Z.W., Ma, Z.Z., Zhou, Y.B., Liu, Y.M., Wang, D.D., Zhao, Y.B., 2017. Hydrocarbon generation potential and depositional environment of shales in the Cretaceous Napo Formation, Eastern Oriente Basin, Ecuador. J. Pet. Geol. 40, 173–193. doi:10.1111/jpg.12671

Figure 1: a) Map showing the situation of oil fields, sampled rock outcroppings, and boreholes in the Oriente Basin. From left to right, Cordillera Real, Subandean Zone, Central Wrench Corridor, and Eastern Inverted System can be distinguished (modified from Baby et al., 1999); b) Schematic cross-section across the central-western part of the basin (after Dashwood and Abbots, 1990) to illustrate the rock sampling strategy (see profile line in Fig. 1a).

Figure 2: Generalized stratigraphic section in the Oriente Basin (adapted from Estupiñán, 2005). Note: source rocks (black circle) and reservoir rocks (black square).

Figure 3: Map representing the rock units (Napo Group and Basal Tena Member) that outcrop in the sampling location at Pungarayacu area and the types of contacts among them.

Figure 4: a) and b), respectively, Pseudo-Van Krevelen diagram and plot of HI against Tmax for rock samples.

Figure 5: a) and b), respectively, representative *m/z* 99 ion chromatograms for the saturate fractions of A Limestone/B Limestone and Basal Shale/U Shale source facies types.

Figure 6: Examples of *m/z* 191 (a and b, respectively) and *m/z* 217 ion chromatograms (c and d, respectively) showing triterpane and sterane distributions for the saturate fractions of representative rock extracts from the A Limestone/B Limestone and Basal Shale/U Shale sub-units.

Figure 7: a) Map showing average API gravity values for oils produced from the study fields in the Central Wrench Corridor; b) Sofer isotopes diagram for the aromatic and saturate fractions of representative oils and rock extracts.

Figure 8: a), b), and c), respectively, example of total ion chromatogram (CON-30 oil) and *m/z* 99 ion chromatograms showing characteristic *n*-paraffin and isoprenoid signals for representative CON-27 and SSF-046 oil samples.

Figure 9: Examples of *m/z* 191 ion chromatograms (a and b) and *m/z* 217 ion chromatograms (c and d) showing triterpane and sterane distributions for the saturate fractions of representative SSF-046 and CON-27 oil samples, respectively.

Figure 10: a), b), c), and d), respectively, *m/z* 198, *m/z* 170, *m/z* 231, and *m/z* 156 ion chromatograms showing methylated dibenzothiophene isomers, as well as trimethylnaphthalene, triaromatic steroid, and dimethylnaphthalene series for the aromatic fraction of a characteristic (GTA-10) oil sample.

Figure 11: *m/z* 184 ion chromatograms (a and c) and *m/z* 178+192 ion chromatograms (b and d), showing tetramethylnaphthalene and phenanthrene series for the aromatic fractions of representative SSF-046 and CON-27 oil samples, respectively.

Figure 12: Dendrogram showing the results of clustering (Ward´s method) and allowing separation into two oil groups.

Figure 13: Dendrogram showing the results of cluster analysis after excluding Auca and Cononaco oil samples.

Figure 14: a) QEDA analysis of four selected oils (continuous lines) and extract mixtures (dotted lines) obtained from B Limestone and Basal Shale facies types confirming oil-oil and oil-source correlations; b) fingerprints of higher diamondoids by QEDA for two representative oils and hydropyrolysates (dashed lines) generated from asphaltenes.

Figure 15: Plot of %20*S* versus %ββ sterane ratios showing the level of thermal maturity of sampled oils.

Figure 16: Whole-oil gas chromatograms (a and b, respectively) and light hydrocarbon fingerprints from *n*-C_5 to *n*-C_9 for representative CON-27 and SSF-046 oil samples from the U reservoir. Abbreviations: DCM (dichloromethane solvent), MCH (methylcyclohexane), and Tol (toluene).

Appendix: Main saturated and aromatic biomarkers identified in the fragmentograms.

Study on spatio-compositional variations and source facies for oils from the Central Wrench Corridor of the Oriente Basin (Ecuador)

G. MÁRQUEZ[a,*], L. GONZÁLEZ[b], A. PERMANYER[c], C. BOENTE[a], M.A. GUZMÁN[a] and E. LORENZO[d]

[a] Center for Research in Sustainable Chemistry (CIQSO), University of Huelva, 21006 Huelva, Spain

[b] School of Geology, Mines and Geophysics, Central University of Venezuela, Caracas, 3895/1010-A, Venezuela

[c] Departament of Mineralogy, Petrology and Applied Geology, University of Barcelona, 08028 Barcelona, Spain

[d] School of Engineering Sciences, State University Santa Elena Peninsula, 240204 La Libertad, Ecuador

Abstract: This research paper contains an integration of classical biomarker work with higher diamondoid examination to better characterize the petroleum systems in the north-central portion of the Sacha-Shushufindi Corridor in the Ecuadorian Oriente Basin. A set of crude oils, cuttings, and outcrop rock samples were analysed to address aspects such as source-rock lithology, paleo-depositional conditions, migration distances, as well as oil-oil and oil-source correlations. For this, gas chromatography-mass spectrometry (GC-MS), GC-triple-quadrupole MS (GC-MS/MS), and carbon isotope ratio mass spectrometry (IRMS) were performed on maltene fractions both from oils and rock extracts. GC-MS/MS analyses of oil-derived asphalthene hydrous pyrolysates were also included on the study. Classical biomarker results suggest mixing of pulses from distant siliciclastic and carbonate-rich Napo source rocks, with former oil charges being slightly biodegraded during the Paleogene and fresher Neogene pulses. These two types of Early-Late Cretaceous source rocks were deposited in shallow marine to nearshore and low-oxygen inner to middle neritic environments, respectively, with considerable and scarce contribution of land-plant material in both cases. Such differentiation of the two source facies types of the Napo Group is supported by results from quantitative extended diamondoid analysis (QEDA).

Keywords: oil-source correlation, oil groups, QEDA method, Sacha-Shushufindi Corridor, Ecuadorian Oriente Basin.

1. Introduction

The petroliferous East Ecuadorian or Oriente Basin is part of the large Amazonian retro-arc foreland basin system that was partially developed in the east of the northern Andean Mountains (Canfield et al., 1982; Estupiñán et al., 2010a; among others; see Fig. 1a). The Oriente Basin lies between the Pre-Cambrian Brazilian-Guyana basement shields to the east and the eastern Andes in Ecuador to the west, and is also geologically continuous to the Putumayo Basin (Colombia) and the Marañón Basin (Peru), northwards and southwards, respectively (Dashwood and Abbots, 1990;

*gonzalo.marquez@diq.uhu.es Tlfn./Fax: +34959217325

Marksteiner and Alemán, 1997; Bès de Berc et al., 2005; Xie et al., 2010). The asymmetric Oriente Basin occupies an area of approximately 100000 km^2 and lies across the shield and Subandean zones of Ecuador (Dashwood and Abbots, 1990). The Basin, underlined by Precambrian rocks from the Guyana shield, preserves a Paleozoic to Quaternary sedimentary sequence (Tschopp, 1953), and it can be divided into two geological and geomorphological zones separated by reverse faults: the Subandean Zone (an inverted sequence of sediments) to the west (adjacent to the Andes); and the Oriente Basin *sensu stricto* (a lowland region) to the east, which were formed during Andean orogenesis in the late Cenozoic (Baldock, 1985; Christophoul et al., 2002a).

Figure 1

Petroleum exploration in the Oriente Basin began in the 1920's (Tschopp, 1953) with the first commercial oilfield discovered by a subsidiary of Texaco at Lago Agrio in 1967. For the next 45 years, Texaco and other companies discovered around 150 oilfields including Shushufindi, Sacha, Auca, and Cononaco (Canfield el al., 1982; Higley, 2000; see Fig. 1), of which nearly 100 are currently active with a total production of half a million barrels per day (Yang et al., 2017). The discovered recoverable reserves in the Oriente Basin and Shushufindi-Aguarico area exceed 13000 and 2000 million barrels of oil (MMBO), respectively (Baby et al., 2014; Ma et al., 2017). Almost all of the East Ecuadorian Basin oil production comes from nearshore marine sandstones of the Hollín and Napo formations (Feininger, 1975).

Previous analyses of sampled oils and Napo rock samples over various tens of Oriente wells were carried out to elucidate oil-oil and oil-source rock correlations (Mello et al., 1995; Estupiñán, 2005; Yang et al., 2017). Although potential Santiago source rocks cannot be totally ruled out (Pindell and Tabbutt, 1995; Vallejo et al., 2002), organic-rich Napo/Chonta intervals appear to be the primary petroleum source rocks in the Oriente/Marañón province (e.g., Canfield et al., 1982). The Albian-Campanian Napo Group is a world-class source rock, equivalent to the Cretaceous La Luna, Gachetá, and Raya/Chonta formations of Venezuela, Colombia, and Peru, respectively (Estupiñán,

2005); and so Cretaceous oils from the Marañón Basin are similar to oils from Napo source rocks in the Oriente Basin (Mathalone and Montoya, 1995). Average total organic carbon (TOC) contents for Napo shales vary from over 4% (Type-II kerogen) in the west to around 1% (more terrigenous subfacies) in the east (Dashwood and Abbots, 1990; Xie et al., 2010). For instance, in the western part of the Oriente Basin, Cenomanian to early Turonian and mid-Coniacian sediments contain marine mature intervals with predominant amorphous organic matter and TOC values about 10% (Vallejo et al., 2002), whilst, to the east, in the segment denominated T block (see Fig. 1a; Hu et al., 2010), Albian to Cenomanian sediments depict organic-rich calcareous shales (TOC contents of 2 to 3%) with marginally mature marine organic matter (Yang et al., 2017). Also noteworthy is the huge absence of mature Napo source rocks in the Oriente Basin (Baby et al., 2013).

Biomarker and carbon isotope analyses of Oriente oils from Hollín, Napo, and Tena reservoirs indicate that they all are genetically correlated and appear to be derived from a common dominantly marine facies type (Mello et al., 1995; Estupiñán, 2005). The varying API gravities in these oils mainly suggest different alteration histories, although no or little in-reservoir oil maturation has occurred. In this regard, the mentioned-above reservoirs contain negligibly to severely altered oils and API gravity does not correlate with reservoir depth (Dashwood and Abbots, 1990). The main reservoirs contain low-sulfur light-to-medium oils in the north-central part of the Central Wrench or Sacha-Shushufindi Corridor (e.g., Lago Agrio), in contrast to sulfur-rich heavy oils on the eastern and western basin flanks (e.g., Tiputini and Pungarayacu, respectively; see Fig. 1a), with the exception of in situ mature light oils related to local volcanic activity at the Bermejo area (Lee et al., 2004). Moreover, medium oils can be found throughout the central-eastern Oriente Basin (e.g., Cuyabeno) while reservoirs also contain heavy oils in several southern locations (Oglan and Nishino, among others). In this sense, fresh water influx from the west resulted in biodegradation of oils in the shallow reservoirs and essentially water-washing in the deeper reservoirs (Smith, 1989);

in addition, re-migrating oils might have been biodegraded at Oglan and other areas (Dashwood and Abbots, 1990).

Given the above, the objectives of this research are: (i) to assess the origin, thermal maturity, and secondary processes of a set of Cretaceous oil samples from the north-central part of the Sacha-Shushufindi Corridor; (ii) to evaluate inter-field compositional changes in oil samples from north to south; (iii) to identify contributions of carbonate and siliciclastic Napo source rock facies; and (iv) to verify the migration model proposed for the Napo reservoirs (as in Dashwood and Abbots, 1990; Bernal, 1998). Such outcomes will improve the level of understanding achieved so far on the petroleum systems in the central-western part of the Ecuadorian Oriente Basin.

2. Geological background

2.1. Tectonic-structural framework

The tectonic and structural settings of the Oriente Basin have been described in numerous works (Tschopp, 1953; Dashwood and Abbots, 1990; Brookfield et al., 2009; among others). In the earliest Paleozoic, tectonic movements along the Ecuadorian margin of the oceanic proto-Pacific Plate led to structures involving Proterozoic metamorphic rocks and igneous cratons (Canfield et al., 1982; Balkwill et al., 1995); whilst in the Late Ordovician a passive margin had already developed after collision of plate boundaries (Mathalone and Montoya, 1995). A stage of mostly subduction-related deposition associated with transtension and transpression occurred during mid-Permian and Early Triassic times (Sempere, 1995). Starting in the Triassic, a period of rifting took place in the eastern Andean area along the proto-Pacific margin (Jaillard et al., 1990), and throughout the Jurassic, magmatic arcs developed (Mathalone and Montoya, 1995). The original Oriente Basin back-arc is the result of this post-rift subsidence (Jaillard et al., 1990; Dashwood and Abbots, 1990); whilst posterior tectonic activity (Late Jurassic to Early Cretaceous) led to a first stage of folding and uplifting of rift structures due to the accretion of allochthonous oceanic rocks onto the Ecuadorian margin (Aspden and Litherland, 1992). Another phase of convergence occurred in late Cretaceous-

Paleocene (Aspden and Litherland, 1992; Balkwill et al., 1995) linked to the Andean orogeny (Feininger and Bristow, 1980), and subsequent transpressive deformation created reverse faults and structural highs in the Oriente Basin (Balkwill et al., 1995). Lastly, transpression of the basin also occurred during the Pliocene-Quaternary (Baby et al., 1999).

The most important structures in the East Ecuadorian Basin comprise steeply dipping faults in en-echelon sets (Balkwill et al., 1995). These faults rose from basement into various stratigraphic horizons and their trends strike in approximately NNE-SSW directions. In general, oilfields are aligned along these structural trends and belong to inverted Pre-Cretaceous extensional systems and have deformed the foreland basin system since the Late Cretaceous (Baby et al., 2013). Main features can be defined as positive flower structures which developed along the three referred NNE-SSW transpressive zones (Christophoul et al., 2002a). From west to east, these tectonic domains are: (i) the Subandean Zone, which hosts two antiforms (the Napo Uplift to the north and the Cordillera of Cutucú to the south, separated by the Pastaza or Puyo Depression) that represent positive flower structures of Neogene age (Bès de Berc et al., 2005); (ii) the Central or Sacha-Shushufindi Corridor, developed in Late Cretaceous and Cenozoic times, resulting from the inversion of Late Triassic-Early Jurassic rift high-angle normal faults; (iii) the Eastern or Capirón-Tiputini Inverted System, generated by the inversion of Late Jurassic half-grabens (Christophoul, 1999). The central Corridor, the Eastern Inverted System, and the Subandean Zone formed, respectively, during Turonian-Maastrichtian, early Eocene, and Neogene ages (Baby et al., 2013).

According to Dashwood and Abbots (1990), the basin axis is distorted by low-relief (< 100 m) anticlinal folds that produce a 50 km-wide axial region and separate the softly dipping eastern flank from the more abrupt western flank. Late Cretaceous to Pliocene tectonic events created low-relief anticlines (Mathalone and Montoya, 1995). According to Dashwood and Abbots (1990), syn-sedimentary compressive deformation occurred throughout the Late Cretaceous on most of the pre-Cretaceous N-S trending normal faults and produced a first type of structures: footwall anticlines associated with normal faults (e.g., Auca and Cononaco oilfields). Subduction of the Nazca

(Pacific) Plate resulted in reverse movement on part of the early N-S faults, particularly on the western flank of the Oriente Basin during the Paleogene period. This led to another type of structures (hanging-wall anticlines over reverse faults; e.g., Lago Agrio and Shushufindi). Most of the productive structures in the area under study are NS-trending anticlines, generally faulted on one of the flanks, which belong to the two referred structural styles (Canfield et al., 1982).

2.2. Stratigraphy and sedimentology

As shown in Fig. 2, a typical stratigraphic section of the Central Wrench Corridor can be divided into a pre-Cretaceous series, a continental to shallow marine Cretaceous sedimentary cycle (White et al., 1995), and a Cenozoic foreland molassic and shallow marine cover (Baby et al., 1999). Stratigraphic nomenclature of the Ecuadorian Oriente Basin is taken from geologic studies by Shell (Faucher et al, 1971) and subsequent modifications (e.g., Jaillard, 1996). The pre-Cretaceous series comprises Paleozoic marine sediments, Triassic and Lower Jurassic marine to continental rift deposits, and Late Jurassic sediments related to the activity of the continental Misahualli volcanic arc (Aspden et al., 1987; Dashwood and Abbots, 1990). Though magmatic rocks have also been identified in the Oriente Basin (Barragán et al., 2005), the Cretaceous series essentially comprises Aptian to Coniacian transitional clastic-carbonate nonmarine-marine sediments (i.e. Hollín and Napo units) deposited in the retro-arc basin during periods of low tectonic activity (Baldock, 1985), which were controlled by marine transgressions and regressions on the continental shelf (Tschopp, 1953). In general, the Cenozoic series is comprised of sediments deposited after stable shelf-rise conditions abruptly ended during the Maastrichtian (Feininger and Bristow, 1980).

Figure 2

In more detail, the Silurian-Devonian Pumbuiza Formation is the most ancient unit and consists of mainly sandstones; while the pre-rift Late Carboniferous-Permian Macuma Formation comprises bedded carbonates and clastics (Ma et al., 2020). Stratigraphically upward, the Early Jurassic Santiago Formation comprises carbonates, shales, and evaporites (Gaibor et al., 2008). The Late Jurassic-Early Cretaceous Chapiza Formation is composed of conglomerates, sandstones, and siltstones (Pindell and Tabbutt, 1995). Above, lays unconformably, the Cretaceous sequence,

initiated with the Hollin unit (Daswhood and Abbots, 1990). The Hollín-Napo sequence is composed by cyclic sequences of sedimentary rocks, which have been historically interpreted as fluvio-deltaic to shallow marine tidal deposits passing westward (Canfield et al., 1982); although more recent interpretations by Shanmugan et al. (2000) and Higgs (2002) suggested a tide-dominated estuarine depositional environment and a tidal shelf model for Napo and Hollín sands. The sedimentation of Hollín (Aptian-Albian) Formation appears to be related to the Aguarico and Cononaco arches to the east (White et al., 1995) and was caused by an Early Cretaceous marine transgression from the western marginal sea, over the Guyana Shield, after which white quartz sandstones interbedded with carbonaceous mudstones were deposited under regressive conditions (De Righi and Bloomer, 1975). The sand-rich Hollín pericratonic Formation constitutes the main oil reservoir in the Ecuadorian Oriente Basin. Both the Hollín unit and Napo sandstone members can be divided into a lower or "main" sub-unit of more permeable quartzose sandstones and upper clay-containing glauconitic sandstones separated by thin shaly layers (Dashwood and Abbots, 1990).

The Napo Group, which rests conformably on Hollín Formation, progressively thins eastwards and was originally divided into three distinct sub-units (Tschopp, 1953). Subsequent studies during petroleum exploration led to a subdivision into Basal, Lower, Middle, and Upper Napo formations (Jaillard, et al., 1997). The Basal Napo Formation (late Albian) consists of a series of alternating sandstones, shales, limestones, and cherts (see Fig. 2). The Lower Napo unit (latest Albian-Cenomanian) consists of sandstones, shales and limestones. The Middle Napo Formation (middle Turonian-early Coniacian?) is dominated by biomicritic limestones with shale partings and subordinate sandstones. Finally, the Upper Napo unit (late Coniacian-Santonian) is dominated by shales with subordinate limestones and sandstones (Jaillard, 1996; Jaillard et al., 2005), and has been informally divided into M1 Limestone, M1 Shale, and M1 Sandstone or San Fernando members (Smith, 1989; Jaillard, 1996). The Basal to Middle Napo formations represent the more significant cycles of transgression and regression. In these units, transgressive packages in the Basal Napo (labelled Basal Shale, C Limestone, T Shale, and T Limestone members), Lower Napo (B Limestone and U Shale intervals), and Middle Napo Formation (A Limestone and M2 Limestone

members) alternate with regressive T, U, and M2 Sandstone members (Vallejo et al., 2002; Fig. 2). The transgressive sequences consist of marine bioclastic limestones and shales, while the regressive packages consist of tide-dominated estuary sandstones rather than fluvio-deltaic deposits (Shanmugan et al., 2000). The Napo sands (mainly the T and U sands) are important reservoirs with similar properties (Dashwood and Abbots, 1990); only slight differences arise between such lower and upper intervals: lower T and U reservoirs have porosity and permeability values ranging from 10 to 22% and up to 1500 mD, respectively, while upper T and U reservoirs exhibit values below 18% and 850 mD (Estupiñán, 2005).

The Maastrichtian-Cenozoic sedimentary cover was deposited after a major non-depositional hiatus at the base of the Maastrichtian-Paleocene Tena Formation (Lebras et al., 1987). This foreland unit comprises fluvial red-coloured claystones and siltstones with basal conglomeratic sandstones (Christophoul et al., 2002a). The Tena Formation ("basal Tena sand") is a secondary petroleum reservoir and gradually truncates the Upper Napo and even Middle Napo units westwards (Dashwood and Abbots, 1990). The Paleogene Tituyacu and Orteguaza formations comprise fluvial to marginal marine deposits composed of clastic sedimentary rocks (Christophoul, 1999). Finally, four diachronous Neogene mainly clastic rock units (Chalcana, Arajuno, Chambira, and Mesa/Mera; Fig. 2) have been also recognized in the Oriente Basin, east of the Pastaza depression (Baby et al., 1999). It has been reported that the late Miocene to Recent sedimentary infill of the Oriente Basin represents an alluvial fan system (Christophoul et al., 2002b).

3. Samples and methods

A set of 125 oil samples from wells in the Cretaceous Hollín, T and U sands of the Auca (19), Cononaco (13), Shushufindi (57), Guanta (14), Lago Agrio (10), Shushuqui (6), and Tetete (6) fields were analysed. Table 1 shows the list of oil samples from the Central Wrench Corridor at different latitudes, the respective reservoir intervals, and complementary data. Table 2 displays information on 6 selected cuttings from wells located in the central-western Oriente Basin, and 4 outcrop samples from the most organic-rich Napo sub-units (i.e. Basal Shale, B Limestone, U

Shale, and A Limestone; Bernal, 1998). These were taken for oil-source rock correlation purposes. Rock sampling sites are located in the Central Wrench Corridor/Subandean Zone from south to north (see cross section shown in Fig. 1b) to discard significant lateral changes in the organofacies of these Napo sub-units. One of the sampled Napo strata outcrops is located on the Namangoza River (4 km southwest of the city of Santiago de Méndez; Fig. 1a), and the rest of them are outcrop along the Misahualli River (Pungarayacu area) at the southern Napo Uplift (about 12 km east of the Tena city; Figs. 1a and 3). The latter location is accessible via a quarry road along the west side of the river.

Table 1

Table 2

Figure 3

Rock samples were disaggregated, air-dried for 24 h, and grounded manually at Barcelona University. A small aliquot was taken to perform Rock-Eval 2/TOC analysis using a Vinci Technologies instrument following the method established by Espitalié et al. (1977). Another aliquot was used for Soxhlet extraction of organic chemicals using a mixture of dichloromethane:methanol (3:1, v/v). These extracts were concentrated by rotary evaporation at 40°C, filtered (0.45 μm) and dissolved in dichloromethane. For some samples (immature Napo B limestones and U shales), another aliquot was taken to carry out artificial maturation for 3 days at 330 °C (Lijmbach et al., 1983). Vitrinite reflectance measurements were also performed in accordance with Escobar et al. (2016).

Oil samples and rock extracts were fractioned into saturates, aromatics, and polar compounds. For this, samples were firstly passed through a batch-type reactor in constant agitation for 1 h at 60 ºC, followed by a 12-h inactive period. Then, asphalthenes were obtained with *n*-heptane in a 1:40 v/v ratio using Whatman filters. Maltenes were fractionated into saturated hydrocarbons, aromatics, and resins by solid-liquid chromatography (De la Cruz et al., 1997). The aliphatic, aromatic, and resin

fractions were eluted with *n*-hexane, toluene, and toluene/methanol (70:30 v/v) using a silica-alumina column. Gas chromatography-mass spectrometry (GC-MS) analysis on saturated and aromatic fractions were performed using a HP 5890 Series II gas chromatograph and an Agilent 5973 N mass spectrometer, operating in "fullscan" mode and with an HP-5 column (60 m × 0.32 mm i.d., 0.5 µm µm film). Helium was used as carrier gas, and initial oven temperature was 50 ºC (held for 2 min), ramped at 2.5 ºC up to 300ºC (held for 70 min).

Whole oil gas chromatographic analyses were carried out using a J&W Agilent PONA GC column (50 m x 0.2 mm i.d.; film thickness 0.25 µm; helium was the carrier gas) in a Delta Chrom Series 9980 instrument with flame ionization detection. The operating conditions were: oven temperature at 35 °C for 15 min, increased from 35 to 320 °C at 2 °C/min, and finally maintained at 320 °C for 30 min. Data were acquired using the Agilent ChemStation program.

Carbon isotopic determination on saturate, aromatic, resin, and asphaltene (SARA) fractions was performed using a Thermo Finnigan 1112 elemental analyzer coupled to a Finnigan Mat Delta C mass spectrometer. USGS 24 graphite, IAEA-CH6 saccharose, IAEA-CH7 polyethylene, and NBS-22 oil were used as reference materials. V and Ni concentrations were determined by inductively coupled plasma atomic emission spectroscopy (ICP-AES) using a Perkin Elmer Optima 3000 sequential spectrometer according to ASTM D5708-05 (ASTM, 2005). Sulfur content in crude oils was determined following the ASTM D4294-10 method (ASTM, 2010) by an energy-dispersive X-ray Panalytical spectrometer (Axios model) with a digital signal processor and a dual multi-channel analyzer.

Quantitative extended diamondoid analysis (QEDA) was carried out on the saturated fractions (maltenes) from rock extracts and representative sampled oils (as in Moldowan et al., 2015). QEDA fingerprints were also observed in asphaltene fraction of these oils after hydrous pyrolysis treatment

(as in Summons et al., 2008). Gas chromatography-triple quadrupole mass spectrometry (GC-MS/MS) was used to determine the composition of higher diamondoids (Dahl et al., 1999; Pytlak et al., 2017). Four deuterated internal standards were used to quantify triamantane and extended diamondoids, namely, triamantane-d4 and cyclohexamantane-d8, as well as tetramantane-d6 and pentamantane-d6 for the four-cage (T1, T2, and T3) and five-cage (P1, P2, P3, and P4) non-enantiomorphic isomers (Moldowan et al., 2015).

4. Results

4.1. Source-rock samples

4.1.1. Rock-Eval results

Low PI values (< 0.1; Table 3) suggest that the studied rocks have been negligibly affected by weathering or contamination by well additives or migrated bitumen (Bissada, 1982). Rock-Eval T_{max} data for the Basal Shale, B Limestone, A Limestone, and U Shale samples lie in the 430-435 ºC, 427-439 ºC, 424-431 ºC, and 425-426 ºC ranges, respectively; these values correspond to calculated vitrinite reflectance (%Ro Calc) between 0.49 and 0.74% (Table 3), indicating immature and early mature organic material (Peters, 1986). Calculated %Ro values are similar to measured %Rr data (Table 3). These maturity data can be suggestive of the problems in unravelling the origin of the oil in the Sacha-Shushufindi Corridor (Dashwood and Abbots, 1990; Bernal, 1998): if the Napo reservoirs are in fact sourced from the same stratigraphic group (Mello et al., 1995), a long-distance migration has to be considered, since vitrinite reflectance data represent thermally immature or marginally mature conditions for oil generation in the north-central Oriente Basin according to Baby et al. (2013).

Table 3

Table 3 shows Rock-Eval 2/TOC data and vitrinite reflectance measurements. TOC values for the so-called B Limestone, Basal Shale, U Shale, and A Limestone samples range, respectively, 0.98 to 1.54 wt.%, 2.54 to 4.97 wt.%, 1.23 to 1.66 wt.%, and 2.12 to 3.09 wt.% (with a cut-off of 0.5%). As

for hydrogen index (HI) data (see Table 3), comparable A and B Limestone sub-units show similar values higher than 430 mg HC/g TOC, thus depicting good liquid hydrocarbon generation attributes; while the samples from the very similar U Shale (HI values of 315.1 and 328.8 mg HC/g TOC) and Basal Shale (HI: 340.1-358.7 mg HC/g TOC) facies also have adequate liquid hydrocarbon generation potential (Peters, 1986). This slight variation in HI values, given relatively similar Tmax values as previously discussed, would indicate a moderate heterogeneity in organic matter type in the carbonate-rich (A and B Limestones) versus shaly (U and Basal Shales) rock samples. PI values exceeding 0.1 for several rock samples from the Basal Shale and A Limestone sub-units (Table 3), would indicate that these samples had entered the oil window (Killops and Killops, 2005). In the pseudo-van Krevelen diagram (Fig. 4a), both A and B Limestone samples plot near the type II organic matter line, whereas the U and Basal Shale samples plot in the organic matter type II/III zonation, indicative of shallower marine settings with higher terrestrial contribution (Tissot and Welte, 1984). This differentiation between samples is also observed in the HI versus T_{max} plot (Fig. 4b), which avoids the uncertainty associated with the oxygen index (Peters, 1986; Cornford et al., 1998).

Figure 4

4.1.2. Carbon isotope signatures

The $\delta^{13}C$ values of the rock extracts from core and outcrop samples are within 2.5‰ of each other (see Table 3). $\delta^{13}C$ analyses of A Limestone and B Limestone rock extracts yield negative CV values, suggesting a predominantly marine source. However, in accordance with literature (Mello et al., 1995; Yang et al., 2017), the five remaining rock extracts have negligibly negative or slightly positive CV values, which might reflect a marine source with certain terrestrial contribution (Basal Shale and U Shale sub-units).

4.1.3. Biomarker-based approaches

Organic geochemical analyses of B Limestone, A Limestone, Basal Shale, and U Shale rock

extracts were conducted after artificial maturation (Lijmbach et al., 1983), as they showed low maturities which make oil-source correlation difficult. The *n*-alkane patterns in the extracted outcrop rock samples from the near-isopic B Limestone and A Limestone sub-units (marly intervals interbedded with calcareous shales and argillaceous limestones) are similar: unimodal type with maximum peaks between *n*-C_{16} and *n*-C_{19}, absence of odd-over-even carbon preference, as well as predominance of *n*-C_{17} over Pr and Pr/Ph < 1.1 (see Table 4, Fig. 5a). All this suggests marine precursor organic matter derived mostly from algae (Type II kerogen) deposited in mid-neritic environments under oxygen-depleted bottom water conditions (Hunt, 1996; Peters et al., 2005). By contrast, the U Shale and Basal Shale rock extracts show bimodal *n*-alkane distributions with maximum peaks at *n*-C_{15} to *n*-C_{17} and *n*-C_{27} to *n*-C_{29} with minor odd/even preference, together with Pr/Ph above 1, and predominance of Pr over *n*-C_{17} (Table 4; Fig. 5b). These features tend to occur in organic matter Type II-III or III (Tocco et al., 1995), and thus it can be inferred that U Shale and Basal Shale source rocks were deposited in shallow-water/nearshore settings with notable terrestrial input exposed during sedimentation to low-oxygen bottom water conditions (Hunt, 1996).

Table 4

Figure 5

The Basal Shale and U Shale extracts also present very similar triterpane and sterane distributions (see Table 4, Figs. 6a and 6c). These two rock extracts show biomarker characteristics typical of sedimentary rocks deposited under nearshore siliciclastic depositional paleo-environments: high abundance of diasteranes, regular sterane distribution dominated by C_{29} counterparts and $C_{28} \approx C_{27}$, stair-step progression of C_{31} to C_{35} homohopanes, 30-norhopane/hopane ratios below 0.7, C_{24}/C_{23} cheilanthane ratios above 0.8, and C_{26}/C_{25} cheilanthane ratios below 1 (Tissot and Welte, 1984; Peters et al., 2005; Huang et al., 2015). On the basis of these results, the environment of deposition for the Basal Shale and U Shale sub-units is inferred to be an inner shelf that experienced periodic influx of land-plant debris likely during times of high fresh water runoff (Mello et al., 1995; Yang et al., 2017). However, Basal Shale and U Shale source rocks have distinct triterpane and sterane

compositions compared with those of A Limestone and B Limestone rock samples (Table 4). These latter two subsets of rock samples have similar *m/z* 191 and 217 mass fragmentograms, which are indicative of marine carbonate-rich source facies (Figs. 6b and 6d). Source-based parameters such as C_{26}/C_{25} cheilanthane ratios below 1, abundance of tricyclopolyprenanes, prominence of C_{27} steranes with respect to their C_{28} and C_{29} counterparts, presence of gammacerane and C_{30} steranes, relatively low abundance of diasteranes, and 30-norhopane/hopane ratios around 1 suggest low-oxygen levels and marine moderately hypersaline depositional conditions with restricted water circulation for the last samples (Seifert and Moldowan, 1978; Cassani and Eglinton; 1986; Peters et al., 1995). As described in literature (Mello et al., 1995; Yang et al., 2017), maximum transgressions of the shoreline might indicate marly depositional regimes (i.e. B Limestone and A Limestone sub-units) in middle neritic environments with algal dominated input and a low influx of terrigenous material. The difference between a shaly source facies (Basal Shale and U Shale) versus a marly source facies (A and B Limestone) is also supported by dibenzothiophene-to-phenanthrene (DBT/P) values (clearly below and near one, respectively; Table 4) and methyl-dibenzothiophene patterns of 4 > 2+3 > 1 and 4 > 2+3 < 1, respectively (Hughes, 1984; Hughes et al., 1995).

Figure 6

4.2. Oil samples

4.2.1. Bulk oil geochemistry

The API gravity, total sulfur content, and SARA compositions of the sampled oils are shown in Table 1. An API map for T, U, and Hollín reservoirs is shown in Figure 7a. With the exception of Cononaco oils, where different API values are obtained in the Hollín (averaging 31º) and Napo reservoirs (20.2-21.3º), burial depth is not a control in oil gravity in any other of the study oilfields. Almost all the Lago Agrio, Guanta, Shushuqui, and Tetete oils from the Hollín, Napo, and basal Tena reservoirs exhibit API gravities (29º-31º) and similar compositions: saturate hydrocarbons (SAT) percentages range between 41% and 44%, aromatics (ARO) from 33% to 36%, and polar compounds (POL) from 22% to 24%.

Most oils from the mentioned-above Cretaceous reservoirs in the Shushufindi field exhibit API gravities in the 26-29º range, with SAT, ARO and POL percentages ranging from 38% to 41%, 33% to 36%, and 25% to 28%, respectively. Auca oils from the Napo and Hollín reservoirs have API gravities between 25º and 28º, as well as SAT, ARO and POL percentages of 36-38%, 34-36%, and 27-29%, respectively. As previously mentioned, Cononaco oils from the Hollín interval have API values around 31º and SARA contents comparable to those of the Shushufindi samples (see Table 1), whilst Cononaco oils produced from Napo reservoir have the lowest API gravities (<22º), ARO (< 35%), and SAT (≤ 36%) contents, as well as the highest POL proportions (> 30%) among all the oils under study. Relatively low total sulfur contents (St < 1%) were also found in oil samples from the Lago Agrio, Guanta, Shushuqui, Shushufindi, and Tetete oilfields, all from the northernmost part of the basin. Low-sulfur oils are characterized by St < 1% (Tissot and Welte, 1984). By contrast, oils from southernmost Auca and Cononaco fields show total sulfur contents exceeding 1%.

V/Ni ratios above 2 (see Table 4) suggest that the study oils originated from predominantly marine organic material deposited under oxygen-deprived conditions (Galarraga et al., 2008). When organic matter is deposited under reducing conditions, low concentrations of iron(II) ions lead to nickel(II) ions precipitating in metal sulphides rather than forming metal-organic compounds, and leading to high V/Ni ratios (Lewan, 1984). By contrast, during deposition of siliciclastic facies under more oxidizing conditions, abundantly available iron(II) ions react mainly with sulphide ions, thus forming pyrite, whereas nickel(II) ions form metal-organic compounds, leading to low V/Ni ratios. Despite the fact that V and Ni concentrations can be influenced by post-accumulation processes, it is reported that the V/Ni ratio tends to be unaltered due to the structural similarities of the metal-organic compounds which contain these two metals (Lewan and Maynard, 1982).

4.2.2. Carbon isotope data

Stable carbon isotope compositions of saturated and aromatic fractions of oil samples are compiled in Table 1. Among all the oils, the $\delta^{13}C$ values are very similar, with variations lower than 1.2‰ and standard deviations close to analytical error (0.5‰). Such similar isotopic compositions can indicate that they originated from the same source rock (Peters et al., 2005). As shown in the Sofer diagram (Sofer, 1984; Fig. 7b), all the sampled oils have negative or negligibly positive canonical variables (CV), suggesting a predominant marine input. However, these data must be interpreted with caution as several processes may alter the $\delta^{13}C$ signature (Peters et al., 2005).

Figure 7

4.2.3. Molecular characteristics

The *n*-alkane distributions for all the studied oils are quite similar and typical of predominantly marine precursor organic matter (Peters et al., 2005): *n*-C_{12} to *n*-C_{35} unimodal shaped, with maximum peaks between *n*-C_{17} and *n*-C_{19} (Fig. 8). Also, all of them have an odd over even carbon preference and pristane-to-phytane ratios (Pr/Ph) varying from 0.9 to 1.1 (Table 4), which is consistent with shaly source rocks deposited in a marine to transitional environment under oxygen-depleted conditions (Tissot and Welte, 1984). Although the relative proportions of pristane and phytane are said to be influenced by complex processes (e.g., Dzou et al., 1995), the Pr/Ph ratio is considered here to indicate the depositional environment. Pr/*n*-$C_{17} \geq 0.5$ (see Fig. 8) would suggest that all the oil samples originated from Type II/III kerogen and/or from multiple sources (Hunt, 1996). However, given that *n*-paraffins in early oil charge(s) could have been affected by paleo-biodegradation (Wenger et al., 2002), as discussed below, *n*-alkane-based parameters should be interpreted with caution in the case of these oils.

Figure 8

All the oil samples have similar *m/z* 191 (triterpanes) and *m/z* 217 (steranes) fragmentograms of the saturated fraction (Fig. 9; peak identifications in the Appendix), suggesting that they were generated from the same source(s). Several features common to all studied oils are: relatively abundant tricyclopolyprenanes, Pr/Ph values lower than 2, 18α(H)-22,29,30-trisnorneohopane to 17α(H)-

22,29,30-trisnorhopane ratios (Ts/Tm) lower than one, $C_{31}R/C_{30}$ hopane ratios exceeding 0.3, ratios between C_{26} and C_{25} tricyclopolyprenanes lower than unity, slightly dominance of C_{27} regular steranes over their C_{28} and C_{29} counterparts (see Table 4), and values above 0.5 (see Table 4) for the ratio of C_{29} regular steranes to C_{30} hopane, which can be indicative of predominantly marine algal precursor organic matter (Seifert and Moldowan, 1978; Seifert and Moldowan, 1981). Based on the significant proportion of C_{28} steranes, the age of the source of sampled oils may be post-Jurassic in age (Peters et al., 2005). As for clay versus carbonate saturated-based indicators, on one hand, pristane/phytane ratios around 1.1, C_{29}/C_{30} hopane values < 0.7, notable presence of diasteranes, low abundance of 18β(H)-des-E-hopane or C_{24}-17,21-secohopane, and carbon preference index values higher than unity may suggest that all the samples originated from clay-rich source rocks (Peters et al., 2005; Permanyer et al., 2013). Whilst on the other hand, significant presence of gammacerane and C_{30} steranes, Ph/*n*-C_{18} values > 0.3, similar abundance of pentahomohopanes with respect to their C_{34} homologues, and whole-oil $\delta^{13}C$ values higher than -28‰ (see Table 4 and Fig. 9) would be indicative of carbonate-rich source rocks (Seifert and Moldowan, 1981; Rullkötter et al., 1985; Chung et al., 1992).

Figure 9

When looking at aromatic-based source-related indicators, similar results are obtained: all oils analysed show the usual methylated dibenzothiophene V shape distribution pattern of carbonate-rich facies (Fig. 10a, peak identifications of aromatics are in the Appendix), with the co-eluting 2- and 3-methyl isomers having the lowest abundances (Hughes, 1984). Also, the higher relative abundance of dibenzothiophene and its alkylated homologues (c.a. 57%) compared to unsubstituted and alkyl-dibenzofurans (about 24%) and fluorenes (nearly 19%) supports carbonate facies (Li et al., 2013). By contrast, DBT/P and Pr/Ph ratios below and above 1 (Table 4), respectively, could suggest that the oil samples were derived from marine siliciclastic source rocks (Hughes et al., 1995). High abundance of 1,2,5-trimethylnaphthalene and 1,2,5,6-tetramethylnaphthalene over their respective counterparts in the oils (Figs. 10b and 11a) might be related to land-plant inputs (van

Aarsen and de Leeuw, 1992). Two representative samples from the Cononaco and Shuhufindi fields show differences in the relative abundances of dibenzothiophene and 1,2,5,6-tetramethyl-naphthalene (Figs. 11a and 11c), while they both show an appreciable presence of phenanthrene and similar methylphenanthrene distribution patterns (Figs. 11b and 11d). These can be interpreted as having distinct contributions of the aforementioned source facies types rather than being caused by different in-reservoir alteration processes (Thomson, 1987; Galarraga et al., 2010).

Figure 10

Figure 11

The mentioned-above results could be explained by a scenario requiring a mixture of charges which originated from two organic facies types: a first one reflecting a carbonate-rich deposition in inner to middle neritic environments under very low-oxygen conditions, and a second one representing siliciclastic source-rocks deposited in shallower water (paralic-neritic) settings.

5. Discussion

5.1. Oils from the north-central part of the Sacha-Shushufindi Corridor

5.1.1. Oil-oil and oil-source correlations

A hierarchical cluster analysis on the basis of 12 parameters (Pr/Ph, 29/30H, 31R/30H, diasterane ratio, sterane-to-hopane ratio, V/Ni, 24/23T, 26/25T, Ts/Tm, DBT/P, $\delta^{13}C_{SAT}$ and $\delta^{13}C_{ARO}$) was performed to classify the oil samples into groups. Multivariate statistical analysis was carried out through the centroid method (Márquez et al., 2016). The similarity percentage was used to quantify divergence after obtaining Euclidean distances. Figures 12 and 13 show dendrogram plots including and without Cononaco/Auca oils, respectively. This clustering was performed using the SPSS 22.0 package for Windows.

Figure 12

Figure 13

Oil samples have a notable degree of similarity between them, indicating that they all are genetically similar. Finally, in an attempt to establish the source rock facies of the study oils from the Hollín, Napo T and U intervals, classical biomarker evidence from the set of oil samples was compared to those from B Limestone/A Limestone and Basal Shale/U Shale rock extracts. Taking into account the distribution patterns of triterpanes, methyldibenzothiophenes (4 > 2+3 < 1), regular steranes ($C_{27} > C_{28} > C_{29}$), and *n*-paraffins (with maximum peaks below *n*-C_{20}), it is possible to state that the sampled oils from the northern-central Sacha-Shushufindi Corridor correlate well with carbonate-rich source-rock facies from the B Limestone and A Limestone intervals, rather than with facies from the Basal Shale and U Shale sub-units. These results are also in agreement with previous studies (Mello et al., 1995; Ma et al., 2020), suggesting A Limestone organic-rich layers of the Napo Group as the best horizons for hydrocarbon generation in the western Oriente Basin. Nevertheless, since analysed oils also show carbon preference indices above 1, DBT/P values below 1, and significant abundance of diasteranes, which are not typical from carbonate source rocks, all this makes plausible the scenario of mixed oils deriving from pulses originated from both post-Jurassic siliciclastic and carbonate-rich sources. In such sense, studied classical biomarker features would preclude the possibility that the studied oils have been appreciably sourced from Santiago organic-rich limestones contradicting previous literature (e.g., Dashwood and Abbots, 1990).

5.1.2. Contributions of carbonate and siliciclastic Napo source facies

Since classical biomarker techniques did not give an entirely unambiguous explanation on the precise origin of the petroleum hydrocarbon liquids from the Hollín, Napo T and U reservoirs in the north-central portion of the Sacha-Shushufindi Corridor, definitive identification of source facies types was conducted by higher diamondoid correlations (Moldowan et al., 2015). Extended diamondoid analysis of the two pairs of representative oils corroborated oil-oil correlations obtained from classical biomarker data (Fig. 14a). In order to further prove mixing processes, the asphaltene fractions from two of the characteristic oil samples from Shushufindi and Auca fields were also

subjected to QEDA analyses. QEDA fingerprint from each asphaltene hydrous pyrolysate is plotted together with that from the respective maltene fraction in Figure 14b. It should be noted that the concentrations of eight higher polymantanes relative to triamantane show significant differences between the maltene and asphaltene QEDA fingerprints. This suggests that these fractions are not fully related to each other and serves as a confirmation that the sampled oils have multiple sources.

Figure 14

QEDA fingerprints in maltenes from two representative oil samples (Shushufindi and Cononaco) were compared to rock extracts of B Limestone/A Limestone, Basal Shale/U Shale facies types, and two mixtures of the extracted A Limestone and Basal Shale rocks (the best potential source facies; see Table 3) with volume ratios 2:1 and 1:1, respectively, to simulate what the QEDA graphs of naturally occurring mixtures would look like (Fig. 14a). The B Limestone/A Limestone extracts show high relative abundances of all higher polymantanes when compared to those of U Shale/Basal Shale. This is in agreement with the fact that Type-II/III kerogens yield lower amounts of higher diamondoids than Type-II kerogens at similar maturities (Jiang et al., 2018). As analysed samples plot between 2:1 and 1:1 mixtures, it can be stated that QEDA provides evidence of oil mixing in the Cretaceous reservoirs of northern Oriente Basin, where significant contributions of various petroleum generation horizons (i.e. the carbonate-rich A Limestone and siliciclastic Basal Shale source facies types) form most of the oil samples. Among all the analysed samples, the Cononaco/Auca oils from the central part of the basin appear to have a similar charge history and are the ones depicting a greater contribution from the carbonate-rich source facies type.

5.1.3. Thermal maturation

The different levels of maturity of the study oils were evaluated using several molecular maturity parameters, such as triaromatic cracking and sterane isomerization ratios (Table 5). The sterane isomerization ratios (%20*S* and %ββ) are restricted to maturation levels from the immature stage to a maximum maturity of about 0.8% and peak oil generation (Fig. 15), respectively (Peters et al.,

2005). None of the oil samples reach the respective "equilibrium" values (55% and 70%) for %20*S* and %ββ: most of them (except for those from Cononaco and Auca fields) showed %20*S* and %ββ ratios close to 50% and 60%. This would denote a maturation level equivalent to the onset of the peak oil generation (%Rc_1≈0.75%). Cononaco and Auca oils showed lower %20*S* and %ββ values (45% and 55%, respectively), indicating maturities equivalent to ≈0.65% within the early oil window (Hunt, 1996).

Table 5

Figure 15

The characteristic triaromatic steroid peaks were identified in the *m/z* ion chromatograms for all the oil samples (Fig. 10c). The triaromatic steroid cracking ratio (TA) can be defined as the ratio of C_{20} triaromatic steroid relative abundance to the sum of the values for its C_{20} and C_{28} 20*R* counterparts (Peters et al., 2005). The sampled oils have similar TA values ranging between 0.32 and 0.35, also suggesting maturation levels in the early oil-generative zone (%Rc_2 about 0.66%). Table 5 shows the values for dimethylnaphthalene ratios (DNR-1; Radke et al., 1984). The oils presented DNR-1 values in the 1.8-2.0 range and DNR-1-based calculated vitrinite reflectance data (%Rc_3) below 0.7%, corroborating a maturity level equivalent to the beginning of the oil window. The predominance of 2-ethylnaphthalene over 1-ethylnaphthalene (Fig. 10d), together with the 4-/1-MDBT ratios slightly higher than one (Fig. 10a), would confirm that all the sampled oils have maturity levels near 0.7% at the early oil window (Radke, 1988; Peters et al., 2005).

Table 5 shows the methylphenanthrene index values (MPI-1; Radke et al., 1982; Radke and Welte, 1983) corresponding to all the oil samples. The studied oils showed MPI-1 values ranging from 0.6 to 0.7 and MPI-1-based calculated vitrinite reflectance data (%Rc_4) in the 0.76-0.81% range. These values suggest maturation levels near the peak of the oil-generative window and they are high when compared to the other calculated vitrinite reflectance data. This is in line with literature (Cassani et

al., 1988) indicating that the MPI-1 ratio is not a useful indicator of thermal maturity for oils predominantly derived from marine organic matter at vitrinite reflectance values lower than 0.9%.

5.1.4. Petroleum alteration processes

As it is well-known in literature (e.g., Philp and Mansuy, 1997), several indicators such as API gravity and total sulfur content of oils can be influenced by factors such as source facies type, migration history, and in-reservoir alteration processes. On the basis of SARA compositions (see Table 1), all the analysed oils have apparently undergone no or negligible biodegradation processes, as the ratio of SAT to ARO is always higher than one (Hakimi et al., 2011). Whole oil gas chromatograms of oil samples showed unaltered isoprenoids and comparable C_4-C_9 *n*-alkanes (Figs. 16a and 16b) with respect to C_{10}^+ *n*-paraffins. The notable presence of light hydrocarbons in the oils might denote refreshing of a biodegraded fluid. Toluene/*n*-C_7 and *n*-C_7/methylcyclohexane values in the 0.7-1.1 and 0.5-0.7 ranges for some representative oils suggest that initial stages of evaporative fractionation and negligible-to-slight biodegradation would not have an appreciable influence on observed specific gravities and total sulphur contents (Thomson, 1987). Furthermore, the *n*-C_6/*n*-C_7 and *i*-C_5/*n*-C_5 ratios are higher than unity for most oil samples, except for 20º API gravity Cononaco oils from the Napo T and U intervals which show values below 1 (Figs. 16a and 16b). In addition, the V contents of Cononaco oils from the T/U reservoirs (V> 21.2 ppm) are appreciably different from those from the Hollín unit (V<18.5 ppm). Such latter values are not what might be expected and can be indicative of variability in partial vaporization and subsequent API gravity variations (Welte et al., 1982; Mango, 1997). API values associated with Napo oils from the Cononaco field may be also partially explained by the role of local re-migration (Smith, 1989).

Figure 16

Total ion current (TIC) chromatograms of the saturated fraction of oil samples show non-depleted isoprenoids and a slight loss of C_{10} to C_{20} *n*-alkanes, suggesting the possibility of biodegradation processes despite the negligible or low presence of unresolved complex mixtures (see Fig. 8a). A lack of 25-norhopanes in the *m/z* 191 ion chromatograms (Figs. 9a and 9b; peak identifications are

in the Appendix) leads to discard severe biodegradation. Specific gravity values below 33º API could be explained by the mixture of biodegraded liquid with unaltered charges (Márquez et al., 2016). Given the Oriente Basin history (e.g., Baby et al., 2014), the most likely explanation consists of presuming the existence of different oil pulses: an early oil charge could have been paleo-biodegraded due to meteoric water influx when the reservoirs were shallow in the late Paleogene, and one or more later pulses could show no biodegradation as the reservoirs subsided in the Miocene and became too hot for microbial activity (Smith, 1989; Dashwood and Abbots, 1990). This hypothesis of crude oil mixtures is coherent with two reported event groups of oil generation and expulsion from the Napo/Chonta source rocks to the northwest (Bermejo area) and southwest ("Situche" and "Santiago" regions) of the basin (Bernal, 1998; Hu et al., 2010). This implies early charge(s) of oil that originated during "Early Andean" (latest Cretaceous-early Oligocene) compressional episodes and uplift of the Western Cordillera, whilst late charge(s) took place during "Late Andean" times when basin subsidence occurred in relation to the Neogene tectonic development of the Cordillera Real (Bernal, 1998), and reservoirs would have been buried again.

5.2. Inter-field compositional changes

Based on hierarchical clustering, we can establish two different sampled oil groups (Fig. 12): those from the southernmost Cononaco and Auca fields on one side, and the nearly identical remaining oils on the other. Some scatter occurs in the major oil group, but without enough differentiation to isolate additional subpopulations (Fig. 13). Sampled oils from the northernmost part of the Central Wrench Corridor showed total sulphur contents (St) lower than one, DBT/P < 1, C_{29}/C_{30} hopane values below 0.6, diasterane ratios exceeding 0.5, and Ts/Tm values near 0.5, which are typical of mostly shaly marine sources; while Cononaco/Auca oils can be characterized by DBT/P < 1, St > 1, C_{29}/C_{30} hopane values exceeding 0.6, diasterane ratios below 0.5, and Ts/Tm clearly below 0.5, indicating mixed carbonate-siliciclastic facies (Moldowan et al., 1994; Hughes et al., 1995). It can be also tentatively stated that there are notable similarities between Cononaco/Auca oils and the liquid hydrocarbons (of ~36 ºAPI) from the northern Peruvian Chonta-Vivian petroleum system

produced from the Piuntza-1X (4º6'52''S, 77º47'28''W) and Situche C-2X (3º8'53''S, 77º17'10''W) wells at depths of over 3 km: the latter show V contents about 30 ppm, as well as V/Ni, total sulfur contents and DBT/P values close to 2.9, 1.6% and 0.7, a slight predominance of C_{27} regular steranes, Pr/Ph ranging from 0.9 to 1.0, Ts/Tm below 0.4, Ph/*n*-C_{18} exceeding 0.3, significant presence of gammacerane and similar abundance of penta- and tetra-homohopanes, along with respective $\delta^{13}C$ values for the saturated and aromatic fractions from -27.7‰ to -27.3‰ and -26.8‰ to -26.3‰ (Navarro, 2005).

5.3. Petroleum migration and generation patterns

Analysed oil samples exhibit %20*S* and %ββ results plotting far off the maturation trendline, with %20*S* values around 50% and inferior to %ββ values. This is suggestive of long-range hydrocarbon migration through relatively permeable long distance carrier beds (Seifert and Moldowan, 1981). Very low ratios (< 0.25) of benzo[a]carbazole to benzo[c]carbazole isomers and low abundances of dibenzofurans corroborate long-range migration from oil kitchens to reservoirs (Terken and Frewin, 2000; Li et al., 2011). These features agree with the hypothesis that long-distance secondary hydrocarbon migrations of a few hundreds of kilometers occurred, particularly through the Hollín sandstones, and across the western Oriente Basin (Dashwood and Abbots, 1990; Baby et al., 2013).

Polar (POL), V and Ni contents are highly correlated among themselves (Pearson's coefficients of V-Ni, V-POL, and Ni-POL equal to 0.969, 0.874, and 0.85). This can reflect geochromatography in petroleum migration (Filby, 1994; Escobar et al., 2012) with hydrocarbon fractioning, where the polar fraction interacts with clay minerals (e.g., Waples, 1981). Particularly, the sampled oils from Cononaco and Auca fields showed the highest values of the three parameters (Table 1), which might indicate that these liquid hydrocarbons migrated from the Auca source kitchen area over shorter distances (Bernal, 1998). In general, it is observed that there is a decrease in POL, V and Ni contents from southwest to northeast: this agrees with northeasternward hydrocarbon migration in the central-western Ecuadorian Oriente Basin as described by several authors (e.g., Hu et al., 2010).

Previous 1D geochemical modeling data agree with the assertion of Napo source rocks across the Oriente Basin becoming thermally mature for oil generation during Cenozoic times (Dashwood and Abbots, 1990; Estupiñán et al., 2010a). In more detail, maturation and burial history suggest that in the Auca region, affected by intraplate magmatism (Barragan et al., 2005), i.e. the areas comprising the NW Oriente and SW Putumayo basins, as well as the Huasaga-Bobonaza Deep in the southwestern basin or further south, the Napo source rocks reached the onset of the oil window during pre-Miocene and mid-Miocene times (Bernal, 1998; Estupiñán et al., 2010b; Xie et al., 2010). Later subsidence in the southwest would have caused re-migration and another pulse of oil generation since the end of the Miocene (Hu et al., 2010). Hence "Situche" and "Santiago" regions located almost at the western Peruvian-Ecuadorian border or beyond and, to a much lesser extent, the "Auca" area linked to magmatic activity, were hypothetical source kitchens for oils in Hollin and Napo oilfields within the NNE-SSW corridor in the central part of the basin (Bernal, 1998; Baby et al., 2013), with carbonate-rich intervals as the major source rock. Particularly, the southernmost rock sample was taken from an outcrop near the Santiago Basin and the "Situche" area and has the highest carbonate character, comparable to that reported for the Chonta Formation in Peru (Pardo and Zúñiga, 1978). Lastly, clastic sediments located at the site of the present-time Andes ("Quito" kitchen) were proposed as alternative target source of the Ecuadorian Oriente oils (Feininger, 1975). This latter kitchen might explain in part the difference between oils from the Cononaco/Auca fields and all the other studied oils.

5. Conclusions

Our integrated geochemical study indicates a multiple petroleum charge of Cretaceous reservoirs in the Central Wrench Corridor of the Oriente Basin. Carbon isotopic signature of SARA fractions, biomarker ratios, along with maltene and asphaltene QEDA fingerprints for the sampled oils and distribution patterns of higher polymantanes at rock extracts point out that all the study oils

originated from the same stratigraphic sub-units of the Napo Group, particularly from the most organic-rich Limestone A and Basal Shale. Thus, Cretaceous-sourced oil samples are interpreted as deriving from at least two source facies types: marine carbonate-rich horizons deposited in inner to middle neritic settings with highly dominant algal input; and clay-rich source rock intervals deposited in a shallow to nearshore marine environment with appreciable terrigenous input.

The genetically related sampled oils can be divided into two slightly different subgroups. Classical biomarkers and QEDA suggest that mixed oils in Cretaceous reservoirs of the northern part of the Sacha-Shushufindi Corridor have higher contributions from the clay-rich source facies type in comparison to the Cononaco/Auca oils. More specifically, Cononaco oils from the T and U sandstone intervals might have experienced alteration processes such as partial vaporization and re-migration. This research work has contributed to adding evidence of the migration oil history within the study area. Petroleum accumulation in Cretaceous studied reservoirs might be explained by long-distance migration, in particular from southwestern source kitchen areas through the Hollín sandstones and across the western Oriente Basin.

Declaration of competing interest

The authors declare that they have no known competing financial interests or personal relationships that could have appeared to influence the work reported in this paper

Acknowledgments

Authors are grateful to Professors Galo Montenegro (ESPOL) and Marcos Escobar[†] (LUZ) for his scientific assistance and facilities to the samples. Carlos Boente obtained a post-doctoral contract within the program PAIDI 2020 (Ref 707 DOC 01097), co-financed by the Junta de Andalucía

(Andalusian Government) and the EU. We are also grateful to the two reviewers for their comments which helped to improve the original version of this manuscript.

References

Aspden, J.A., Litherland, M., 1992. The geology and Mesozoic collisional history of the Cordillera Real, Ecuador. Tectonophysics 205, 187–204. doi:10.1016/0040-1951(92)90426-7

Aspden, J.A., McCourt, W.J., Brook, M., 1987. Geometrical control of subduction-related magmatism: the Mesozoic and Cenozoic plutonic history of western Colombia. J. Geol. Soc. London. 144, 893–905. doi:10.1144/gsjgs.144.6.0893

ASTM, 2005. Standard Test Methods for Determination of Nickel, Vanadium, and Iron in Crude Oils and Residual Fuels by Inductively Coupled Plasma (ICP) Atomic Emission Spectrometry. Annual Book of the American Society For Testing Materials Standards, v. 05.03. West Conshohocken, Pennsylvania, ASTM International.

ASTM, 2010. Standard Test Method for Sulfur in Petroleum and Petroleum Products by Energy Dispersive X-ray Fluorescence Spectrometry. Annual Book of the American Society For Testing Materials Standards, v. 05.03. West Conshohocken, Pennsylvania, ASTM International.

Baby, P., Rivadeneira, M., Barragan, R., 2014. La Cuenca Oriente: geología y petróleo, Tercera edición. Institut Français d'Études Andines (IFEA), Petroamazonas EP, Lima, 414 p.

Baby, P., Rivadeneira, M., Barragan, R., Christophoul, F., 2013. Thick-skinned tectonics in the Oriente foreland basin of Ecuador. In: Nemcok, M., Mora, A., Cosgrove, J.W. (Eds.), Thick-skin-

dominated Orogens: from initial inversion to full accretion, vol. 377. Geol. Soc. Lond. Spec. Publ., 59–76.

Baby, P., Rivadeneira, M., Christophoul, F., Barragán, R., 1999. Style and timing of deformation in the Oriente Basin of Ecuador. 4th International Symposium on Andean Geodynamics, Extended Abstract, Gottingen, Germany, pp. 68–72.

Baldock, I.W., 1985. The Northern Andes: a review of the Ecuadorian Pacific Margin. In: Nairn, A.E.M., Stehli, H., Uyeda, E. (Eds.), The Ocean Basins and Margins. Plenum Press, NewYork, 181–218.

Balkwill, H., Rodriguez, G., Paredes, F., Almeida, J., 1995. Northern part of Oriente Basin, Ecuador: reflection seismic expression of structures. In: Tankard, A.J., Suárez, S.R., Welsink H.J. (Eds.), Petroleum Basins of South America, Am. Assoc. Pet. Geol. Memoir 62, 559–572.

Barragán, R., Baby, P., Duncan, R., 2005. Cretaceous alkaline intra-plate magmatism in the Ecuadorian Oriente Basin: Geochemical, geochronological and tectonic evidence. Earth Planet. Sci. Lett. 236, 670–690. doi:10.1016/j.epsl.2005.03.016

Bernal, C., 1998. Modelo teórico de generación y migración de hidrocarburos de la Formación Napo en la Cuenca Oriental del Ecuador. Thesis, Escuela Politécnica Nacional, Quito, 99 p.

Bès de Berc, S., Soula, J.C., Baby, P., Souris, M., Christophoul, F., Rosero, J., 2005. Geomorphic evidence of active deformation and uplift in a modern continental wedge-top-foredeep transition: Example of the eastern Ecuadorian Andes. Tectonophysics 399, 351–380. doi:10.1016/j.tecto.2004.12.030

Bissada, K.K., 1982. Geochemical constraints on petroleum generation and migration. In: Proceedings of the 2nd ASEAN Council on Petroleum (ASCOPE '81), Manila, Philippines, October 7-11, 1981, pp. 69–87.

Boreham, C.J., Crick, I.H., Powell, T.G., 1988. Alternative calibration of the Methylphenanthrene Index against vitrinite reflectance: Application to maturity measurements on oils and sediments. Org. Geochem. 12, 289–294. doi:10.1016/0146-6380(88)90266-5

Brookfield, M.E., Hemmings, D.P., Van Straaten, P., 2009. Paleoenvironments and origin of the sedimentary phosphorites of the Napo Formation (Late Cretaceous, Oriente Basin, Ecuador). J. South Am. Earth Sci. 28, 180–192. doi:10.1016/j.jsames.2009.02.004

Canfield, R.W., Bonilla, G., Robbins, R.K., 1982. Sacha oilfield of Ecuadorian Oriente. Am. Assoc. Pet. Geol. Bull. 66, 1076–1090.

Cassani, F., Eglinton, G., 1986. Organic geochemistry of Venezuelan extra-heavy oils. 1. Pyrolysis of asphaltenes: A technique for the correlation and maturity evaluation of crude oils. Chem. Geol. 56, 167–183. doi:10.1016/0009-2541(86)90001-X

Cassani, F., Gallango, O., Talukdar, S., Vallejos, C., Ehrmann, U., 1988. Methylphenanthrene maturity index of marine source rock extracts and crude oils from the Maracaibo Basin. Org. Geochem. 13, 73–80. doi:10.1016/0146-6380(88)90027-7

Christophoul, F., 1999. Discrimination des influences Tectoniques et Eustatiques dans les bassins liés a des zones de convergence: exemples du Bassin Subandin d'Équateur. Ph.D. thesis, Université Paul Sabatier-Toulouse III, 184 p.

Christophoul, F., Baby, P., Dávila, C., 2002a. Stratigraphic responses to a major tectonic event in a foreland basin: The Ecuadorian Oriente Basin from Eocene to Oligocene times. Tectonophysics 345, 281–298. doi:10.1016/S0040-1951(01)00217-7

Christophoul, F., Baby, P., Soula, J.-C., Rosero, M., Burgos, J., 2002b. Les ensembles fluviatiles néogènes du bassin subandin d'Équateur et implications dynamiques. Comptes Rendus Geosci. 334, 1029–1037. doi:10.1016/s1631-0713(02)01825-4

Chung, H.M., Rooney, M.A., Toon, M.B., Claypool, G.E., 1992. Carbon isotope composition of marine crude oils. Am. Assoc. Pet. Geol. Bull. 76, 1000–1007. doi:10.1306/bdff8952-1718-11d7-8645000102c1865d

Cornford, C., Gardner, P., Burgess, C., 1998. Geochemical truths in large data sets. I: Geochemical screening data. Org. Geochem. 29, 519–530. doi:10.1016/S0146-6380(98)00189-2

Dahl, J.E., Moldowan, J.M., Peters, K.E., Claypool, G.E., Rooney, M.A., Michael, G.E., Mello, M.R., Kohnen, M.L., 1999. Diamondoid hydrocarbons as indicators of natural oil cracking. Nature 399, 54–57. doi:10.1038/19953

Dashwood, M., Abbots, I., 1990. Aspects of the petroleum geology of the Oriente Basin, Ecuador. In: Brooks, J. (Ed.), Classic Petroleum Provinces, Special Publication-Geological Society of London, vol. 50, Blackwell, London, pp. 89–117.

De La Cruz, C., Márquez, N., Escobar, M., Segovia, S., 1997. An improved chromatographic method for the separation of saturated hydrocarbons, aromatic hydrocarbons, resins and asphaltenes

from heavy crude oils. 213th American Chemical Society National Meeting, San Francisco, April 13-17, pp. 416–418.

De Righi, M., Bloomer, G., 1975. Oil and gas developments in the Upper Amazon basin-Colombia, Ecuador and Peru. In: 9th World Petroleum Congress Proceedings, Tokyo, May 1-4, pp. 181–192.

Dzou, L.I., Holba, A.G., Ramón, J.C., Moldowan, J.M., Zinniker, D., 1999. Application of new diterpane biomarkers to source, biodegradation and mixing effects on Central Llanos Basin oils, Colombia. Org. Geochem. 30, 515–534. doi:10.1016/S0146-6380(99)00039-X

Escobar, M., Márquez, G., Azuaje, V., Da Silva, A., Tocco, R., 2012. Use of biomarkers, porphyrins, and trace elements to assess the origin, maturity, biodegradation, and migration of Alturitas oils in Venezuela. Fuel 97, 186–196. doi:10.1016/j.fuel.2012.03.002

Escobar, M., Márquez, G., Suárez-Ruiz, I., Juliao, T.M., Carruyo, G., Martínez, M., 2016. Source-rock potential of the lowest coal seams of the Marcelina Formation at the Paso Diablo mine in the Venezuelan Guasare Basin: Evidence for the correlation of Amana oils with these Paleocene coals. Int. J. Coal Geol. 163, 149–165. doi:10.1016/j.coal.2016.07.003

Espitalié, J., Laporte, J., Madec, M., Marquis, F., Leplat, P., Paulet, J., Boutefeu, A., 1977. Méthode rapide de caractérisation des roches mères, de leur potentiel pétrolier et de leur degré d'évolution. Revue Institut Francais du Pétrole 32, 23–42.

Estupiñán, J., 2005. Control diagenético sobre la calidad de los reservorios de las areniscas "U" y "T" de la Formación Napo del Cretácico de la Cuenca Oriente, Ecuador. Modelización térmica y su

relación con la generación de hidrocarburos. Tesis Doctoral, Universidad Complutense de Madrid, Madrid, 261 p.

Estupiñán, J., Marfil, R., Scherer, M., Permanyer, A., 2010a. Reservoir sandstones of the Cretaceous Napo Formation U and T members in the Oriente Basin, Ecuador: Links between diagenesis and sequence stratigraphy. J. Pet. Geol. 33, 221–245. doi:10.1111/j.1747-5457.2010.00475.x

Estupiñán, J., Permanyer, A., Marfil, R., Barbero, L., 2010b. Burial history and thermal evolution of the Cretaceous Napo Formation in the Oriente Basin of Ecuador. In: World Academy of Science, Engineering and Technology (WASET) Conference, Amsterdam, September 28-29, pp. 1299–1307.

Faucher, B., Vernet, R., Bizon, G., Bizon, J., Grekoff, N., Lys, M., Sigal, J., 1971. Sedimentary formations in Ecuador: A Stratigraphic and micropaleontological survey. Institut Francais du Pétrole, Paris, 220 pp.

Feininger, T., 1975. Origin of petroleum in the Oriente of Ecuador. American Association of Petroleum. Am. Assoc. Pet. Geol. Bull. 59, 1166–1175. doi:10.1306/83d91f4c-16c7-11d7-8645000102c1865d

Feininger, T., Bristow, C.R., 1980. Cretaceous and Paleocene geologic history of coastal Ecuador. Geologische Rundschau 69, 849–874.

Filby, R.H., 1994. Origin and nature of trace element species in crude oils, bitumens and kerogens: Implications for correlation and other geochemical studies.In: Parnell, J. (Ed.), Geofluids: Origin,

migration and evolution of fluids in sedimentary basins, Geological Society Special Publication No. 78, London, pp. 203-218.

Gaibor, J., Hochuli, J.P.A., Winkler, W., Toro, J., 2008. Hydrocarbon source potential of the Santiago Formation, Oriente Basin, SE of Ecuador. J. South Am. Earth Sci. 25, 145–156. doi:10.1016/j.jsames.2007.07.002

Galarraga, F., Reategui, K., Martïnez, A., Martínez, M., Llamas, J.F., Márquez, G., 2008. V/Ni ratio as a parameter in palaeoenvironmental characterisation of nonmature medium-crude oils from several Latin American basins. J. Pet. Sci. Eng. 61, 9–14. doi:10.1016/j.petrol.2007.10.001

Galarraga, F., Urbani, F., Escobar, M., Márquez, G., Martínez, M., Tocco, R., 2010. Main factors controlling the compositional variability of seepage oils from Trujillo State, Western Venezuela. J. Pet. Geol. 33, 255–267. doi:10.1111/j.1747-5457.2010.00477.x

Hakimi, M.H., Abdullah, W.H., Shalaby, M.R., 2011. Organic geochemical characteristics of crude oils from the Masila Basin, eastern Yemen. Org. Geochem. 42, 465–476. doi:10.1016/j.orggeochem.2011.03.015

Higgs, R., 2002. Tide-dominated estuarine facies in the Hollin and Napo (T and U) formations (Cretaceous), Sacha Field, Oriente Basin, Ecuador: Discussion. Am. Assoc. Pet. Geol. Bull. 86, 329–334. doi:10.1306/C9EBCE7D-1735-11D7-8645000102C1865D

Higley, D.K., 2001. The Putumayo-Oriente-Marañon Province of Colombia, Ecuador, and Peru—Mesozoic-Cenozoic and Paleozoic Petroleum Systems. USGS Digit. Data Ser., 40 p.

Hu, Y., Yin, J., Su, Y., Xin, Y., Wang, X., Xiao, G., Yu, Z., Wang, L., 2010. Geochemistry of heavy oil in the T Block, Oriente Basin and its origin mechanism. Acta Geol. Sin. 84, 406–414. doi:10.1111/j.1755-6724.2010.00143.x

Huang, H., Zhang, S., Su, J., 2015. Geochemistry of Tri- and Tetracyclic Terpanes in the Palaeozoic Oils from the Tarim Basin, Northwest China. Energy and Fuels 29, 7014–7025. doi:10.1021/acs.energyfuels.5b01613

Hughes, W.B., 1984. Use of thiophenic organosulphur compounds in characterizing of oils derived from carbonate versus siliciclastic sources. In: Palacas, G. (Ed.), Petroleum geochemistry and source rock potential of carbonate rocks. Am. Assoc. Pet. Geol. Studies in Geology No. 18, pp. 181–196.

Hughes, W.B., Holba, A.G., Dzou, L.I.P., 1995. The ratios of dibenzothiophene to phenanthrene and pristane to phytane as indicators of depositional environment and lithology of petroleum source rocks. Geochim. Cosmochim. Acta 59, 3581–3598. doi:10.1016/0016-7037(95)00225-O

Hunt, J.M., 1996. Petroleum Geochemistry and Geology, 2nd Edition. Freeman and Company, San Francisco, 743 p.

Jaillard, E., 1996. Sedimentary model for the Oriente Basin of Ecuador during the Cretaceous. In: Extended Abstracts of 3rd International Symposium on Andean Geodynamics (ISAG), Saint Malo, September 17-19, pp. 395–398.

Jaillard, E., Bengtson, P., Dhondt, A. V., 2005. Late Cretaceous marine transgressions in Ecuador and northern Peru: A refined stratigraphic framework. J. South Am. Earth Sci. 19, 307–323. doi:10.1016/j.jsames.2005.01.006

Jaillard, E., Soler, P., Carlier, G., Mourier, T., 1990. Geodynamic evolution of the northern and central Andes during early to middle Mesozoic times: A Tethyan model. J. Geol. Soc. London. 147, 1009–1022. doi:10.1144/gsjgs.147.6.1009

Jarvie, D.M., Claxton, B.L., Henk, B., Breyer, J., 2001. Oil and shale gas from the Barnett Shale, Fort Worth basin, Texas. Am. Assoc. Pet. Geol. Annual National Convention, Denver, June 3-6, p. A100.

Jiang, W., Li, Y., Xiong, Y., 2018. The effect of organic matter type on formation and evolution of diamondoids. Mar. Pet. Geol. 89, 714–720. doi:10.1016/j.marpetgeo.2017.11.003

Killops, S.D., Killops, V.J., 2005. Introduction to Organic Geochemistry, 2nd Edition. Wiley-Blackwell Publishing, Oxford, 393 p.

Lebras, M., Megard, F., Dupuy, C., Dostal, J., 1987. Geochemistry and tectonic setting of pre-collision Cretaceous and Paleogene volcanic rocks of Ecuador. Geol. Soc. Am. Bull. 99, 569–578. doi:10.1130/0016-7606(1987)99<569:GATSOP>2.0.CO;2

Lee, G.H., Eissa, M.A., Decker, C.L., Castagna, J.P., O'Meara, D.J., Marín, H.D., 2004. Aspects of the petroleum geology of the Bermejo field, Northwestern Oriente Basin, Ecuador. J. Pet. Geol. 27, 335–356. doi:10.1111/j.1747-5457.2004.tb00062.x

Lewan, M.D., 1984. Factors controlling the proportionality of vanadium to nickel in crude oils. Geochim. Cosmochim. Acta 48, 2231–2238. doi:10.1016/0016-7037(84)90219-9

Lewan, M.D., Maynard, J.B., 1982. Factors controlling enrichment of vanadium and nickel in the bitumen of organic sedimentary rocks. Geochim. Cosmochim. Acta 46, 2547–2560. doi:10.1016/0016-7037(82)90377-5

Li, M.J., Wang, T.G., Yang, F.L., Shi, Y., 2011. Molecular tracers for filling pathway in condensate pools: Alkyldibenzofuran. J. Oil Gas Technol. 33, 6–11.

Li, M., Wang, T., Zhong, N., Zhang, W., Sadik, A., Li, H., 2013. Ternary diagram of fluorenes, dibenzothiophenes and dibenzofurans: Indicating depositional environment of crude oil source rocks. Energy Explor. Exploit. 31, 569–588. doi:10.1260/0144-5987.31.4.569

Lijmbach, G.W.M., van der Veen, F.M., Englehardt, E D., 1983. Geochemical characterization of crude oils and source rocks using field ionization mass spectrometry. In: Bjorøy, M., Albrecht, C., Cornford, C. (Eds.), Advances in Organic Geochemistry, John Wiley and Sons, New York, pp. 788–798.

Ma, Z.Z., Chen, H., Xie, Y., Zhang, Z., Liu, Y., Yang, X., Zhou, Y., Wang, D., 2017. Division and resources evaluation of hydrocarbon plays in Putomayo-Oriente-Maranon Basin, South America. Pet. Explor. Dev. 44, 247–256. doi:10.1016/S1876-3804(17)30027-7

Ma, Z.Z., Tian, Z.T., Zhou, Y.B., Yang, X.F., Tian, Y., 2020. Geochemical characterization and origin of crude oils in the Oriente basin, Ecuador, South America. J. South Am. Earth Sci. 104, 102790. doi:10.1016/j.jsames.2020.102790

Mango, F.D., 1997. The light hydrocarbons in petroleum: A critical review. Org. Geochem. 26, 417–440. doi:10.1016/S0146-6380(97)00031-4

Marksteiner, R., Alemán, A., 1997. Petroleum systems along the fold belt associated to the Marañon-Oriente-Putumayo foreland basin. Memoirs of 6th Bolivarian Symposium: Petroleum Exploration in the Sub-Andean Basins, Cartagena, Colombia, September 14-17, pp. 63–74.

Márquez, G., Escobar, M., Lorenzo, E., Duno, L., Esquinas, N., Gallego, J.R., 2016. Intra- and inter-field compositional changes of oils from the Misoa B4 reservoir in the Ceuta Southeast Area (Lake Maracaibo, Venezuela). Fuel 167, 118–134. doi:10.1016/j.fuel.2015.11.046

Mathalone, J.M.P., Montoya R., M., 1995, Petroleum geology of the Sub-Andean basins of Peru. In: Tankard, A.J., Suárez, S.R., Welsink H.J. (Eds.), Petroleum Basins of South America, Am. Assoc. Pet. Geol. Memoir 62, pp. 423–444.

Mello, M.R., Koutsoukos, E.A.M., Erazo, W.Z., 1995. The Napo Formation, Oriente basin, Ecuador: hydrocarbon source potential and paleo environmental assessment. In: Katz, B.J. (Ed.), Petroleum source rocks, Springer-Verlag, Berlin, pp. 167–181.

Moldowan, J.M., Dahl, J., Zinniker, D., Barbanti, S.M., 2015. Underutilized advanced geochemical technologies for oil and gas exploration and production-1. The diamondoids. J. Pet. Sci. Eng. 126, 87–96. doi:10.1016/j.petrol.2014.11.010

Moldowan, J.M., Peters, K.E., Carlson, R.M.K., Schoell, M., Abu-Ali, M., 1994. Diverse applications of petroleum biomarker maturity parameters. Arab. J. Sci. Eng. 19, 273–298.

Navarro, L., 2005. The Santiago Basin: Structural style and petroleum systems. BSc thesis, San Agustín National University, Arequipa, Peru, 112 p.

Pardo A., Zúñiga F., 1976. Stratigraphy and tectonic evolution of the jungle region of Peru. In: Proceedings of the II Latin American Congress on Geology, Caracas, November 11-16, 1973, pp. 569–608.

Permanyer, A., Márquez, G., Gallego, J.R., 2013. Compositional variability in oils and formation waters from the Ayoluengo and Hontomín fields (Burgos, Spain). Implications for assessing biodegradation and reservoir compartmentalization. Org. Geochem. 54, 125–139. doi:10.1016/j.orggeochem.2012.10.007

Peters, K.E., 1986. Guidelines for evaluating petroleum source rocks using programmed pyrolysis. Am. Assoc. Pet. Geol. Bull. 70, 318–329.

Peters, K.E., Clark, M.E., das Gupta, U., McCaffrey, M.A., Lee, C.Y., 1995. Recognition of an Infracambrian source rock based on biomarkers in the Bagehwala-1 oil, India. Am. Assoc. Pet. Geol. Bull. 79, 1481–1494.

Peters, K., Walters, C.C., Moldowan, J.M., 2005. The Biomarker Guide: Biomarkers and Isotopes in Petroleum Systems and Earth history, 2nd Edition. Cambridge University Press, London, 1132 p.

Pindell, J., Tabbutt, K., 1995. Mesozoic–Cenozoic Andean paleogeography and regional controls on hydrocarbon systems. In: Tankard, A.J., Suárez, R., Welsink, H.J. (Eds.), Petroleum Basins of South America. Am. Assoc. Pet. Geol. Memoir 62, pp. 101–128.

Philp, R.P., Mansuy, L., 1997. Petroleum geochemistry: concepts, applications, and results. Energy and Fuels 11, 749–760. doi:10.1021/ef960174v

Pytlak L., Kowalski A., Gross D., Sachsenhofer R.F., 2017. Composition of diamondoids in oil samples from the alpine foreland basin, Austria: potential as indices of source rock facies, maturity and biodegradation. J. Pet. Geol. 40, 153–171. doi:10.1111/jpg.12670

Radke, M., 1988. Application of aromatic compounds as maturity indicators in source rocks and crude oils. Mar. Pet. Geol. 5, 224–236. doi:10.1016/0264-8172(88)90003-7

Radke, M., Welte, D. H., 1983. The methylphenantrene index (MPI): a maturity parameter based on aromatic hydrocarbons. In: Bjoroy, M., Albrecht, C., Cornford, C., de Groot, K., Eglinton, G., Galimov, E., Leythaeuser, D., Pelet, R., Rullkötter, J., Speers, G. (Eds.), Advances in Organic Geochemistry. John Wiley and Sons, New York, pp. 504-512.

Radke, M., Leythaeuser, D., Teichmüller, M., 1984. Relationship between rank and composition of aromatic hydrocarbons for coals of different origins. Org. Geochem. 6, 423–430. doi:10.1016/0146-6380(84)90065-2

Radke, M., Welte, D.H., Willsch, H., 1982. Geochemical study on a well in the Western Canada Basin: relation of the aromatic distribution pattern to maturity of organic matter. Geochim. Cosmochim. Acta 46, 1–10. doi:10.1016/0016-7037(82)90285-X

Rullkötter, J., Spiro, B., Nissenbaum, A., 1985. Biological marker characteristics of oils and asphalts from carbonate source rocks in a rapidly subsiding graben, Dead Sea, Israel. Geochim. Cosmochim. Acta 49, 1357–1370. doi:10.1016/0016-7037(85)90286-8

Seifert W.K., Moldowan, J.M., 1978. Application of steranes, terpanes and monoaromatic to the maturation, migration and source of crude oils. Geochim. Cosmochim. Acta 42, 77–95.

Seifert, W.K., Moldowan, J.M., 1981. Palaeoreconstruction by biological markers. Geochim. Cosmochim. Acta 45, 783–794.

Sempere, T., 1995. Phanerozoic evolution of Bolivia and adjacent regions. In: Tankard, A.J., Suarez S.R., Welsink, H.J. (Eds.). Petroleum Basins of South America, Am. Assoc. Pet. Geol. Memoir 62, pp. 207–230.

Shanmugam, G., Poffenberger, M., Toro Álava, J., 2000. Tide-dominated estuarine facies in the Hollin and Napo ('T' and "U") formations (Cretaceous), Sacha field, Oriente Basin, Ecuador. Am. Assoc. Pet. Geol. Bull. 84, 652–682. doi:10.1306/c9ebce7d-1735-11d7-8645000102c1865d

Smith, L.R., 1989. Regional variations in formation water salinity, Hollin and Napo Formations (Cretaceous), Oriente Basin, Ecuador. Am. Assoc. Pet. Geol. Bull. 73, 757–776. doi:10.1306/44b4a258-170a-11d7-8645000102c1865d

Sofer, Z., 1984. Stable Carbon Isotope composition of crude oils: application to source depositional environments and petroleum alteration. Am. Assoc. Pet. Geol. Bull. 68, 31–49. doi:10.1306/ad460963-16f7-11d7-8645000102c1865d

Summons, R.E., Hope, J.M., Swart, R., Walter, M.R., 2008. Origin of Nama Basin bitumen seeps: Petroleum derived from a Permian lacustrine source rock traversing southwestern Gondwana. Org. Geochem. 39, 589–607. doi:10.1016/j.orggeochem.2007.12.002

Terken, J.M.J., Frewin, N.L., 2000. The Dhahaban petroleum system of Oman. Am. Assoc. Pet. Geol. Bull. 84, 523–544. doi:10.1306/c9ebce41-1735-11d7-8645000102c1865d

Thompson, K.F.M., 1987. Fractionated aromatic petroleums and the generation of gas-condensates. Org. Geochem. 11, 573–590. doi:10.1016/0146-6380(87)90011-8

Tissot, B.P., Welte, D.H., 1984. Petroleum Formation and Occurrence, 2nd Edition. Springer-Verlag, New York, 699 p. doi:10.1007/978-3-642-87813-8

Tocco, R., Escobar, M., Ruggiero, A., Galarraga, F., 1995. Geochemistry of seep oils and rock samples of the early Tertiary section from the Northandean Flank of the Venezuelan Los Andes. Org. Geochem. 23, 311–327. doi:10.1016/0146-6380(95)00013-5

Tschopp, H.J., 1953. Oil explorations in the Oriente of Ecuador, 1938-50. Am. Assoc. Pet. Geol. Bull. 37, 2303–2347. doi:10.1306/5ceadd94-16bb-11d7-8645000102c1865d

Vallejo, C., Hochuli, P.A., Winkler, W., von Salis, K., 2002. Palynological and sequence stratigraphic analysis of the Napo Group in the Pungarayacu 30 well, Sub-Andean Zone, Ecuador. Cretac. Res. 23, 845–859. doi:10.1006/cres.2002.1028

van Aarssen, B.G.K., de Leeuw, J.W., 1992. High-molecular-mass substances in resinites as possible precursors of specific hydrocarbons in fossil fuels. Org. Geochem. 19, 315–326. doi:10.1016/0146-6380(92)90002-F

Waples, D.W., 1981. Organic geochemistry for exploration geologist. Burges Publishing Company, Minneapolis, 151 p.

Welte, D.H., Kratochvil, H., Rullkötter, J., Ladwein, H., Schaefer, R.G., 1982. Organic geochemistry of crude oils from the Vienna Basin and an assessment of their origin. Chem. Geol. 35, 33–68. doi:10.1016/0009-2541(82)90018-3

Wenger, L.M., Davis, C.L., Isaksen, G.H., 2002. Multiple controls on petroleum biodegradation and impact on oil quality. SPE Reserv. Eval. Eng. 5, 375–383. doi:10.2118/80168-PA

White, H., Skopec, R., Ramirez, F., Rodas, J., Bonilla, G., 1995. Reservoir characteristics of the Hollin and Napo formations, western Oriente Basin, Ecuador. In: Tankard, A.J., Suarez S.R., Welsink, H.J. (Eds.). Petroleum Basins of South America, Am. Assoc. Pet. Geol. Memoir 62, pp. 573–596.

Xie, Y., Cheng, J., Su, Y., Hu, Y., 2010. Petroleum geology and exploration potential of Oriente-Marañon Basin. Pet. Explor. Dev. 37, 51–56. doi:10.1016/S1876-3804(10)60014-6

Yang, X.F., Xie, Y.F., Zhang, Z.W., Ma, Z.Z., Zhou, Y.B., Liu, Y.M., Wang, D.D., Zhao, Y.B., 2017. Hydrocarbon generation potential and depositional environment of shales in the Cretaceous Napo Formation, Eastern Oriente Basin, Ecuador. J. Pet. Geol. 40, 173–193. doi:10.1111/jpg.12671

Figure 1: a) Map showing the situation of oil fields, sampled rock outcroppings, and boreholes in the Oriente Basin. From left to right, Cordillera Real, Subandean Zone, Central Wrench Corridor, and Eastern Inverted System can be distinguished (modified from Baby et al., 1999); b) Schematic cross-section across the central-western part of the basin (after Dashwood and Abbots, 1990) to illustrate the rock sampling strategy (see profile line in Fig. 1a).

Figure 2: Generalized stratigraphic section in the Oriente Basin (adapted from Estupiñán, 2005). Note: source rocks (black circle) and reservoir rocks (black square).

Figure 3: Map representing the rock units (Napo Group and Basal Tena Member) that outcrop in the sampling location at Pungarayacu area and the types of contacts among them.

Figure 4: a) and b), respectively, Pseudo-Van Krevelen diagram and plot of HI against Tmax for rock samples.

Figure 5: a) and b), respectively, representative *m/z* 99 ion chromatograms for the saturate fractions of A Limestone/B Limestone and Basal Shale/U Shale source facies types.

Figure 6: Examples of *m/z* 191 (a and b, respectively) and *m/z* 217 ion chromatograms (c and d, respectively) showing triterpane and sterane distributions for the saturate fractions of representative rock extracts from the A Limestone/B Limestone and Basal Shale/U Shale sub-units.

Figure 7: a) Map showing average API gravity values for oils produced from the study fields in the Central Wrench Corridor; b) Sofer isotopes diagram for the aromatic and saturate fractions of representative oils and rock extracts.

Figure 8: a), b), and c), respectively, example of total ion chromatogram (CON-30 oil) and *m/z* 99 ion chromatograms showing characteristic *n*-paraffin and isoprenoid signals for representative CON-27 and SSF-046 oil samples.

Figure 9: Examples of *m/z* 191 ion chromatograms (a and b) and *m/z* 217 ion chromatograms (c and d) showing triterpane and sterane distributions for the saturate fractions of representative SSF-046 and CON-27 oil samples, respectively.

Figure 10: a), b), c), and d), respectively, *m/z* 198, *m/z* 170, *m/z* 231, and *m/z* 156 ion chromatograms showing methylated dibenzothiophene isomers, as well as trimethylnaphthalene, triaromatic steroid, and dimethylnaphthalene series for the aromatic fraction of a characteristic (GTA-10) oil sample.

Figure 11: *m/z* 184 ion chromatograms (a and c) and *m/z* 178+192 ion chromatograms (b and d), showing tetramethylnaphthalene and phenanthrene series for the aromatic fractions of representative SSF-046 and CON-27 oil samples, respectively.

Figure 12: Dendrogram showing the results of clustering (Ward´s method) and allowing separation into two oil groups.

Figure 13: Dendrogram showing the results of cluster analysis after excluding Auca and Cononaco oil samples.

Figure 14: a) QEDA analysis of four selected oils (continuous lines) and extract mixtures (dotted lines) obtained from B Limestone and Basal Shale facies types confirming oil-oil and oil-source correlations; b) fingerprints of higher diamondoids by QEDA for two representative oils and hydropyrolysates (dashed lines) generated from asphaltenes.

Figure 15: Plot of %20*S* versus %ββ sterane ratios showing the level of thermal maturity of sampled oils.

Figure 16: Whole-oil gas chromatograms (a and b, respectively) and light hydrocarbon fingerprints from *n*-C_5 to *n*-C_9 for representative CON-27 and SSF-046 oil samples from the U reservoir. Abbreviations: DCM (dichloromethane solvent), MCH (methylcyclohexane), and Tol (toluene).

Appendix: Main saturated and aromatic biomarkers identified in the fragmentograms.

Figure 1

Click here to access/download;Figure;Figure 1.tif

Figure 2

Click here to access/download;Figure;Figure 2.tif

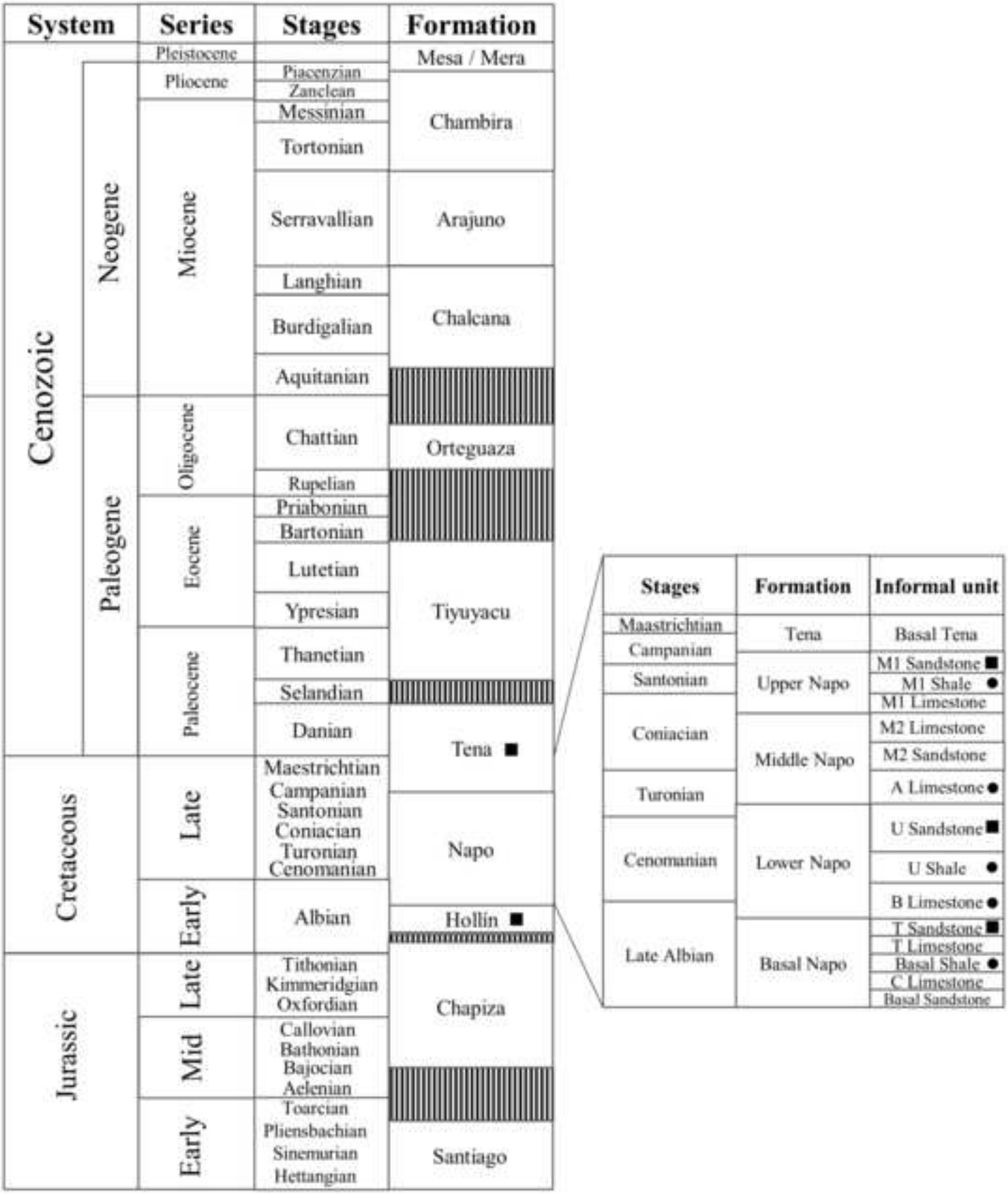

Figure 3

Click here to access/download;Figure;Figure 3.tif

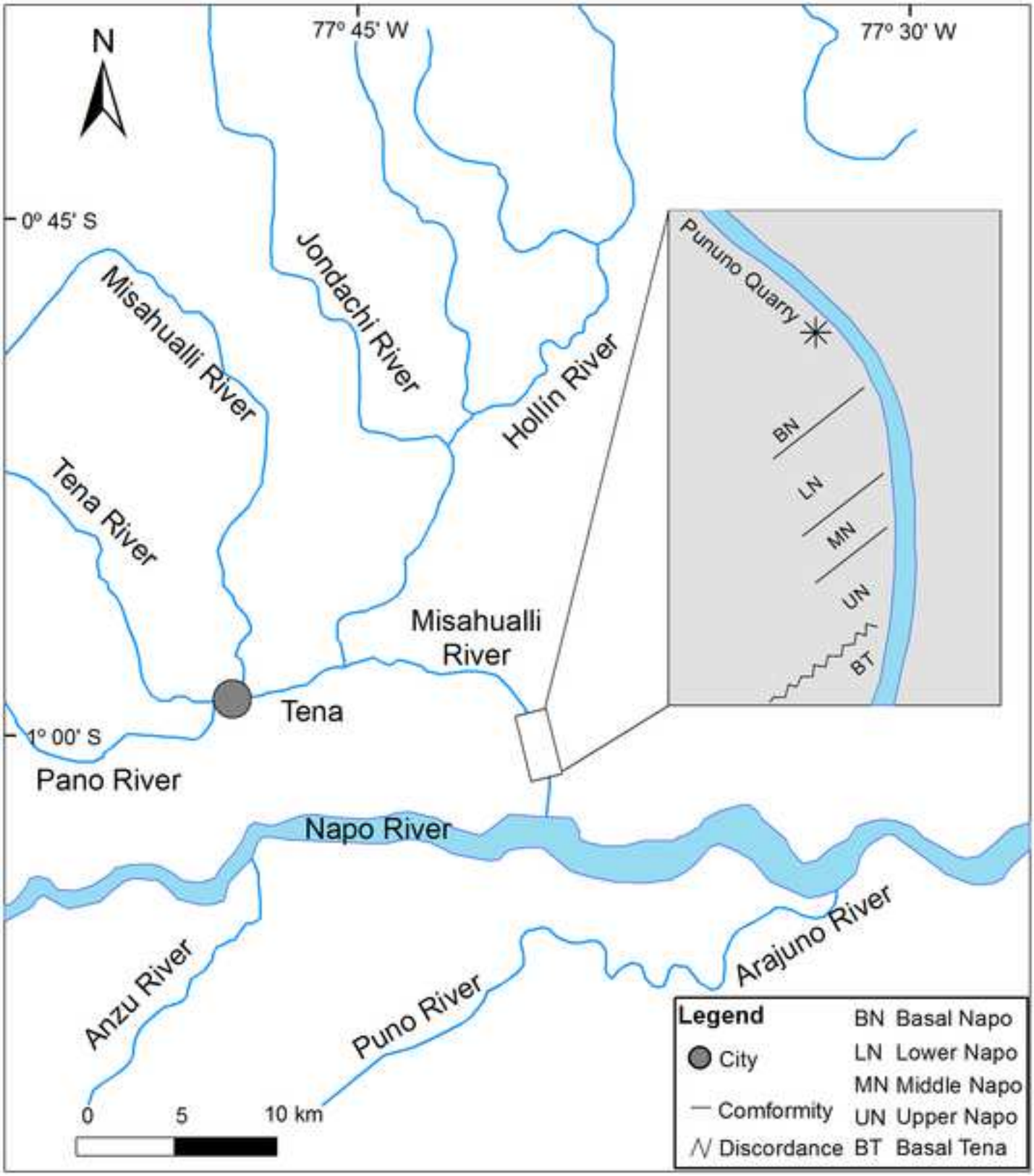

Figure 4

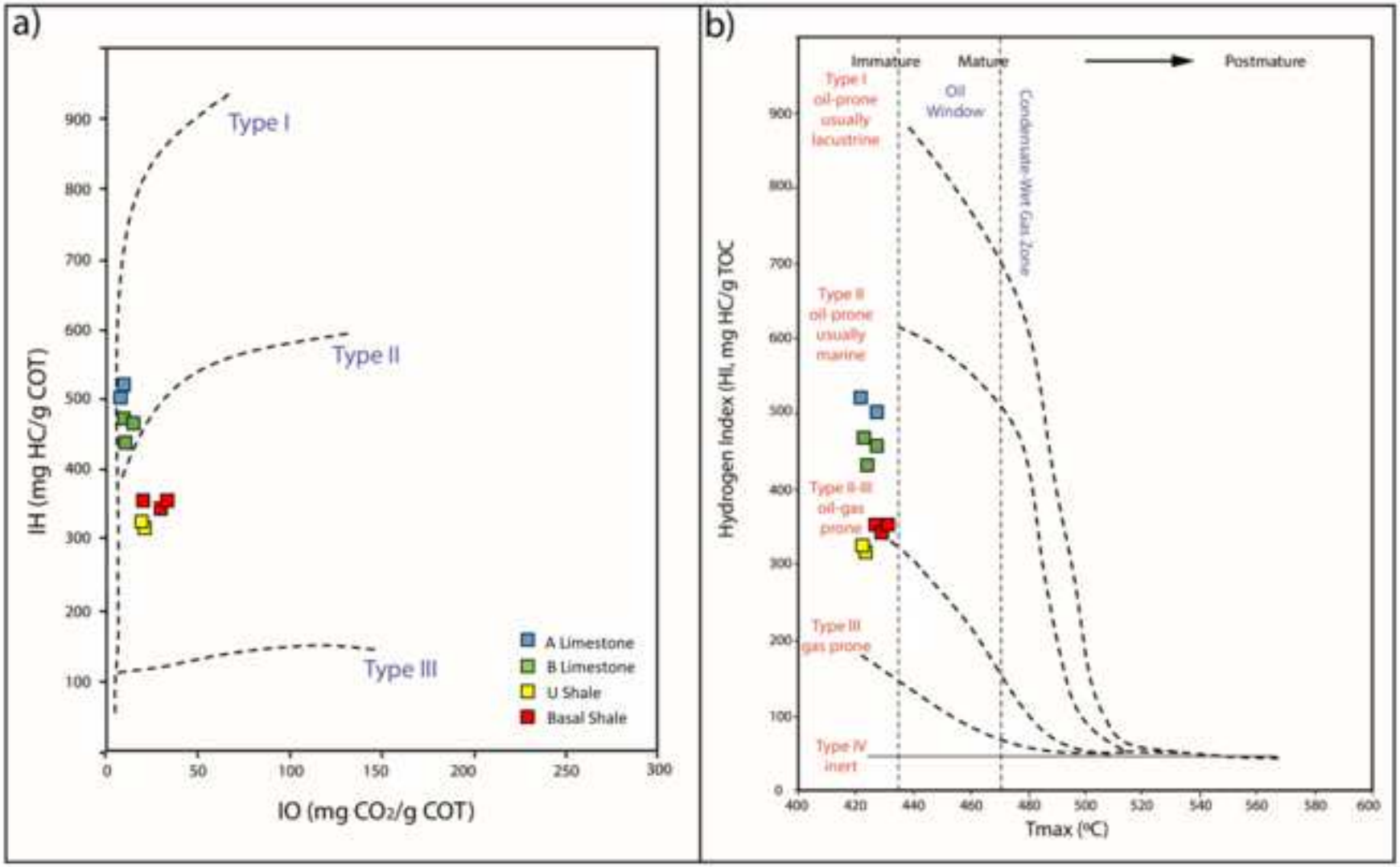

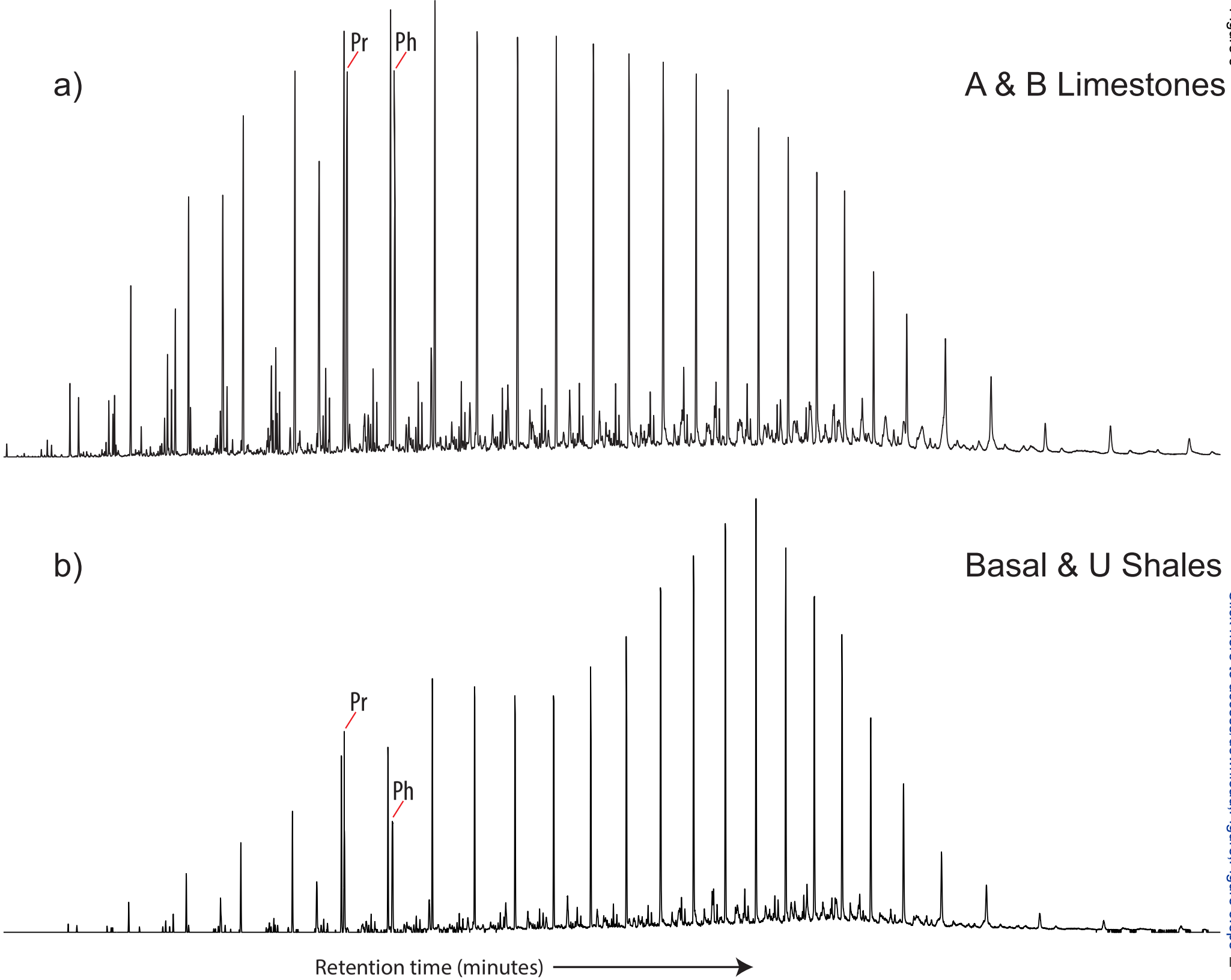

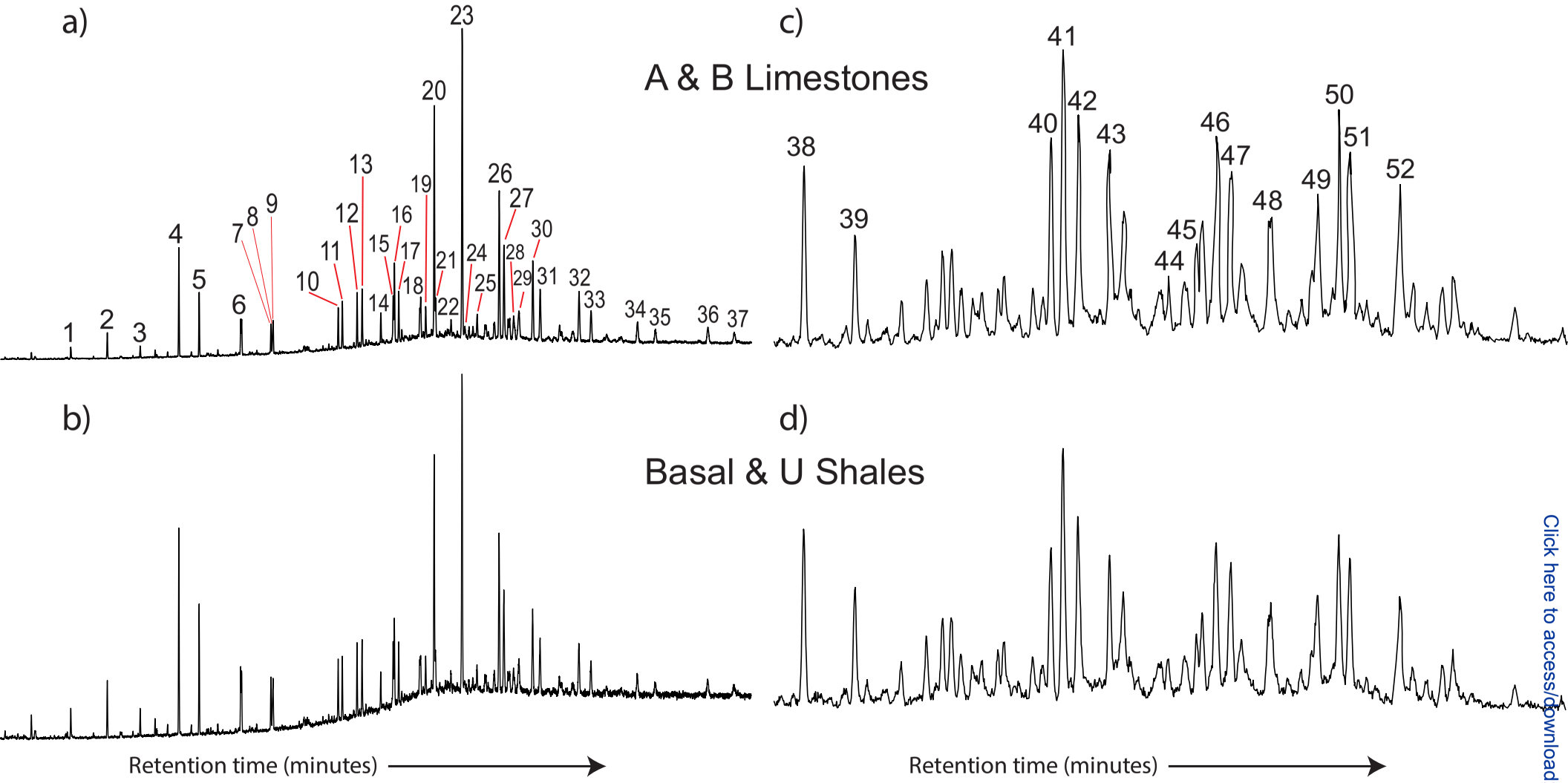

Figure 7

Click here to access/download;Figure;Figure 7.tif

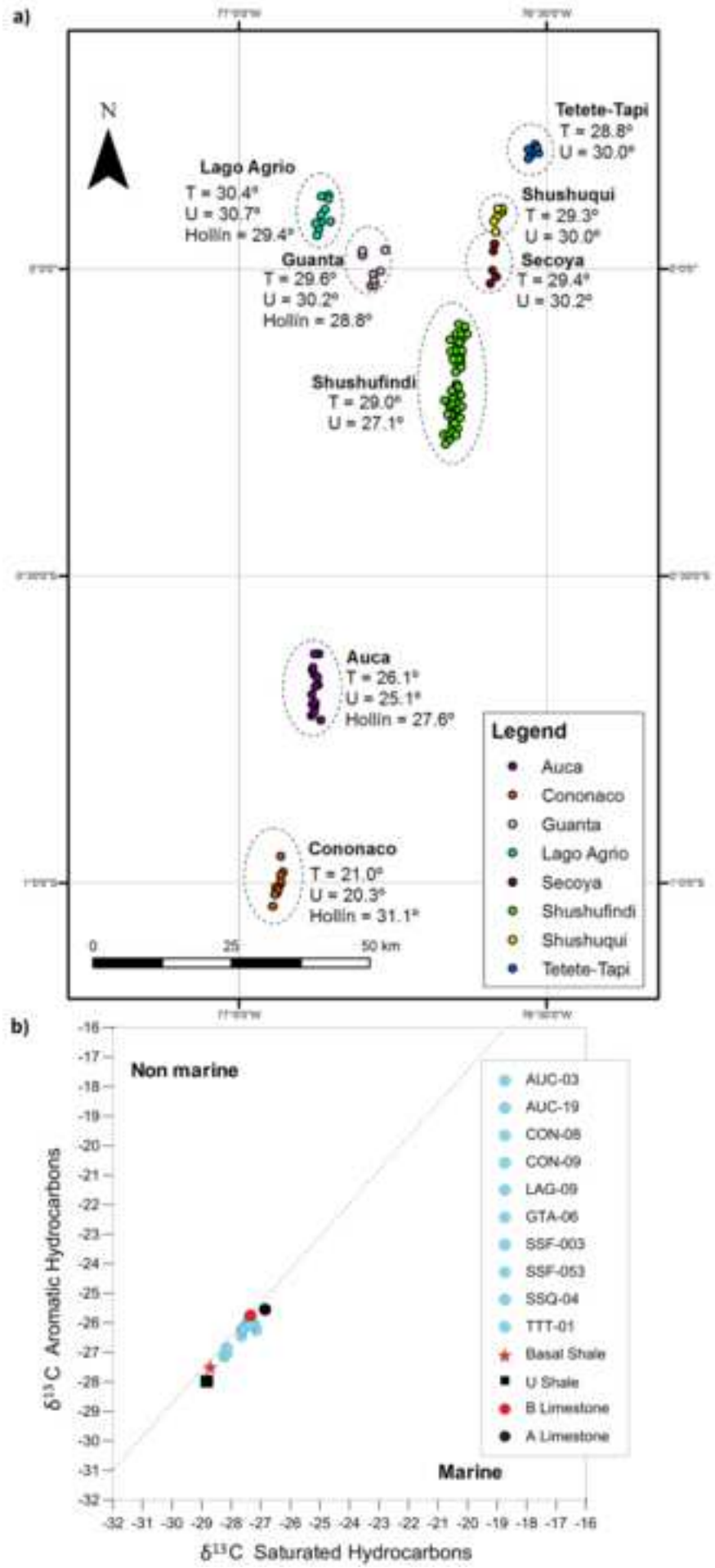

Figure 8

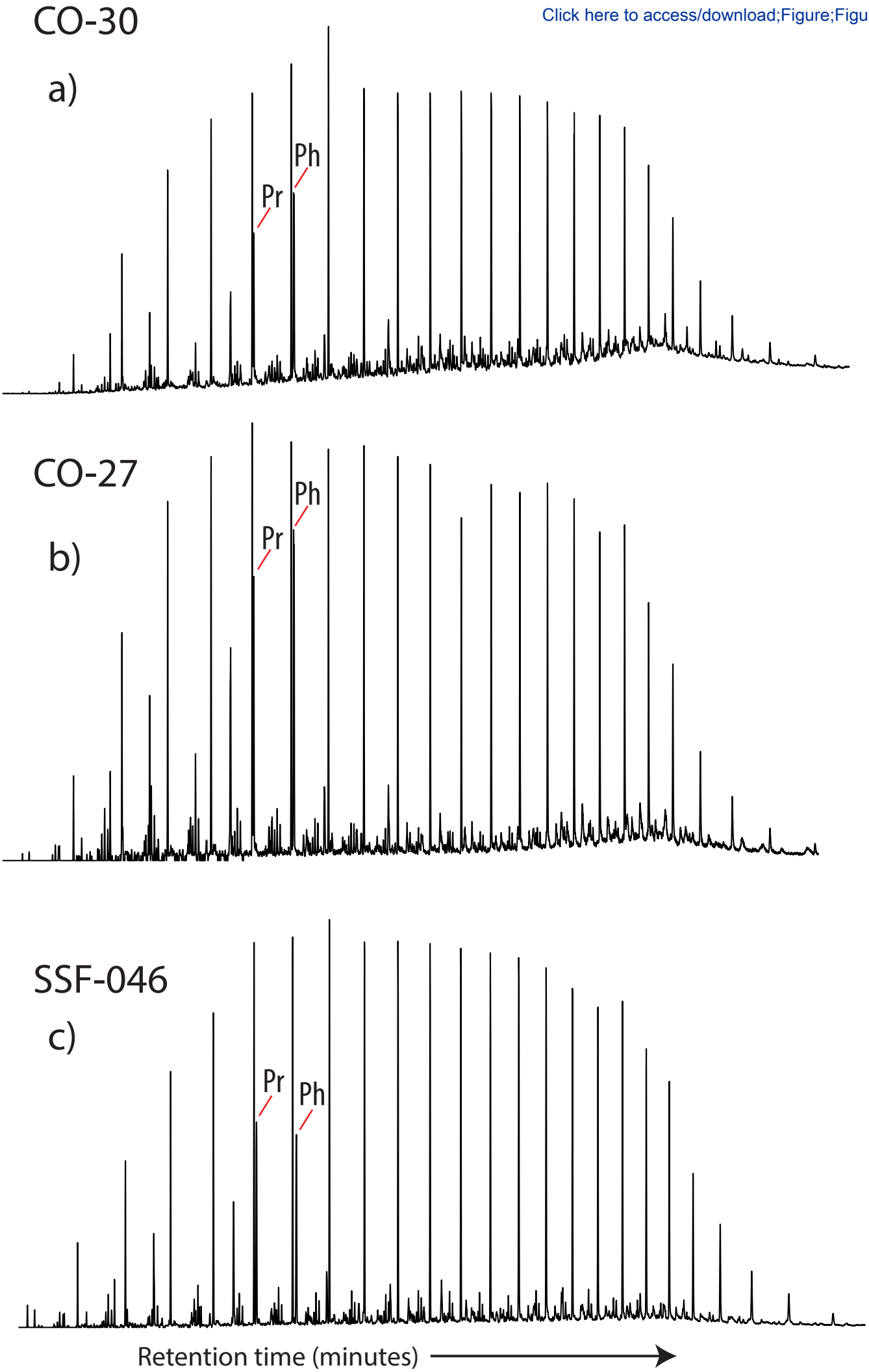

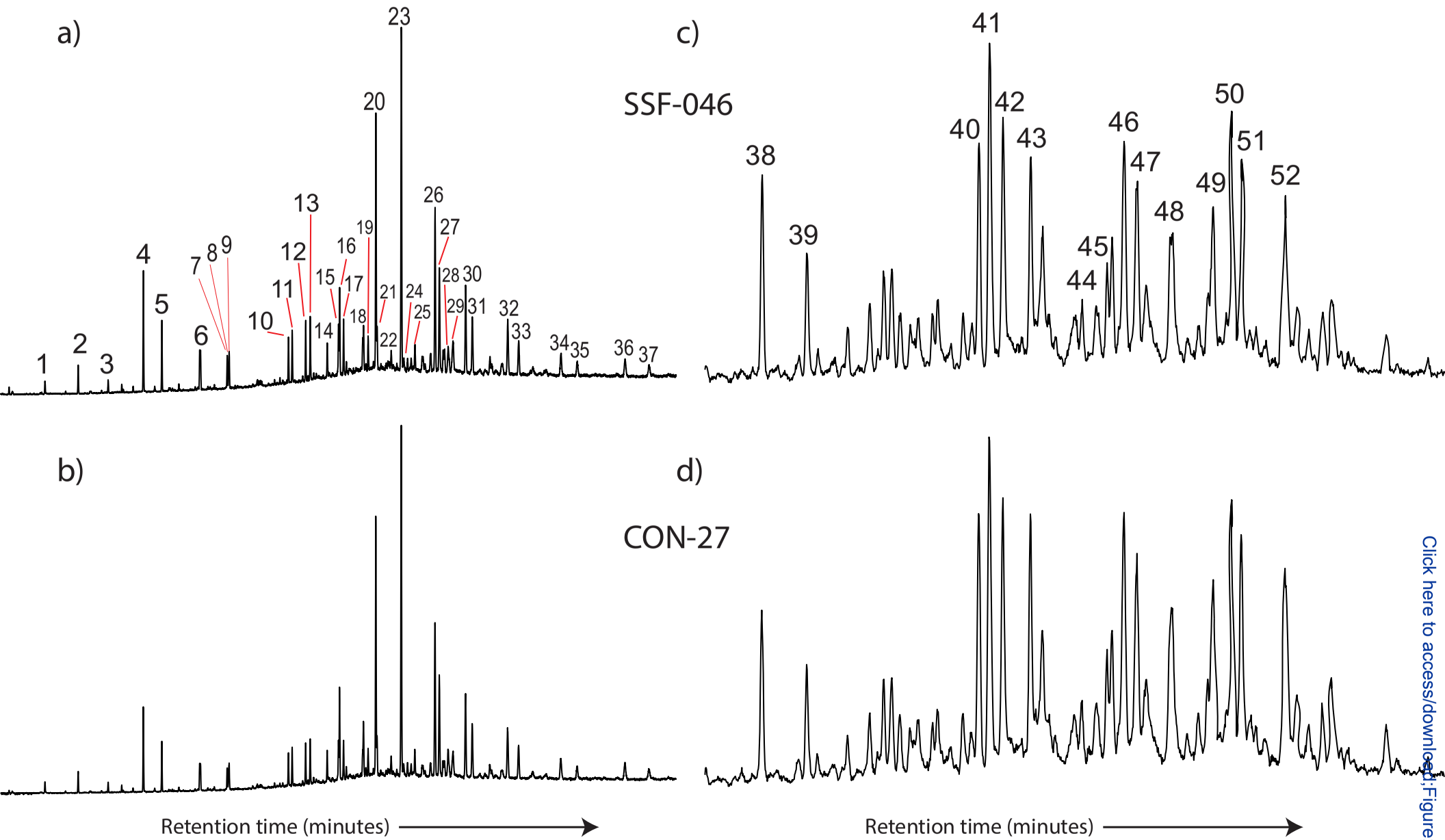

Figure 9

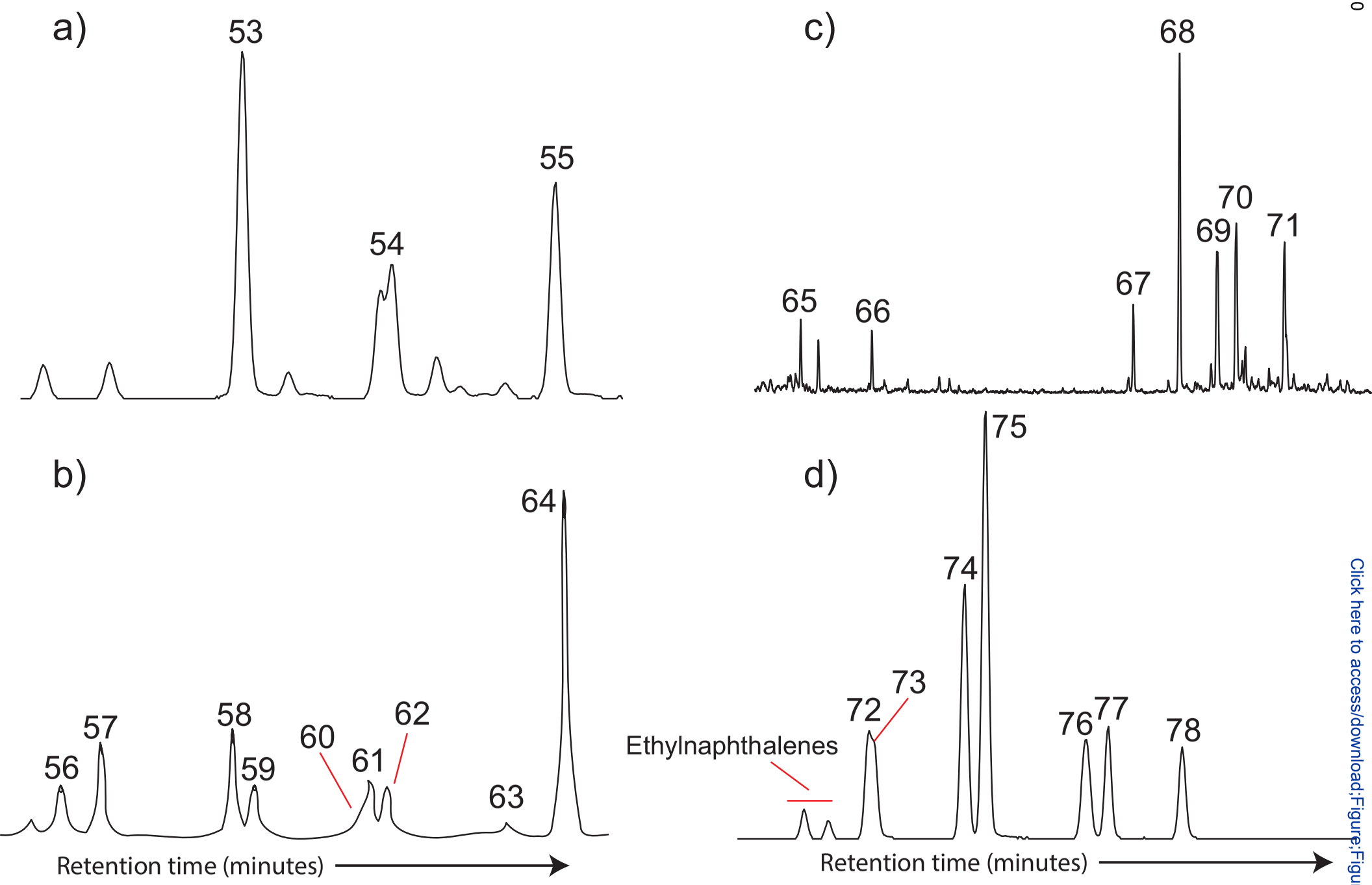

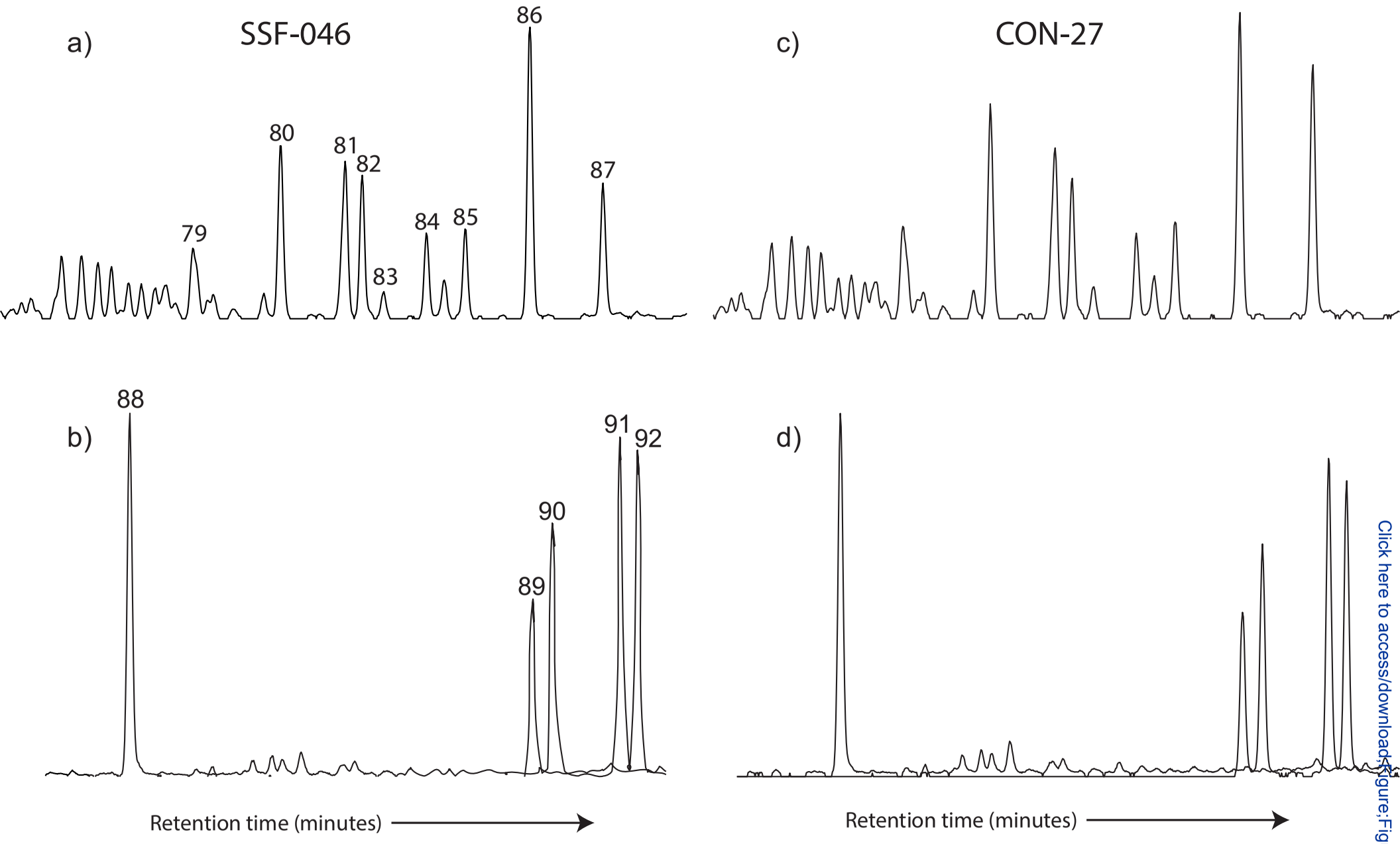

Figure 12

Click here to access/download;Figure;Figure 12.tif

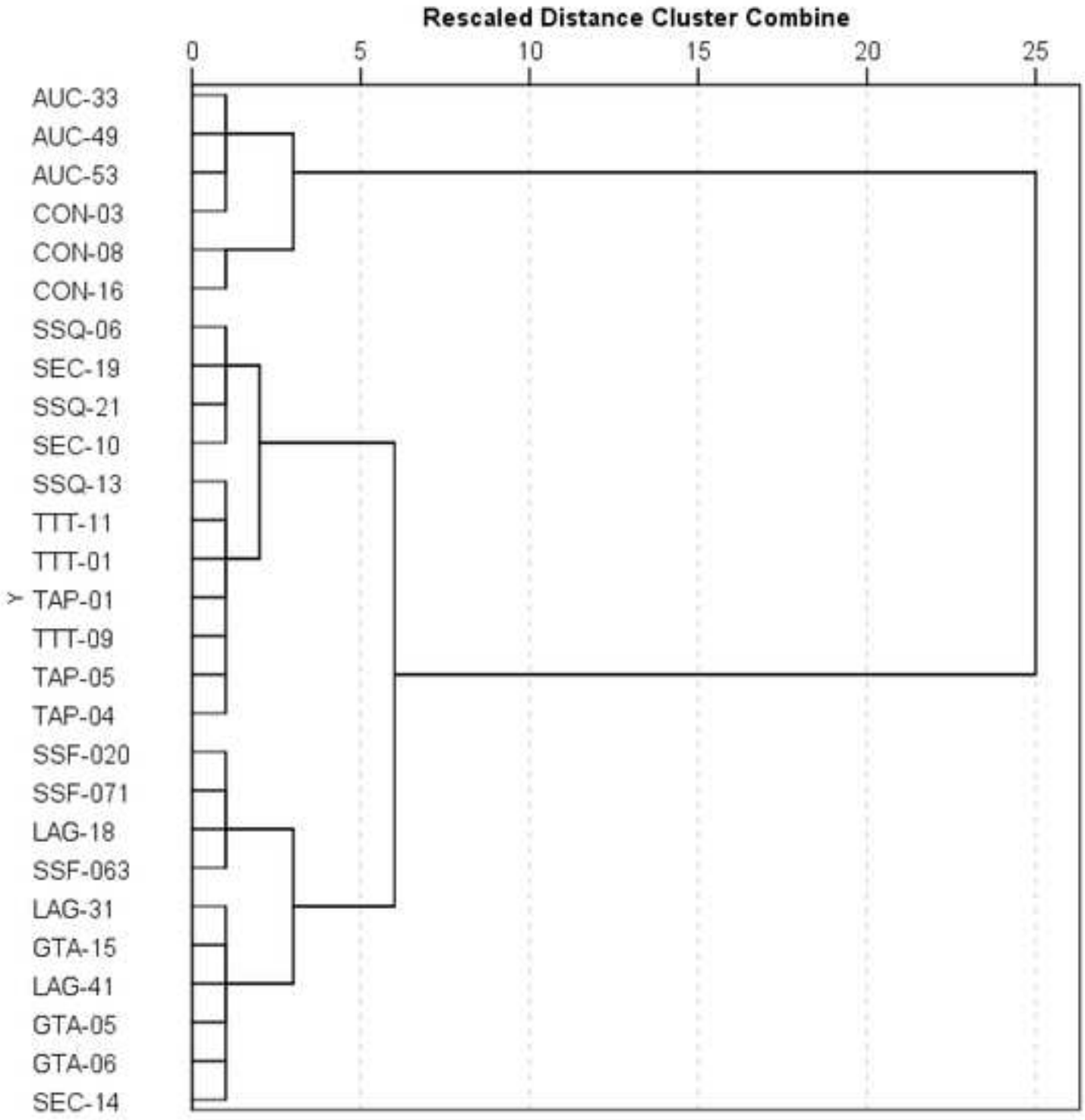

Figure 13

Click here to access/download;Figure;Figure 13.tif

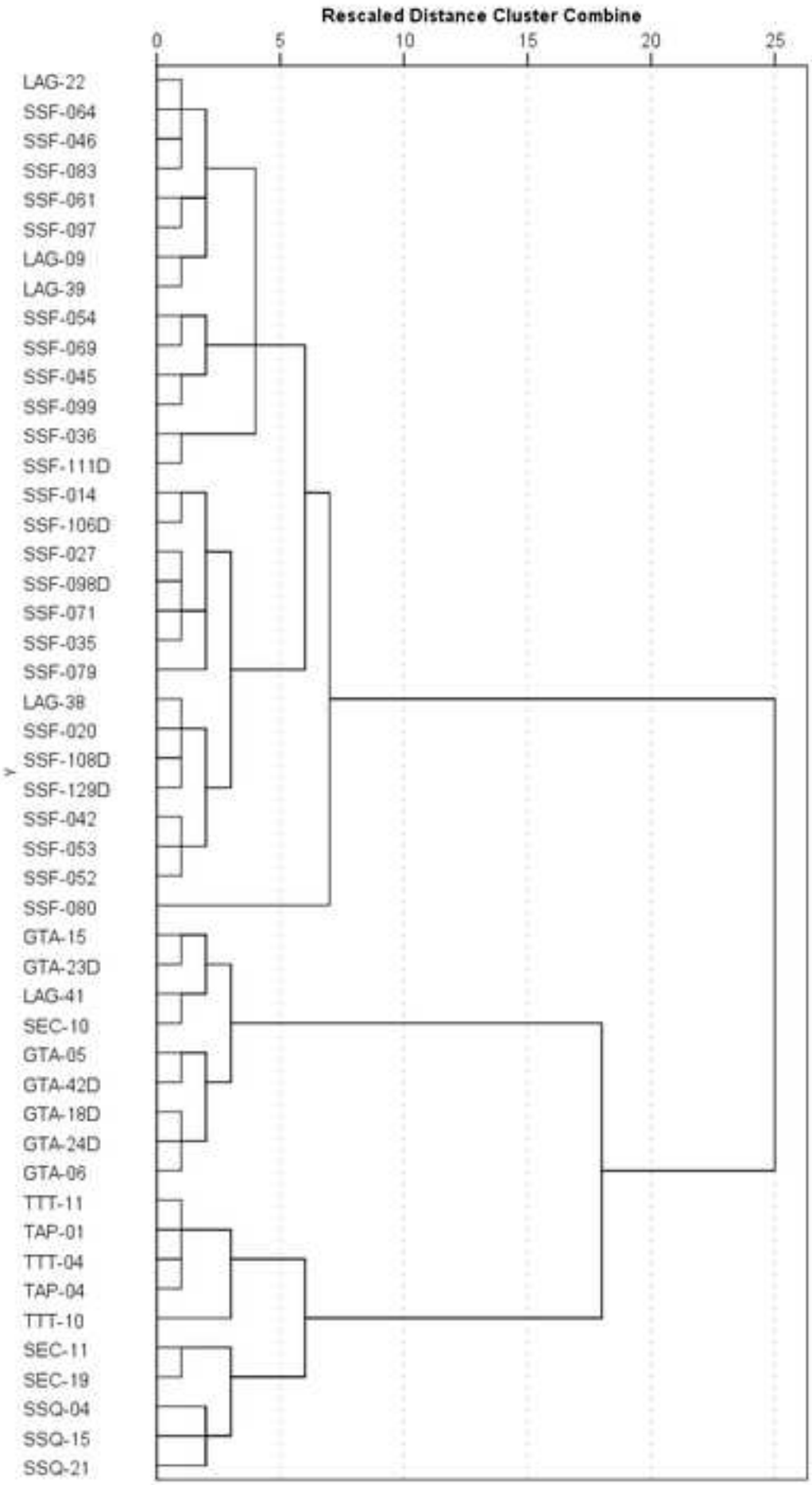

Figure 14

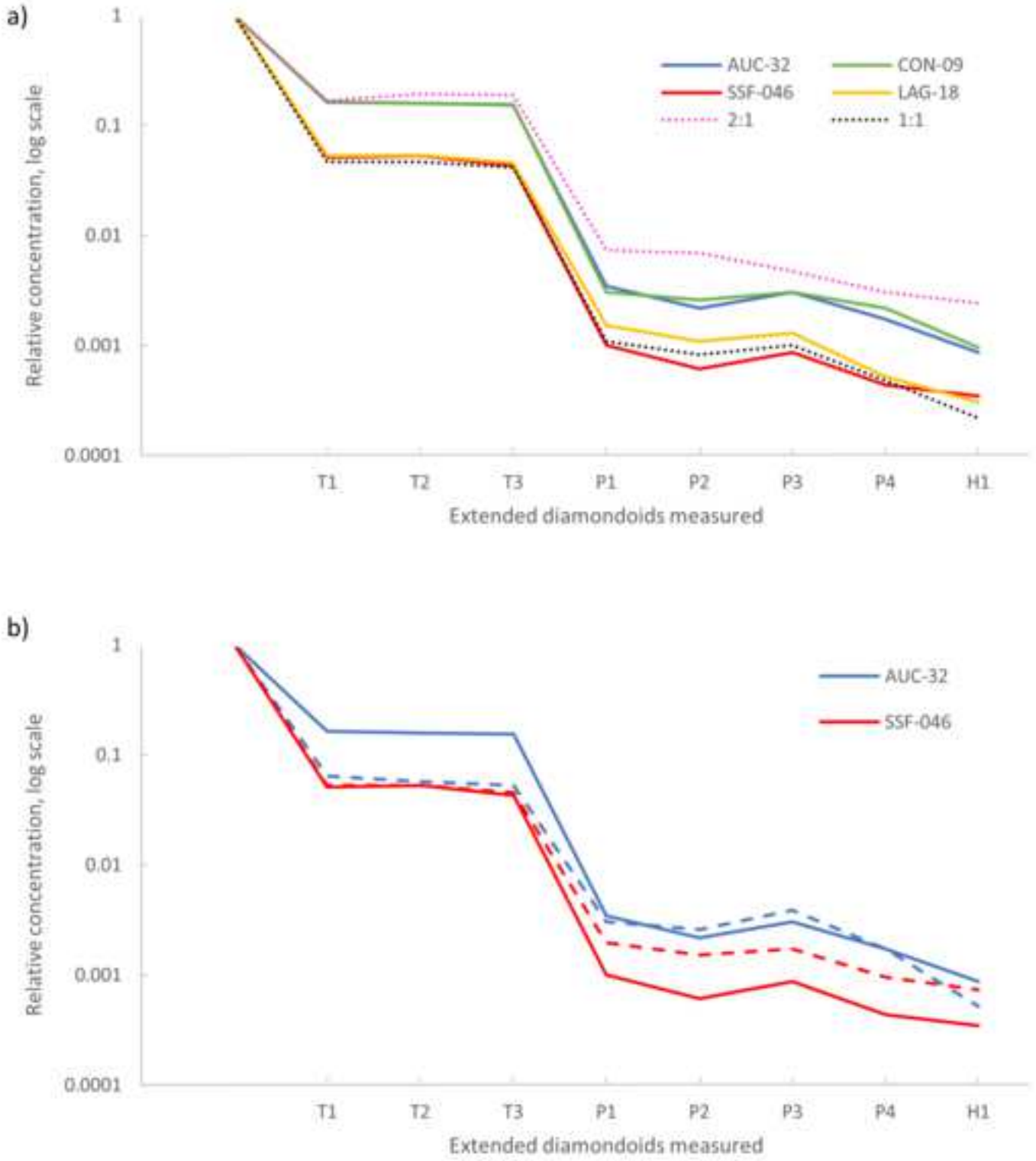

Figure 15

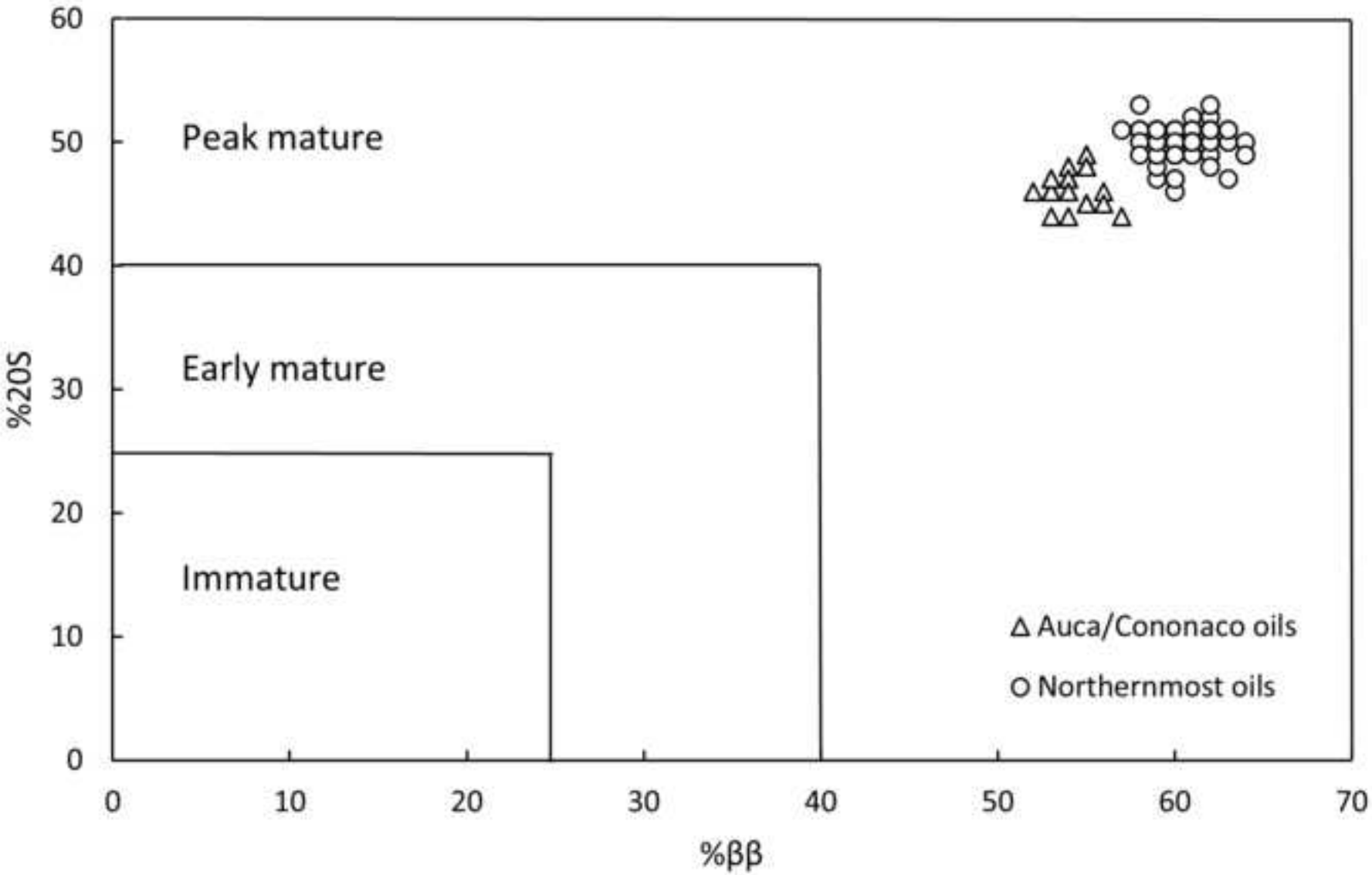

Figure 16

Click here to access/download;Figure;Figure 16.tif

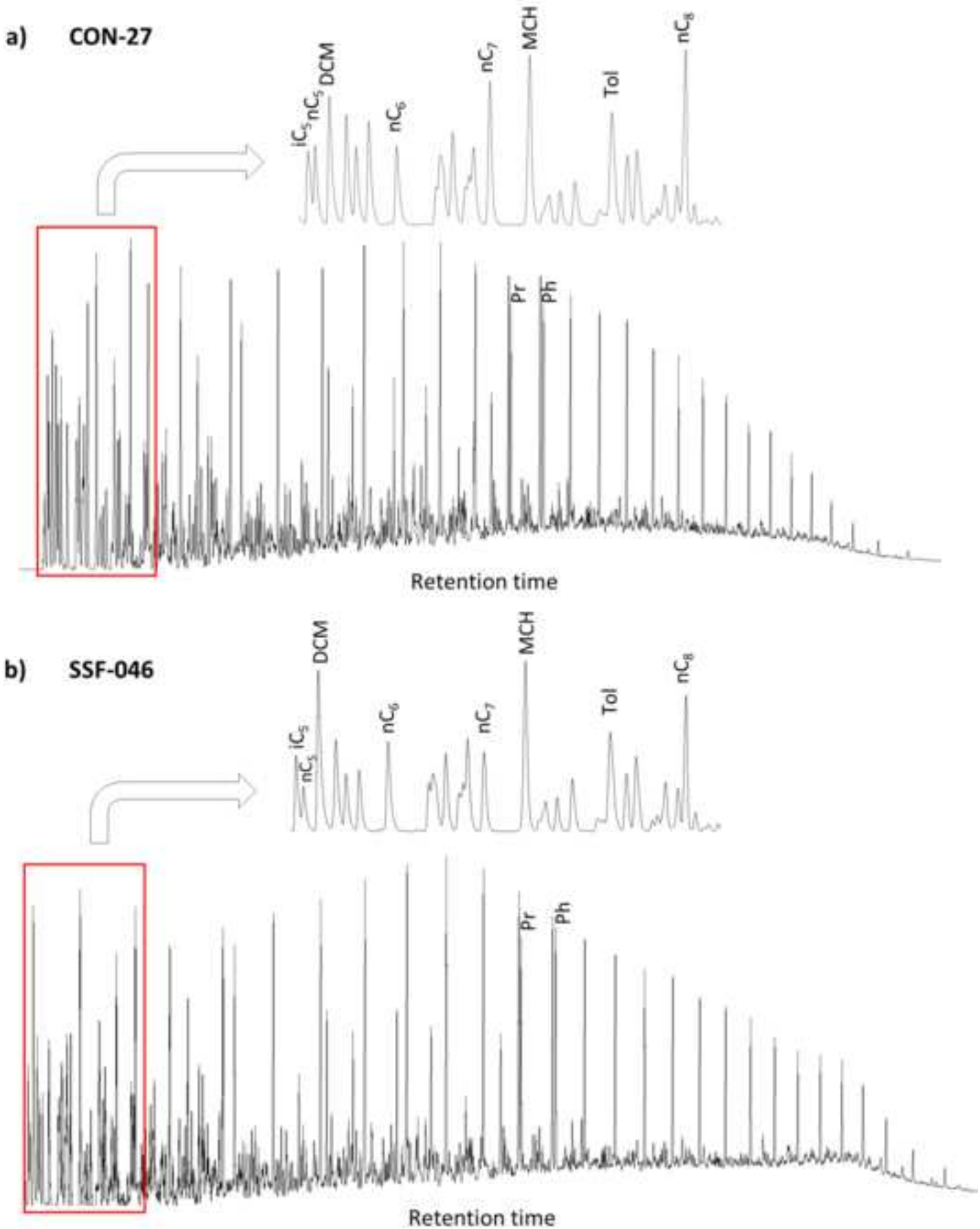

Table 1: List of wells studied; API gravities, SARA fractionating, $\delta^{13}C$ (‰) in SARA fractions, Ni concentration (ppm), V/Ni, and sulfur content (wt.%) for sampled oils

Well	Depth (m)	Latitude	Longitude	Reservoir	ºAPI	V	V/Ni	St	SAT	ARO	POL	$\delta^{13}C_{ARO}$	$\delta^{13}C_{SAT}$
AUC-03	3264	00º43’44”S	76º52’57”W	U	25.2	15.3	2.16	1.20	37	35	28	-26.0	-27.4
AUC-19	3060	00º40’41”S	76º52’20”W	T	26.4	15.9	2.22	1.13	37	36	27	-26.5	-27.6
AUC-31	3119	00º39’14’’S	76º52’53’’W	U	25.0	16.1	2.34	1.09	37	35	28	-26.3	-27.5
AUC-32	3118	00º39’42”S	76º52’42”W	Hollín	27.1	14.7	2.67	1.12	38	35	27	-26.2	-27.3
AUC-33	3156	00º39’57”S	76º52’23”W	T	25.8	14.8	3.12	1.15	37	35	28	-26.8	-27.5
AUC-34	3135	00º38’60”S	76º52’46”W	Hollín	27.9	15.6	2.30	1.12	37	36	27	-26.1	-27.4
AUC-35	3121	00º42’36”S	76º52’36”W	T	26.2	16.0	2.73	1.01	38	34	28	-26.6	-27.3
AUC-36	3128	00º42’46”S	76º52’37”W	Hollín	27.8	15.8	2.13	1.11	37	35	28	-26.3	-27.2
AUC-38	3138	00º37’42’’S	76º52’15’’W	Hollín	28.0	15.7	2.26	1.06	38	35	27	-26.4	-27.4
AUC-39	3165	00º37’42’’S	76º52’40’’W	Hollín	27.5	16.3	2.67	1.08	37	35	28	-26.5	-27.3
AUC-43	3146	00’41’39’’S	76º52’54’’W	U	24.9	14.9	2.81	1.08	38	34	28	-26.3	-27.5
AUC-49	3133	00º43’42’’S	76º52’54’’W	T	26.0	16.5	3.08	1.02	37	36	27	-26.9	-27.5
AUC-50	3137	00º42’38’’S	76º52’51’’W	Lower U	25.3	15.9	2.37	1.03	36	36	28	-26.4	-27.6
AUC-53	3138	00º40’49’’S	76º52’34’’W	Hollín	28.1	16.2	2.55	1.04	38	34	28	-26.8	-27.8
AUC-57D	3056	00º42’26”S	76º52’36”W	T	26.2	15.1	2.42	1.17	37	35	28	-26.2	-27.5
AUC-59D	3048	00º42’26”S	76º52’36”W	T	26.3	15.0	2.76	1.10	37	36	27	-26.1	-27.2
AUC-73D	2991	00º37’42”S	76º52’40”W	U	24.8	15.4	2.63	1.20	36	36	28	-26.4	-27.6
AUC-74	3134	00º44’10”S	76º52’05”W	Hollín	27.7	15.3	2.54	1.05	38	34	28	-26.6	-27.4
AUC-99	3103	00º43’21”S	76º52’42”W	T	26.1	15.2	2.45	1.14	38	35	27	-26.5	-27.5
CON-03	3180	01º00’27”S	76º56’27”W	Hollín	31.2	18.4	3.01	1.04	36	35	29	-26.9	-27.9
CON-08	3168	01º00’09”S	76º55’56”W	Hollín	30.7	18.0	2.34	1.07	37	35	28	-27.2	-28.2
CON-09	3202	01º01’03”S	76º56’22”W	U	20.2	22.2	2.56	1.29	36	33	31	-27.1	-28.1
CON-13	3261	00º58’59”S	76º55’42”W	Hollín	30.8	17.8	2.41	1.05	37	34	29	-27.0	-28.0
CON-14	3219	00º59’17”S	76º55’55”W	T	20.9	21.5	2.70	1.20	35	34	31	-26.8	-27.8
CON-16	3197	00º59’51”S	76º55’55”W	T	21.1	21.7	2.18	1.18	36	34	30	-27.0	-28.0
CON-18	3175	01º00’47”S	76º56’13”W	Hollín	31.0	18.2	2.29	1.08	36	36	28	-27.2	-28.2
CON-23	3210	01º01’12”S	76º56’31”W	T	21.3	21.9	2.62	1.21	36	34	30	-27.3	-28.3
CON-27	3198	01º02’20”S	76º56’45”W	T	20.6	21.4	2.94	1.27	35	34	31	-27.0	-28.0
CON-30D	3209	00º59’17”S	76º55’55”W	Hollín	31.5	17.6	2.80	1.03	36	35	29	-27.1	-28.1
CON-36D	3114	00º59’17”S	76º55’55”W	T	21.2	21.1	2.58	1.19	36	33	31	-26.8	-27.8
CON-46D	3105	00º57’28”S	76º55’55”W	Upper U	20.4	21.6	2.23	1.26	35	34	31	-26.7	-27.7
CON-48D	3203	00º57’28”S	76º55’55”W	T	21.0	21.3	2.17	1.22	36	34	30	-26.9	-27.9
LAG-09	3171	00º04’31”N	76º52’03”W	T	30.4	7.5	2.47	0.68	41	36	23	-26.3	-27.6

Well	Depth (m)	Latitude	Longitude	Reservoir	°API	V	V/Ni	St	SAT	ARO	POL	$\delta^{13}C_{ARO}$	$\delta^{13}C_{SAT}$
LAG-11	3201	00º05'45"N	76º51'39"W	Hollín	28.9	7.9	2.28	0.71	42	34	24	-26.4	-27.7
LAG-18	3190	00º07'10"N	76º51'15"W	Hollín	29.6	7.4	2.58	0.77	41	34	25	-26.2	-27.5
LAG-22	2875	00º03'53"N	76º52'13"W	Tena	30.2	7.3	2.71	0.93	41	36	23	-26.3	-27.6
LAG-31	2870	00º07'03"N	76º51'58"W	Tena	30.5	7.8	2.96	0.78	43	35	22	-26.6	-27.8
LAG-38	3098	00º05'13"N	76º52'00"W	U	30.3	7.9	2.41	0.65	42	35	23	-26.1	-27.5
LAG-39	3183	00º04'25"N	76º52'32"W	Hollín	29.5	7.7	2.69	0.78	41	36	23	-26.5	-27.8
LAG-40D	3192	00º06'46"N	76º51'19"W	Hollín	29.3	7.9	2.35	0.72	42	35	23	-26.3	-27.6
LAG-41	3180	00º03'14"N	76º52'25"W	Hollín	29.6	7.6	2.61	0.76	43	34	23	-26.9	-28.2
LAG-50	3178	00º04'37"N	76º51'05"W	Hollín	29.1	7.5	2.21	0.80	41	36	23	-26.8	-28.0
GTA-04	3048	00º00'17"S	76º46'13"W	T	29.5	7.8	2.69	0.92	42	35	23	-27.1	-28.2
GTA-05	2717	00º01'47"N	76º45'47"W	Tena	31.1	7.4	2.54	0.59	43	33	24	-26.9	-28.1
GTA-06	3060	00º01'42"S	76º47'07"W	U	29.7	7.2	2.42	0.86	43	33	24	-26.6	-27.9
GTA-10	3078	00º01'15"N	76º47'58"W	U	30.7	7.3	2.31	0.80	44	34	22	-27.2	-28.1
GTA-11	3034	00º01'42"N	76º47'58"W	U	30.1	7.0	3.19	0.82	42	35	23	-27.1	-28.0
GTA-15	3069	00º01'35"S	76º46'45"W	Hollín	28.6	7.3	2.73	0.94	41	35	24	-27.0	-27.9
GTA-17D	2951	00º00'34"S	76º46'55"W	Lower U	30.0	7.1	2.50	0.85	42	34	24	-26.7	-27.8
GTA-18D	2959	00º01'10"S	76º46'50"W	Lower U	30.2	7.8	2.46	0.86	42	34	24	-26.8	-28.1
GTA-20D	3027	00º01'10"S	76º46'50"W	T	30.2	7.5	2.31	0.91	41	35	24	-26.9	-27.7
GTA-23D	3080	00º00'34"S	76º46'55"W	Hollín	28.9	7.3	3.00	0.92	41	35	24	-27.1	-28.0
GTA-24D	2952	00º00'34"S	76º46'55"W	Lower U	30.3	7.6	2.29	0.84	43	35	22	-27.1	-28.1
GTA-40D	2958	00º01'10"S	76º46'50"W	Lower U	30.5	7.5	2.89	0.89	43	35	22	-27.2	-27.7
GTA-41D	2710	00º01'10"S	76º46'50"W	Tena	31.3	7.7	2.48	0.52	44	34	22	-26.9	-28.2
GTA-42D	3026	00º01'10"S	76º46'50"W	T	29.7	7.6	2.15	0.88	42	35	23	-26.8	-28.3
SSF-002	2894	00º14'37"S	76º38'25"W	U	26.7	8.4	2.40	0.93	39	36	25	-26.3	-27.1
SSF-003	2842	00º07'36"S	76º38'44"W	T	28.8	8.0	2.59	0.74	40	34	26	-26.2	-27.5
SSF-014	2853	00º09'09"S	76º38'19"W	T	29.0	8.5	3.08	0.67	39	35	26	-26.2	-27.3
SSF-017	2890	00º12'55"S	76º39'57"W	T	29.5	8.7	2.53	0.75	38	36	26	-26.5	-27.6
SSF-020	2866	00º13'30"S	76º39'28"W	Upper U	26.9	8.4	2.39	0.91	40	35	25	-26.1	-27.2
SSF-024	2907	00º16'45"S	76º39'29"W	T	29.6	8.3	2.24	0.75	38	36	26	-26.3	-27.5
SSF-026	2879	00º16'13"S	76º38'57"W	T	29.3	7.9	2.60	0.68	39	35	26	-26.6	-27.1
SSF-027	2926	00º16'13"S	76º40'03"W	U	27.1	8.6	2.69	0.99	39	36	25	-26.4	-27.0
SSF-035	2932	00º17'11"S	76º39'51"W	U	27.5	8.6	2.84	0.98	38	36	26	-26.5	-27.1
SSF-036	2854	00º08'34"S	76º38'54"W	U	27.3	8.2	2.96	0.90	39	35	26	-26.5	-27.5
SSF-042	2841	00º12'22"S	76º38'50"W	T	28.9	7.8	2.41	0.72	39	35	26	-26.1	-27.5

Well	Depth (m)	Latitude	Longitude	Reservoir	°API	V	V/Ni	St	SAT	ARO	POL	$\delta^{13}C_{ARO}$	$\delta^{13}C_{SAT}$
SSF-045	2843	00º14’28”S	76º38’57’’W	T	30.0	7.9	2.09	0.76	39	35	26	-26.3	-27.1
SSF-046	2845	00º08’07”S	76º39’22”W	T	26.6	8.1	2.37	0.95	39	36	25	-26.3	-27.0
SSF-049	2761	00º08’02”S	76º38’16”W	U	27.0	8.2	2.42	0.93	38	36	26	-26.0	-27.2
SSF-052	2892	00º06’26”S	76º37’44”W	Tena	26.1	8.4	2.14	1.00	39	35	26	-26.2	-27.5
SSF-053	2881	00º06’59”S	76º39’25”W	U	26.7	8.5	2.65	0.95	40	35	25	-26.2	-27.6
SSF-054	2740	00º06’58”S	76º38’16”W	Tena	26.4	8.1	2.33	0.91	39	35	26	-26.1	-27.0
SSF-056	2886	00º05’29”S	76º38’36”W	T	29.7	8.4	2.51	0.71	40	35	25	-26.0	-27.2
SSF-057	2850	00º06’23”S	76º38’50”W	T	29.9	8.5	2.66	0.69	39	35	26	-26.6	-27.2
SSF-059	2860	00º05’41”S	76º37’57”W	Upper U	27.4	8.4	2.87	0.90	39	35	25	-26.4	-27.3
SSF-061	2888	00º15’38”S	76º38’44”W	T	28.5	8.4	3.02	0.68	40	34	26	-26.4	-27.5
SSF-062	2865	00º10’09”S	76º38’52”W	U	27.2	8.2	2.62	0.92	40	34	26	-26.3	-27.3
SSF-063	2852	00º09’09”S	76º38’52”W	T	29.1	8.6	2.59	0.74	38	36	26	-26.5	-27.3
SSF-064	2863	00º09’41”S	76º38’19”W	Upper U	27.1	8.4	2.43	1.01	39	35	26	-26.3	-27.6
SSF-065	2752	00º11’20”S	76º38’50”W	Upper U	26.9	8.5	2.26	0.98	40	34	26	-26.4	-27.4
SSF-066	2760	00º08’30”S	76º38’19”W	U	27.4	8.7	2.70	0.95	39	35	26	-26.1	-27.0
SSF-067	2848	00º13’34”S	76º38’57”W	T	29.7	8.1	2.18	0.69	40	34	26	-26.2	-27.5
SSF-069	2897	00º16’10”S	76º39’32”W	U	26.4	8.4	2.06	0.97	39	35	26	-26.0	-27.4
SSF-071	2894	00º06’26”S	76º38’19”W	T	29.7	8.0	2.64	0.72	40	35	25	-26.1	-27.1
SSF-073	2857	00º12’43”S	76º39’09”W	U	27.6	8.3	2.25	0.93	39	36	25	-26.0	-27.4
SSF-079	2866	00º14’47”S	76º39’13”W	U	27.1	7.9	2.63	0.94	40	34	26	-26.2	-27.3
SSF-080	2851	00º13’14”S	76º39’10”W	T	28.8	8.4	2.72	0.77	38	36	26	-26.3	-27.0
SSF-082	2855	00º14’15”S	76º39’19”W	U	27.3	8.0	2.41	0.90	39	35	26	-26.3	-27.2
SSF-083	2875	00º11’20”S	76º38’45”W	U	26.6	8.6	2.57	0.93	39	36	25	-26.4	-27.1
SSF-084	2780	00º11’58”S	76º39’19”W	Lower U	27.0	8.4	2.13	0.92	39	36	25	-26.6	-27.2
SSF-085	2872	00º15’22”S	76º39’13”W	T	29.9	8.2	2.75	0.78	40	34	26	-26.1	-27.3
SSF-086	2747	00º08’02”S	76º38’47”W	U	26.8	8.5	2.35	0.98	40	35	25	-26.1	-27.5
SSF-087	2847	00º08’53”S	76º38’35”W	U	26.6	8.8	2.94	0.89	39	35	26	-26.0	-27.4
SSF-088	2858	00º08’53”S	76º39’09”W	U	27.2	8.3	2.60	0.97	39	35	26	-26.5	-27.6
SSF-091	2825	00º13’14”S	76º38’38”W	U	27.7	8.2	2.87	0.91	38	36	26	-26.2	-27.0
SFF-092	2817	00º13’46”S	76º38’38”W	T	29.4	7.9	2.46	0.75	40	35	25	-26.2	-27.5
SSF-095	2864	00º15’57”S	76º39’10”W	T	29.5	8.4	2.17	0.73	40	34	26	-26.1	-27.2
SSF-096	3070	00º11’58”S	76º39’19”W	Upper U	27.1	8.0	2.51	0.92	40	34	26	-26.6	-27.3
SSF-097	2850	00º14’15”S	76º39’38”W	T	28.7	8.2	2.84	0.78	39	36	25	-26.4	-27.4
SSF-098D	2840	00º10’09”S	76º38’52”W	T	29.5	8.4	2.88	0.74	39	35	26	-26.2	-27.1

Well	Depth (m)	Latitude	Longitude	Reservoir	°API	V	V/Ni	St	SAT	ARO	POL	$\delta^{13}C_{ARO}$	$\delta^{13}C_{SAT}$
SSF-099	2853	00º07’14”S	76º38’31”W	T	29.2	8.0	2.04	0.74	41	33	26	-26.2	-27.1
SSF-104D	2839	00º15’06”S	76º38’57”W	T	30.0	8.2	2.26	0.66	40	35	25	-26.3	-27.5
SSF-106D	2871	00º13’30’’S	76º38’16’’W	Lower U	26.1	8.3	2.83	0.92	39	35	26	-26.2	-27.0
SSF-107D	2562	00º06’26”S	76º37’44”W	Tena	26.0	7.9	2.65	1.02	39	35	26	-26.1	-27.4
SSF-108D	2748	00º08’02”S	76º38’16”W	Lower U	27.3	8.1	2.34	0.97	39	35	26	-26.0	-27.1
SSF-109D	2844	00º10’09”S	76º38’52”W	T	28.8	8.5	2.68	0.71	39	35	26	-26.4	-27.0
SSF-110D	2728	00º11’36”S	76º38’38”W	Lower U	26.6	8.0	2.51	0.91	39	35	26	-26.1	-27.2
SSF-111D	2799	00º06’26”S	76º37’44”W	Lower U	27.5	8.6	2.47	0.93	39	35	26	-26.5	-27.3
SSF-116D	2816	00º10’09”S	76º38’52”W	T	29.6	8.2	2.18	0.73	41	33	26	-26.4	-27.1
SSF-118D	2805	00º12’23’’S	76º38’19”W	T	28.7	8.5	2.75	0.68	39	36	25	-26.5	-27.5
SSF-122D	2820	00º14’37”S	76º38’25”W	T	29.0	7.9	2.34	0.70	40	34	26	-26.1	-27.5
SSF-129D	2837	00º16’16”S	76º38’51”W	T	29.3	8.3	2.53	0.72	40	35	25	-26.0	-27.0
SSQ-04	2525	00º05’31”N	76º34’21”W	T	29.0	7.0	2.79	0.81	41	35	24	-26.2	-27.2
SSQ-06	2478	00º05’01”N	76º34’51”W	Lower U	30.3	7.2	2.83	0.89	42	35	23	-26.5	-27.5
SSQ-12	2499	00º04’36”N	76º35’08”W	Lower U	29.7	7.1	2.57	0.90	41	35	24	-26.3	-27.3
SSQ-13	2450	00º03’35”N	76º34’59”W	Tena	32.7	7.1	3.02	0.76	43	34	23	-26.1	-27.1
SSQ-15	2485	00º05’50”N	76º34’21”W	Lower U	30.0	7.0	3.13	0.89	43	34	23	-26.1	-27.1
SSQ-21	2520	00º05’50”N	76º34’46”W	T	29.6	7.1	2.45	0.85	42	35	23	-26.4	-27.4
SEC-10	2541	00º00’11”S	76º35’16”W	T	29.3	7.3	2.52	0.90	42	34	24	-26.6	-27.9
SEC-11	2538	00º00’50”S	76º34’55”W	T	29.8	--	--	0.87	41	35	24	-26.8	-28.0
SEC-14	2496	00º01’40”N	76º35’12”W	Lower U	30.1	7.7	2.65	0.88	43	34	23	-26.7	-28.0
SEC-19	2490	00º02’24”N	76º35’06”W	Upper U	30.3	--	--	0.86	42	35	23	-26.5	-27.7
SEC-37D	2546	00º01’29”S	76º35’30”W	T	29.2	--	--	0.92	41	35	24	-26.8	-28.1
TTT-01	2866	00º11’02”N	76º31’34”W	T	28.7	7.1	2.81	0.78	42	35	23	-26.1	-27.3
TTT-03	2879	00º11’15”N	76º30’45”W	Lower U	30.1	7.0	2.59	0.81	43	35	22	-26.5	-27.6
TTT-04	2864	00º12’06”N	76º31’07”W	T	28.8	6.8	3.07	0.88	42	35	23	-26.3	-27.4
TTT-09	2808	00º11’47”N	76º30’55”W	Lower U	29.8	6.9	2.63	0.79	42	35	23	-26.0	-27.2
TTT-10	2846	00º11’37”N	76º31’47”W	Lower U	30.0	6.8	2.46	0.82	43	34	23	-25.9	-27.0
TTT-11	2847	00º10’45”N	76º31’48”W	Lower U	30.2	6.8	3.14	0.80	43	35	22	-26.1	-27.3
TAP-01	2814	00º12’13”N	76º33’05”W	T	28.8	--	--	0.84	43	34	23	-26.3	-27.4
TAP-04	2823	00º12’10”N	76º32’33”W	Lower U	29.6	--	--	0.78	42	35	23	-26.2	-27.2
TAP-05	2828	00º13’01”N	76º32’42”W	Lower U	29.8	7.2	2.60	0.81	44	34	22	-26.0	-27.1

Note: St = sulfur content, SAT = saturates, ARO = aromatics, and POL = polar compounds (resins plus asphalthenes)

Table 2: Information of cutting and outcrop samples under study.

Sample	Latitude	Longitude	Rock unit	Lithology	Location
Rock-1 (2480 m)	00º22’11”S	76º53’08”W	A Limestone	Argillaceous marl	Sacha-132 well
Rock-2 (3012 m)	00º29’14”S	76º45’59”W	Basal Shale	Claystone	Yuca-02 well
Rock-3 (outcrop)	01º00’06”S	77º45’46”W	Basal Shale	Claystone	Misahualli River
Rock-4 (outcrop)	02º43’42”S	78º14’25”W	B Limestone	Shaly limestone	Namangoza River
Rock-5 (outcrop)	01º00’29”S	77º45’43”W	U Shale	Claystone	Misahualli River
Rock-6 (1768 m)	01º22’06”S	77º40’34”W	U Shale	Claystone	Oglan A-1 well
Rock-7 (1270 m)	00º07’15”N	77º17’57”W	Basal Shale	Claystone	Bermejo Sur-19 well
Rock-8 (3046 m)	00º59’49”S	76º56’18”W	B Limestone	Marlstone	Cononaco-19 well
Rock-9 (1190 m)	02º08’22”S	77º33’54”W	B Limestone	Marlstone	Macuma-1 well
Rock-0 (outcrop)	01º00’36”S	77º45’41”W	A Limestone	Argillaceous marl	Misahualli River

Table 3: TOC, vitrinite reflectances (Ro Calc and %Rr), $\delta^{13}C$ (‰) in SARA fractions, and Rock-Eval data for the sampled rocks.

Sample	Rock unit	TOC	Tmax	Ro Calc	Rr	S1	S2	S3	HI	OI	PI	$\delta^{13}C_{SAT}$	$\delta^{13}C_{ARO}$
Rock-1 (2480 m)	A Limestone	3.09	431	0.59%	0.60%	1.87	15.48	0.42	500.8	13.62	0.11	-26.8	-25.6
Rock-2 (3012 m)	Basal Shale	4.97	430	0.58%	0.59%	1.66	21.05	1.30	350.0	22.01	0.08	-28.5	-27.2
Rock-3 (outcrop)	Basal Shale	3.90	433	0.63%	0.62%	1.80	13.26	1.18	340.1	29.97	0.12	-28.7	-27.5
Rock-4 (outcrop)	B Limestone	1.41	428	0.55%	0.55%	0.39	6.09	0.21	431.7	14.77	0.06	-27.2	-25.9
Rock-5 (outcrop)	U Shale	1.23	426	0.50%	0.49%	0.31	3.87	0.28	315.1	22.48	0.08	-28.9	-27.8
Rock-6 (1768 m)	U Shale	1.66	425	0.49%	0.49%	0.37	5.45	0.38	328.8	21.58	0.07	-29.0	-28.0
Rock-7 (1270 m)	Basal Shale	2.54	435	0.67%	0.65%	1.12	9.09	0.86	349.7	32.63	0.11	-28.9	-27.7
Rock-8 (3046 m)	B Limestone	1.54	427	0.53%	0.54%	0.54	7.23	0.21	469.3	14.28	0.07	-27.4	-25.9
Rock-9 (1190 m)	B Limestone	0.98	431	0.59%	0.59%	0.51	4.47	0.14	456.5	15.40	0.10	-27.0	-25.8
Rock-0 (outcrop)	A Limestone	2.12	424	0.48%	0.48%	0.57	10.86	0.29	512.4	13.95	0.05	-26.9	-25.7

Notes: TOC data in wt.%; S1and S2 in mg HC/g rock, while S3 in mg CO_2/g rock; HI=S2/TOC; OI=S3/TOC; HI in mg HC/g TOC; Tmax in ºC; IO in mg CO_2/g TOC; PI=S1/(S1+S2); %Ro Calc = 0.018·Tmax-7.16 (Jarvie et al.. 2001).

Table 4: Geochemical indicators of source type and depositional environment for saturated and aromatic fractions in oils and extracts analysed.

Sample	%27ST	%28ST	%29ST	Ts/Tm	Ph/nC_{18}	Pr/Ph	29/30H	31R/30H	26/25T	24/23T	ST/30H	DBT/P	Dia/ST
AUC-03	35	33	32	0.35	0.63	1.02	0.71	0.34	0.74	0.60	0.62	0.61	0.43
AUC-19	36	32	32	0.33	0.60	1.01	0.70	0.35	0.72	0.58	0.64	0.63	0.41
AUC-31	35	32	33	0.38	0.62	0.99	0.69	0.36	0.76	0.59	0.65	0.66	0.42
AUC-32	37	31	32	0.35	0.64	0.95	0.71	0.34	0.73	0.60	0.62	0.62	0.43
AUC-33	35	33	32	0.34	0.61	1.00	0.68	0.37	0.72	0.58	0.63	0.63	0.44
AUC-34	36	32	32	0.37	0.62	1.00	0.67	0.36	0.75	0.61	0.64	0.64	0.43
AUC-35	35	32	33	0.36	0.63	0.97	0.70	0.35	0.74	0.62	0.62	0.62	0.43
AUC-36	35	33	32	0.33	0.64	0.93	0.67	0.33	0.75	0.59	0.63	0.65	0.44
AUC-38	36	33	31	0.37	0.65	1.02	0.68	0.36	0.73	0.60	0.61	0.65	0.45
AUC-39	37	32	31	0.35	0.63	1.03	0.70	0.34	0.74	0.59	0.62	0.62	0.42
AUC-43	35	33	32	0.35	0.66	0.94	0.67	0.35	0.72	0.61	0.63	0.61	0.44
AUC-49	36	32	32	0.34	0.63	1.03	0.69	0.37	0.71	0.59	0.62	0.64	0.43
AUC-50	37	32	31	0.36	0.66	1.02	0.69	0.34	0.73	0.60	0.63	0.66	0.44
AUC-53	35	33	32	0.34	0.65	0.96	0.70	0.35	0.74	0.59	0.65	0.65	0.45
AUC-57D	35	32	33	0.36	0.62	0.98	0.68	0.36	0.75	0.61	0.65	0.63	0.43
AUC-59D	36	33	31	0.35	0.66	0.96	0.67	0.33	0.73	0.60	0.64	0.64	0.42
AUC-73D	37	32	31	0.33	0.63	1.01	0.70	0.34	0.72	0.58	0.63	0.62	0.42
AUC-74	36	32	32	0.38	0.64	1.02	0.68	0.35	0.75	0.59	0.62	0.63	0.44
AUC-99	35	32	33	0.35	0.65	1.03	0.67	0.36	0.74	0.60	0.63	0.64	0.43
CON-03	36	32	32	0.33	0.67	1.01	0.70	0.34	0.73	0.60	0.65	0.61	0.42
CON-08	35	33	32	0.35	0.66	1.02	0.68	0.35	0.76	0.60	0.64	0.59	0.44
CON-09	34	34	32	0.34	0.70	1.00	0.71	0.36	0.75	0.58	0.61	0.60	0.43
CON-13	37	32	31	0.33	0.65	1.03	0.69	0.33	0.74	0.59	0.63	0.60	0.44
CON-14	35	33	32	0.35	0.71	0.97	0.72	0.35	0.73	0.59	0.62	0.62	0.42
CON-16	36	32	32	0.35	0.70	1.02	0.71	0.33	0.75	0.61	0.63	0.58	0.41
CON-18	37	32	31	0.32	0.67	0.95	0.69	0.37	0.72	0.60	0.64	0.59	0.43
CON-23	34	33	33	0.34	0.71	1.00	0.71	0.34	0.74	0.59	0.62	0.61	0.43
CON-27	34	34	32	0.36	0.72	0.94	0.68	0.36	0.74	0.61	0.60	0.62	0.44
CON-30D	37	32	31	0.32	0.64	0.92	0.72	0.38	0.72	0.62	0.61	0.63	0.45

Sample	%27ST	%28ST	%29ST	Ts/Tm	Ph/nC_{18}	Pr/Ph	29/30H	31R/30H	26/25T	24/23T	ST/30H	DBT/P	Dia/ST
CON-36D	36	33	31	0.34	0.73	1.02	0.69	0.36	0.74	0.59	0.62	0.60	0.43
CON-46D	35	33	32	0.33	0.70	1.01	0.72	0.35	0.73	0.61	0.61	0.61	0.42
CON-48D	34	34	32	0.35	0.73	0.96	0.70	0.34	0.72	0.60	0.63	0.59	0.44
LAG-09	35	33	32	0.48	0.54	1.04	0.57	0.36	0.79	0.73	0.56	0.42	0.52
LAG-11	36	32	32	0.47	0.55	1.03	0.56	0.37	0.78	0.72	0.59	0.41	0.51
LAG-18	34	34	32	0.50	0.54	1.08	0.54	0.38	0.77	0.75	0.56	0.43	0.53
LAG-22	37	32	31	0.48	0.56	1.07	0.57	0.35	0.78	0.71	0.59	0.44	0.52
LAG-31	35	33	32	0.47	0.53	1.12	0.55	0.37	0.79	0.72	0.57	0.41	0.54
LAG-38	34	34	32	0.48	0.54	1.05	0.55	0.36	0.78	0.74	0.58	0.43	0.53
LAG-39	35	32	33	0.49	0.56	1.10	0.56	0.36	0.77	0.73	0.56	0.43	0.51
LAG-40D	37	32	31	0.49	0.54	1.07	0.56	0.37	0.78	0.72	0.59	0.43	0.52
LAG-41	35	32	33	0.47	0.57	1.06	0.54	0.38	0.79	0.73	0.55	0.44	0.53
LAG-50	37	32	31	0.49	0.55	1.05	0.55	0.36	0.78	0.71	0.58	0.42	0.53
GTA-04	35	33	32	0.46	0.59	1.02	0.54	0.39	0.81	0.74	0.55	0.48	0.54
GTA-05	36	32	32	0.47	0.56	1.09	0.57	0.38	0.78	0.73	0.59	0.47	0.51
GTA-06	36	33	31	0.48	0.57	1.07	0.55	0.37	0.77	0.72	0.58	0.48	0.53
GTA-10	37	32	31	0.50	0.56	1.11	0.57	0.36	0.78	0.71	0.59	0.46	0.52
GTA-11	38	31	31	0.49	0.57	1.05	0.56	0.35	0.79	0.72	0.56	0.49	0.52
GTA-15	36	33	31	0.47	0.57	1.06	0.56	0.36	0.78	0.73	0.58	0.48	0.53
GTA-17D	36	32	32	0.48	0.55	1.04	0.55	0.38	0.80	0.73	0.59	0.48	0.53
GTA-18D	37	32	31	0.49	0.58	1.03	0.57	0.37	0.78	0.72	0.57	0.49	0.52
GTA-20D	35	33	32	0.47	0.57	1.12	0.56	0.37	0.79	0.71	0.59	0.46	0.52
GTA-23D	38	31	31	0.48	0.56	1.08	0.54	0.36	0.77	0.73	0.58	0.47	0.53
GTA-24D	36	33	31	0.49	0.57	1.06	0.55	0.37	0.79	0.72	0.56	0.49	0.53
GTA-40D	36	32	32	0.48	0.58	1.10	0.56	0.36	0.78	0.71	0.59	0.50	0.51
GTA-41D	35	33	32	0.49	0.57	1.04	0.57	0.35	0.80	0.72	0.59	0.47	0.52
GTA-42D	37	32	31	0.47	0.58	1.08	0.56	0.37	0.79	0.73	0.58	0.48	0.52
SSF-002	36	32	32	0.49	0.55	1.05	0.56	0.36	0.78	0.73	0.58	0.44	0.53
SSF-003	37	32	31	0.50	0.57	1.06	0.54	0.37	0.77	0.70	0.60	0.45	0.52
SSF-014	38	31	31	0.48	0.58	1.10	0.55	0.35	0.78	0.71	0.59	0.43	0.53

Sample	%27ST	%28ST	%29ST	Ts/Tm	Ph/nC_{18}	Pr/Ph	29/30H	31R/30H	26/25T	24/23T	ST/30H	DBT/P	Dia/ST
SSF-017	36	33	31	0.49	0.57	1.04	0.55	0.36	0.79	0.71	0.61	0.44	0.54
SSF-020	37	32	31	0.48	0.58	1.07	0.54	0.37	0.78	0.73	0.59	0.45	0.52
SSF-024	37	32	31	0.50	0.57	1.09	0.57	0.35	0.80	0.72	0.62	0.46	0.51
SSF-026	35	32	33	0.48	0.56	1.05	0.56	0.36	0.77	0.72	0.60	0.43	0.53
SSF-027	36	32	32	0.48	0.57	1.06	0.55	0.37	0.79	0.72	0.61	0.45	0.52
SSF-035	38	31	31	0.47	0.58	1.04	0.56	0.37	0.78	0.73	0.59	0.42	0.53
SSF-036	37	31	32	0.49	0.56	1.10	0.56	0.38	0.79	0.70	0.62	0.45	0.51
SSF-042	35	33	32	0.50	0.58	1.08	0.54	0.36	0.79	0.71	0.60	0.44	0.53
SSF-045	37	32	31	0.48	0.59	1.03	0.58	0.35	0.80	0.72	0.61	0.46	0.52
SSF-046	35	32	33	0.49	0.58	1.11	0.56	0.36	0.79	0.72	0.59	0.45	0.51
SSF-049	38	31	31	0.51	0.57	1.02	0.54	0.35	0.77	0.73	0.61	0.43	0.50
SSF-052	36	32	32	0.49	0.56	1.13	0.53	0.37	0.79	0.70	0.60	0.44	0.52
SSF-053	36	32	32	0.49	0.58	1.08	0.55	0.36	0.78	0.71	0.60	0.45	0.53
SSF-054	36	33	31	0.48	0.57	1.09	0.56	0.36	0.80	0.72	0.59	0.42	0.53
SSF-056	37	32	31	0.47	0.56	1.07	0.55	0.35	0.78	0.71	0.62	0.45	0.52
SSF-057	37	32	31	0.49	0.59	1.06	0.57	0.37	0.78	0.73	0.62	0.45	0.51
SSF-059	38	31	31	0.46	0.58	1.05	0.56	0.38	0.78	0.70	0.60	0.44	0.51
SSF-061	37	31	32	0.49	0.57	1.03	0.58	0.36	0.79	0.72	0.59	0.44	0.52
SSF-062	36	33	31	0.48	0.56	1.08	0.57	0.34	0.79	0.69	0.63	0.42	0.52
SSF-063	37	32	31	0.51	0.57	1.12	0.57	0.37	0.79	0.71	0.60	0.43	0.53
SSF-064	36	32	32	0.48	0.57	1.06	0.58	0.36	0.78	0.70	0.59	0.45	0.52
SSF-065	36	33	31	0.48	0.56	1.05	0.56	0.36	0.80	0.72	0.61	0.46	0.52
SSF-066	38	31	31	0.49	0.58	1.02	0.55	0.37	0.78	0.72	0.60	0.44	0.50
SSF-067	37	32	31	0.50	0.57	1.03	0.57	0.36	0.78	0.71	0.61	0.45	0.52
SSF-069	36	32	32	0.49	0.56	1.09	0.58	0.36	0.79	0.71	0.58	0.43	0.53
SSF-071	35	32	33	0.48	0.57	1.08	0.56	0.37	0.79	0.73	0.62	0.43	0.51
SSF-073	38	31	31	0.47	0.58	1.06	0.57	0.38	0.77	0.72	0.61	0.45	0.52
SSF-079	38	31	31	0.47	0.57	1.07	0.55	0.37	0.81	0.70	0.60	0.44	0.54
SSF-080	35	32	33	0.49	0.55	1.05	0.56	0.35	0.79	0.60	0.62	0.44	0.53
SSF-082	35	33	32	0.48	0.57	1.04	0.58	0.36	0.77	0.71	0.60	0.45	0.51

Sample	%27ST	%28ST	%29ST	Ts/Tm	Ph/nC_{18}	Pr/Ph	29/30H	31R/30H	26/25T	24/23T	ST/30H	DBT/P	Dia/ST
SSF-083	36	33	31	0.49	0.58	1.10	0.57	0.36	0.78	0.70	0.61	0.44	0.52
SSF-084	38	31	31	0.50	0.58	1.13	0.57	0.37	0.79	0.73	0.60	0.45	0.52
SSF-085	37	32	31	0.49	0.57	1.06	0.56	0.36	0.80	0.71	0.61	0.43	0.53
SSF-086	37	32	31	0.47	0.56	1.11	0.56	0.34	0.78	0.72	0.62	0.44	0.51
SSF-087	36	32	32	0.48	0.55	1.03	0.58	0.37	0.79	0.70	0.61	0.45	0.52
SSF-088	38	31	31	0.49	0.57	1.09	0.57	0.36	0.77	0.74	0.59	0.43	0.50
SSF-091	37	32	31	0.48	0.57	1.07	0.55	0.37	0.78	0.70	0.62	0.46	0.53
SFF-092	36	32	32	0.50	0.59	1.08	0.56	0.36	0.78	0.71	0.60	0.45	0.51
SSF-095	37	32	31	0.49	0.56	1.11	0.55	0.35	0.81	0.72	0.61	0.46	0.51
SSF-096	38	31	31	0.47	0.57	1.06	0.54	0.38	0.79	0.70	0.59	0.44	0.52
SSF-097	35	32	33	0.49	0.58	1.05	0.58	0.35	0.79	0.73	0.62	0.45	0.53
SSF-098D	38	31	31	0.48	0.56	1.04	0.56	0.37	0.80	0.71	0.60	0.42	0.52
SSF-099	36	33	31	0.50	0.57	1.05	0.57	0.36	0.79	0.69	0.61	0.46	0.52
SSF-104D	35	32	33	0.47	0.58	1.06	0.56	0.35	0.79	0.72	0.59	0.44	0.53
SSF-106D	37	32	31	0.49	0.56	1.07	0.57	0.36	0.77	0.71	0.61	0.43	0.54
SSF-107D	37	31	32	0.48	0.58	1.12	0.55	0.35	0.80	0.71	0.60	0.44	0.52
SSF-108D	38	31	31	0.47	0.56	1.07	0.53	0.36	0.78	0.72	0.62	0.45	0.53
SSF-109D	37	32	31	0.48	0.57	1.08	0.56	0.35	0.79	0.73	0.59	0.43	0.53
SSF-110D	36	33	31	0.49	0.56	1.10	0.57	0.34	0.80	0.69	0.62	0.42	0.52
SSF-111D	36	32	32	0.50	0.58	1.10	0.56	0.38	0.79	0.70	0.61	0.43	0.50
SSF-116D	37	32	31	0.48	0.57	1.04	0.58	0.35	0.76	0.73	0.59	0.45	0.52
SSF-118D	35	33	32	0.49	0.57	1.09	0.57	0.37	0.80	0.72	0.60	0.42	0.53
SSF-122D	38	31	31	0.48	0.59	1.07	0.55	0.37	0.78	0.71	0.60	0.44	0.51
SSF-129D	37	32	31	0.47	0.55	1.10	0.56	0.36	0.77	0.72	0.62	0.45	0.52
SSQ-04	38	31	31	0.50	0.60	1.11	0.55	0.37	0.76	0.70	0.54	0.44	0.52
SSQ-06	37	32	31	0.49	0.58	1.03	0.55	0.39	0.75	0.71	0.55	0.43	0.51
SSQ-12	36	32	32	0.48	0.59	1.07	0.56	0.36	0.76	0.72	0.56	0.44	0.52
SSQ-13	37	32	31	0.49	0.62	1.00	0.57	0.38	0.74	0.73	0.56	0.45	0.50
SSQ-15	35	33	32	0.48	0.59	0.98	0.56	0.37	0.75	0.72	0.55	0.44	0.53
SSQ-21	36	32	32	0.47	0.58	0.99	0.58	0.38	0.76	0.71	0.54	0.43	0.51

Sample	%27ST	%28ST	%29ST	Ts/Tm	Ph/nC_{18}	Pr/Ph	29/30H	31R/30H	26/25T	24/23T	ST/30H	DBT/P	Dia/ST
SEC-10	37	32	31	0.47	0.60	1.12	0.55	0.37	0.76	0.72	0.55	0.44	0.52
SEC-11	38	31	31	0.49	0.61	1.06	0.56	0.39	0.75	0.71	0.56	0.43	0.51
SEC-14	37	32	31	0.48	0.59	1.07	0.54	0.38	0.74	0.73	0.54	0.45	0.50
SEC-19	35	33	32	0.49	0.60	1.05	0.56	0.40	0.77	0.70	0.54	0.45	0.53
SEC-37D	36	32	32	0.48	0.59	1.10	0.55	0.37	0.75	0.72	0.55	0.43	0.51
TTT-01	37	32	31	0.47	0.60	1.10	0.54	0.37	0.76	0.70	0.53	0.51	0.50
TTT-03	38	31	31	0.48	0.59	1.06	0.57	0.38	0.75	0.71	0.52	0.52	0.51
TTT-04	37	32	31	0.48	0.60	1.03	0.55	0.38	0.74	0.72	0.54	0.50	0.52
TTT-09	36	32	32	0.49	0.58	1.05	0.56	0.37	0.77	0.72	0.52	0.52	0.50
TTT-10	35	33	32	0.50	0.61	0.99	0.56	0.40	0.76	0.71	0.53	0.51	0.49
TTT-11	37	32	31	0.49	0.59	1.04	0.57	0.40	0.75	0.70	0.53	0.52	0.51
TAP-01	36	32	32	0.48	0.58	1.13	0.58	0.38	0.75	0.71	0.52	0.51	0.51
TAP-04	35	33	32	0.49	0.60	1.12	0.56	0.39	0.73	0.72	0.53	0.52	0.52
TAP-05	37	32	31	0.47	0.59	1.04	0.57	0.37	0.74	0.70	0.52	0.51	0.50
Rock-3 (Basal Shale)	32	32	36	0.58	0.48	1.73	0.52	0.39	0.97	0.71	0.48	0.38	0.66
Rock-4 (B Limestone)	38	31	31	0.37	0.85	1.01	0.75	0.37	0.59	0.69	0.68	0.86	0.34
Rock-5 (U Shale)	32	31	37	0.60	0.42	1.52	0.63	0.38	0.89	0.57	0.50	0.39	0.63
Rock-0 (A Limestone)	39	31	30	0.32	0.80	0.89	0.81	0.40	0.57	0.55	0.67	1.03	0.29

Notes: 24/23T= C_{24}-cheilanthane/C_{23}-cheilanthane; 29/30H=30-norhopane/hopane; Pr/nC_{17}=pristane/*n*-heptadecane; DBT/P=dibenzothiophene/phenanthene; 31R/30H=homohopane 22R/hopane; %27ST=percentage of C_{27} regular steranes; 26/25T=C_{26}-tricyclopolyprenanes/C_{25}-tricyclopolyprenane; ST/30H=ratio of C_{29}-regular steranes to C_{30}-hopane; Ts/Tm=18α(H)-22,29,30 trisnorneohopane/17α(H)-22,29,30 trisnorhopane; Pr/Ph=pristane/phytane; and Dia/ST=diasterane ratio or C_{27}-diasteranes/C_{27}-regular steranes.

Table 5: Some maturity-related molecular parameters for saturated and aromatic hydrocarbons in representative source-rock extracts and all the oil samples.

Sample	%20S	%ββ	Rc_1	TA	Rc_2	DNR-1	Rc_3	MPI-1	Rc_4	CPI
AUC-03	46	54	0.68	0.33	0.63	1.93	0.66	0.64	0.78	1.04
AUC-19	46	53	0.68	0.32	0.62	1.90	0.66	0.63	0.77	1.02
AUC-31	48	55	0.70	0.32	0.62	1.99	0.67	0.62	0.77	1.03
AUC-32	47	54	0.69	0.34	0.64	1.92	0.66	0.64	0.78	1.03
AUC-33	46	53	0.68	0.32	0.61	1.98	0.67	0.63	0.77	1.02
AUC-34	48	55	0.70	0.35	0.66	1.90	0.66	0.62	0.77	1.01
AUC-35	49	55	0.71	0.33	0.63	2.02	0.66	0.65	0.79	1.03
AUC-36	47	54	0.69	0.34	0.64	1.96	0.66	0.63	0.77	1.03
AUC-38	48	55	0.70	0.34	0.64	1.98	0.66	0.64	0.78	1.03
AUC-39	46	52	0.67	0.33	0.63	1.90	0.66	0.65	0.79	1.02
AUC-43	48	54	0.71	0.35	0.66	1.89	0.66	0.63	0.77	1.02
AUC-49	47	54	0.70	0.34	0.64	1.90	0.66	0.62	0.77	1.03
AUC-50	47	53	0.69	0.33	0.63	1.99	0.67	0.64	0.78	1.04
AUC-53	46	53	0.68	0.35	0.66	1.91	0.66	0.63	0.77	1.03
AUC-57D	49	55	0.71	0.32	0.61	1.99	0.67	0.63	0.77	1.04
AUC-59D	47	54	0.69	0.33	0.63	2.00	0.67	0.65	0.79	1.03
AUC-73D	47	54	0.69	0.34	0.64	1.95	0.66	0.63	0.77	1.02
AUC-74	48	55	0.70	0.34	0.6	1.94	0.66	0.62	0.77	1.03
AUC-99	46	54	0.68	0.33	0.63	2.00	0.67	0.64	0.78	1.04
CON-03	44	53	0.66	0.33	0.63	1.92	0.66	0.65	0.79	1.02
CON-08	45	55	0.67	0.34	0.64	2.00	0.67	0.66	0.79	1.02
CON-09	48	54	0.70	0.35	0.66	1.99	0.66	0.67	0.80	1.04
CON-13	47	53	0.69	0.34	0.64	1.96	0.66	0.65	0.79	1.03
CON-14	45	55	0.67	0.35	0.66	1.89	0.66	0.66	0.79	1.03
CON-16	44	54	0.66	0.34	0.64	1.92	0.66	0.65	0.79	1.02
CON-18	44	57	0.66	0.34	0.64	1.91	0.66	0.68	0.80	1.01
CON-23	45	55	0.67	0.35	0.66	1.93	0.66	0.66	0.79	1.03
CON-27	46	56	0.68	0.36	0.67	1.90	0.66	0.67	0.80	1.04
CON-30D	45	56	0.67	0.34	0.64	1.95	0.66	0.66	0.79	1.02
CON-36D	48	55	0.70	0.33	0.63	1.95	0.66	0.65	0.79	1.03
CON-46D	47	54	0.69	0.34	0.64	1.94	0.66	0.68	0.80	1.01
CON-48D	46	54	0.68	0.33	0.63	2.00	0.67	0.64	0.78	1.03
LAG-09	50	60	0.73	0.34	0.64	1.98	0.67	0.67	0.80	1.04
LAG-11	49	59	0.71	0.35	0.66	1.90	0.66	0.66	0.79	1.03
LAG-18	50	61	0.73	0.33	0.63	1.88	0.66	0.62	0.76	1.05
LAG-22	51	62	0.74	0.34	0.64	1.92	0.66	0.65	0.79	1.02
LAG-31	49	60	0.72	0.35	0.65	1.93	0.66	0.65	0.79	1.03
LAG-38	50	60	0.73	0.34	0.64	1.95	0.66	0.64	0.78	1.01
LAG-39	49	62	0.72	0.34	0.64	1.92	0.66	0.63	0.77	1.02
LAG-40D	50	61	0.73	0.33	0.63	1.91	0.66	0.64	0.78	1.03

Sample	%20S	%ββ	Rc_1	TA	Rc_2	DNR-1	Rc_3	MPI-1	Rc_4	CPI
LAG-41	51	59	0.74	0.34	0.64	1.92	0.66	0.64	0.78	1.03
LAG-50	50	61	0.73	0.33	0.63	1.93	0.66	0.63	0.77	1.02
GTA-04	51	62	0.74	0.34	0.64	1.96	0.66	0.70	0.82	1.05
GTA-05	49	59	0.72	0.33	0.63	1.98	0.67	0.69	0.81	1.03
GTA-06	50	61	0.73	0.34	0.64	1.90	0.66	0.66	0.80	1.02
GTA-10	50	60	0.73	0.35	0.65	1.88	0.65	0.67	0.80	1.04
GTA-11	49	60	0.72	0.34	0.64	1.95	0.66	0.68	0.81	1.02
GTA-15	51	61	0.74	0.34	0.64	1.93	0.66	0.67	0.80	1.03
GTA-17D	50	62	0.73	0.32	0.62	1.94	0.66	0.66	0.80	1.04
GTA-18D	50	60	0.73	0.33	0.63	1.93	0.66	0.68	0.81	1.02
GTA-20D	51	59	0.74	0.34	0.64	1.92	0.66	0.68	0.81	1.03
GTA-23D	50	61	0.73	0.35	0.65	1.98	0.66	0.69	0.81	1.04
GTA-24D	51	60	0.74	0.34	0.64	1.90	0.66	0.67	0.80	1.03
GTA-40D	49	60	0.72	0.33	0.63	1.88	0.66	0.68	0.81	1.03
GTA-41D	50	62	0.73	0.34	0.64	1.90	0.66	0.67	0.80	1.02
GTA-42D	51	61	0.74	0.33	0.63	1.93	0.66	0.68	0.81	1.01
SSF-002	49	62	0.72	0.33	0.63	1.97	0.67	0.65	0.79	1.04
SSF-003	51	59	0.74	0.34	0.64	1.89	0.66	0.66	0.80	1.03
SSF-014	51	60	0.74	0.35	0.65	1.90	0.66	0.62	0.77	1.02
SSF-017	50	61	0.73	0.33	0.63	1.88	0.66	0.67	0.80	1.03
SSF-020	50	60	0.73	0.35	0.65	1.92	0.66	0.64	0.78	1.02
SSF-024	51	60	0.74	0.32	0.62	1.93	0.66	0.64	0.78	1.04
SSF-026	50	62	0.73	0.33	0.63	1.87	0.66	0.63	0.78	1.04
SSF-027	49	61	0.72	0.35	0.65	1.91	0.66	0.65	0.78	1.03
SSF-035	51	59	0.74	0.34	0.64	1.95	0.66	0.67	0.80	1.03
SSF-036	50	60	0.73	0.33	0.63	1.98	0.67	0.63	0.78	1.04
SSF-042	49	61	0.72	0.33	0.63	1.94	0.66	0.62	0.77	1.03
SSF-045	51	59	0.74	0.34	0.64	1.87	0.66	0.66	0.80	1.02
SSF-046	51	62	0.74	0.34	0.64	1.90	0.66	0.65	0.80	1.02
SSF-049	50	60	0.73	0.33	0.63	1.88	0.66	0.66	0.80	1.01
SSF-052	49	62	0.72	0.34	0.64	1.85	0.66	0.62	0.77	1.02
SSF-053	51	59	0.74	0.34	0.64	1.93	0.66	0.67	0.80	1.03
SSF-054	49	60	0.72	0.33	0.63	1.91	0.66	0.65	0.79	1.04
SSF-056	51	61	0.74	0.35	0.65	1.83	0.65	0.63	0.78	1.05
SSF-057	50	60	0.73	0.32	0.62	1.92	0.66	0.64	0.78	1.04
SSF-059	50	59	0.73	0.33	0.63	1.96	0.66	0.64	0.78	1.02
SSF-061	49	61	0.72	0.34	0.64	1.90	0.66	0.66	0.80	1.03
SSF-062	50	60	0.73	0.33	0.63	1.81	0.65	0.65	0.79	1.04
SSF-063	51	62	0.74	0.33	0.63	2.00	0.67	0.65	0.79	1.03
SSF-064	49	59	0.72	0.34	0.64	1.98	0.67	0.66	0.80	1.02
SSF-065	50	60	0.73	0.34	0.64	1.93	0.66	0.64	0.78	1.04
SSF-066	50	61	0.73	0.35	0.65	1.88	0.66	0.63	0.78	1.03

Sample	%20S	%ββ	Rc_1	TA	Rc_2	DNR-1	Rc_3	MPI-1	Rc_4	CPI
SSF-067	51	60	0.74	0.34	0.64	1.95	0.66	0.62	0.77	1.03
SSF-069	50	60	0.73	0.33	0.63	1.97	0.67	0.64	0.78	1.02
SSF-071	49	62	0.72	0.35	0.65	1.90	0.66	0.64	0.78	1.03
SSF-073	50	61	0.73	0.34	0.64	1.87	0.66	0.63	0.78	1.04
SSF-079	51	59	0.74	0.33	0.63	2.00	0.67	0.65	0.79	1.03
SSF-080	49	60	0.72	0.33	0.63	1.92	0.66	0.63	0.78	1.02
SSF-082	50	61	0.73	0.34	0.64	1.94	0.66	0.62	0.77	1.02
SSF-083	50	62	0.73	0.35	0.65	1.93	0.66	0.64	0.78	1.04
SSF-084	51	59	0.74	0.32	0.62	1.92	0.66	0.65	0.79	1.03
SSF-085	50	60	0.73	0.33	0.63	1.89	0.66	0.64	0.78	1.04
SSF-086	49	61	0.72	0.34	0.64	1.91	0.66	0.63	0.78	1.03
SSF-087	50	62	0.73	0.35	0.65	1.97	0.67	0.64	0.78	1.01
SSF-088	51	60	0.74	0.35	0.65	1.89	0.66	0.65	0.79	1.05
SSF-091	50	61	0.73	0.34	0.64	1.90	0.66	0.63	0.78	1.03
SFF-092	49	61	0.72	0.34	0.64	1.88	0.66	0.65	0.79	1.02
SSF-095	51	62	0.74	0.33	0.63	1.92	0.66	0.64	0.78	1.05
SSF-096	49	60	0.72	0.32	0.62	1.93	0.66	0.66	0.80	1.03
SSF-097	50	59	0.73	0.33	0.63	1.87	0.66	0.63	0.78	1.04
SSF-098D	51	60	0.74	0.34	0.64	1.91	0.66	0.65	0.79	1.02
SSF-099	49	60	0.72	0.35	0.65	1.96	0.66	0.63	0.78	1.01
SSF-104D	50	60	0.73	0.34	0.64	1.97	0.67	0.65	0.79	1.03
SSF-106D	51	62	0.74	0.33	0.63	1.94	0.66	0.64	0.78	1.02
SSF-107D	50	60	0.73	0.33	0.63	1.95	0.66	0.67	0.80	1.04
SSF-108D	51	59	0.74	0.34	0.64	1.89	0.66	0.64	0.78	1.05
SSF-109D	49	61	0.72	0.35	0.65	1.94	0.66	0.62	0.77	1.04
SSF-110D	50	60	0.73	0.34	0.64	1.91	0.66	0.64	0.78	1.03
SSF-111D	49	59	0.72	0.33	0.63	1.93	0.66	0.67	0.80	1.03
SSF-116D	50	62	0.73	0.33	0.63	2.01	0.67	0.63	0.78	1.05
SSF-118D	51	60	0.74	0.34	0.64	1.88	0.66	0.65	0.79	1.03
SSF-122D	51	59	0.74	0.34	0.64	1.91	0.66	0.63	0.78	1.03
SSF-129D	49	61	0.72	0.33	0.63	1.97	0.67	0.66	0.80	1.02
SSQ-04	51	62	0.74	0.35	0.65	2.03	0.67	0.63	0.78	1.03
SSQ-06	50	60	0.73	0.34	0.64	2.08	0.68	0.62	0.77	1.04
SSQ-12	51	59	0.74	0.33	0.63	1.99	0.67	0.64	0.78	1.02
SSQ-13	50	60	0.73	0.32	0.62	2.11	0.68	0.61	0.77	1.05
SSQ-15	49	60	0.72	0.33	0.63	2.00	0.67	0.62	0.77	1.03
SSQ-21	50	61	0.73	0.34	0.64	2.02	0.67	0.64	0.78	1.04
SEC-10	51	61	0.74	0.33	0.63	1.95	0.66	0.63	0.78	1.02
SEC-11	51	60	0.74	0.32	0.62	1.93	0.66	0.62	0.77	1.03
SEC-14	49	60	0.72	0.35	0.65	2.01	0.67	0.64	0.78	1.03
SEC-19	51	62	0.74	0.34	0.64	1.94	0.66	0.65	0.79	1.04
SEC-37D	50	59	0.73	0.33	0.63	1.98	0.67	0.64	0.78	1.02

Sample	%20S	%ββ	Rc_1	TA	Rc_2	DNR-1	Rc_3	MPI-1	Rc_4	CPI
TTT-01	51	59	0.74	0.35	0.65	1.94	0.66	0.65	0.79	1.04
TTT-03	49	61	0.72	0.34	0.64	1.89	0.66	0.62	0.77	1.02
TTT-04	50	60	0.73	0.34	0.64	1.90	0.66	0.64	0.78	1.05
TTT-09	49	60	0.72	0.33	0.63	1.97	0.67	0.63	0.78	1.03
TTT-10	50	61	0.73	0.35	0.65	1.85	0.65	0.61	0.77	1.06
TTT-11	50	61	0.73	0.34	0.64	1.99	0.67	0.63	0.78	1.04
TAP-01	49	60	0.72	0.34	0.64	1.93	0.66	0.65	0.79	1.03
TAP-04	51	60	0.74	0.33	0.63	1.97	0.67	0.64	0.78	1.02
TAP-05	50	61	0.73	0.34	0.64	2.00	0.67	0.66	0.80	1.03
Rock-3 (Basal Shale)	43	26	0.63	0.36	0.64	1.76	0.64	0.80	1.00	1.05
Rock-4 (B Limestone)	--	--	--	--	--	--	--	--	--	0.99
Rock-5 (U Shale)	--	--	--	--	--	--	--	--	--	1.04
Rock-0 (A Limestone)	--	--	--	--	--	--	--	--	--	0.99

Notes: %20*S*=5α,14α,17α(H)-stigmastane 20S and 20R ratio (%); %ββ=ratio (%) of C_{29} isosteranes (20*S*+20*R*) to C_{29} regular steranes (20*S*+20*R*); $\%Rc_1=0.01\cdot(33.33+0.487\cdot\%20S)$; TA=$C_{20}$ homologue to C_{20} plus C_{28} 20R triaromatic steroid ratio; $Rc_2=0.37+0.7\cdot TA$; MPI-1=1.5·(2-MP+3-MP)/(P+1-MP+9-MP); $Rc_4=0.4+0.6\cdot$ MPI-1, Ro from 0.65 to 1.35% (Boreham et al., 1988); DNR-1=(2,6+2,7)/1,5-DMN; $\%Rc_3=0.49+0.09\cdot$DNR-1; and CPI=$2\cdot n$-$C_{22+25+27+29}$ to n-C_{22+30}+$2\cdot n$-$C_{24+26+28}$ ratio.

Appendix: Main saturated and aromatic biomarkers identified in the fragmentograms.

1	C_{20}-Tricyclic terpane	47	5α(H),14β(H),17β(H)-Ergostane 20S
2	C_{21}-Tricyclic terpane	48	5α(H),14α(H),17α(H)-Ergostane 20R
3	C_{22}-Tricyclic terpane	49	5α(H),14α(H),17α(H)-Stigmastane 20S
4	C_{23}-Tricyclic terpane	50	5α(H),14β(H),17β(H)-Stigmastane 20R
5	C_{24}-Tricyclic terpane	51	5α(H),14β(H),17β(H)-Stigmastane 20S
6	C_{25}-Tricyclic terpane 17R+17S	52	5α(H),14α(H),17α(H)-Stigmastane 20R
7	C_{26}-Tricyclic terpane 17R	53	4-Methyldibenzothiophene
8	C_{24}-Tricyclic terpane?	54	2-Methyldibenzothiophene *
9	C_{26}-Tricyclic terpane 17S	55	1-Methyldibenzothiophene
10	C_{28}-Tricyclic terpane 17R	56	1,3,7-Trimethylnaphthalene
11	C_{28}-Tricyclic terpane 17S	57	1,3,6-Trimethylnaphthalene
12	C_{29}-Tricyclic terpane 17R	58	1,3,5+1,4,6-Trimethylnaphthalene*
13	C_{29}-Tricyclic terpane 17S	59	2,3,6-Trimethylnaphthalene
14	18α(H)-22,29,30-Trisnorneohopane	60	1,2,7-Trimethylnaphthalene
15	C_{30}-Tricyclic terpane 17R	61	1,6,7-Trimethylnaphthalene
16	17α(H)-22,29,30-Trisnorhopane	62	1,2,6-Trimethylnaphthalene
17	C_{30}-Tricyclic terpane 17S	63	1,2,4-Trimethylnaphthalene
18	17α(H),21β(H)-28,30-Bisnorhopane	64	1,2,5-Trimethylnaphthalene
19	17β(H),21α(H)-28,30-Bisnorhopane	65	20-triaromatic steroid hydrocarbon
20	17α(H),21β(H)-30-Norhopane	66	21-triaromatic steroid hydrocarbon
21	18α(H)-30-Norneohopane	67	26-triaromatic steroid hydrocarbon 20S
22	17β(H),21α(H)-30-Normoretane	68	26 (20R) + 27 (20S)-triaromatic steroid*
23	17α(H),21β(H)-Hopane	69	28-triaromatic steroid hydrocarbon 20S
24	18α(H)-Neohopane	70	27-triaromatic steroid hydrocarbon 20R
25	17β(H),21α(H)-Moretane	71	28-triaromatic steroid hydrocarbon 20R
26	17α(H),21β(H)-29-Homohopane 22S	72	2,6-Dimethylnaphthalene
27	17α(H),21β(H)-29-Homohopane 22R	73	2,7-Dimethylnaphthalene
28	Gammacerane	74	1,3+1,7-Dimethylnaphthalene*
29	17β(H),21α(H)-29-Homomoretane 22S+22R	75	1,6-Dimethylnaphthalene
30	17α(H),21β(H)-29-Bishomohopane 22S	76	1,4+2,3-Dimethylnaphthalene*
31	17α(H),21β(H)-29-Bishomohopane 22R	77	1,5-Dimethylnaphthalene
32	17α(H),21β(H)-29-Trishomohopane 22S	78	1,2-Dimethylnaphthalene
33	17α(H),21β(H)-29-Trishomohopane 22R	79	1,3,5,7-Tetramethylnaphthalene
34	17α(H),21β(H)-29-Tetrahomohopane 22S	80	1,3,6,7-Tetramethylnaphthalene
35	17α(H),21β(H)-29-Tetrahomohopane 22R	81	1,2,4,6+1,2,4,7-Tetramethylnaphthalene*
36	17α(H),21β(H)-29-Pentahomohopane 22S	82	1,2,5,7-Tetramethylnaphthalene
37	17α(H),21β(H)-29-Pentahomohopane 22R	83	2,3,6,7-Tetramethylnaphthalene
38	13β(H),17α(H)-Diacholestane 20S	84	1,2,6,7-Tetramethylnaphthalene
39	13β(H),17α(H)-Diacholestane 20R	85	1,2,3,6-Tetramethylnaphthalene
40	5α(H),14α(H),17α(H)-Cholestane 20S*	86	1,2,5,6+1,2,3,5-Tetramethylnaphthalene*
41	5α(H),14β(H),17β(H)-Cholestane 20R*	87	Dibenzothiophene
42	5α(H),14 β(H),17β(H)-Cholestane 20S	88	Phenanthrene
43	5α(H),14α(H),17α(H)-Cholestane 20R	89	3-Methylphenanthrene
44	13α(H),17βH)-Diastigmastane 20S	90	2-Methylphenanthrene
45	5α(H),14α(H),17α(H)-Ergostane 20S	91	9-Methylphenanthrene
46	5α(H),14β(H),17β(H)-Ergostane 20R*	92	1-Methylphenanthrene

*Peak co-elution

Declaration of interests

☒ The authors declare that they have no known competing financial interests or personal relationships that could have appeared to influence the work reported in this paper.

☐The authors declare the following financial interests/personal relationships which may be considered as potential competing interests:

CRediT author statement for manuscript entitled *Study on spatio-compositional variations and source facies for oils from the Central Wrench Corridor of the Oriente Basin (Ecuador)*

CRediT author statement

Gonzalo Márquez: Investigation, Conceptualization, Writing – Original Draft, Methodology; **Lenin González**: Methodology, Resources, Validation; **Albert Permanyer**: Writing – Review & Editing, Supervision; **Carlos Boente**: Investigation, Data Curation, Software; **Marco Antonio Guzmán**: Investigation; **Erica Lorenzo**: Visualization, Formal analysis, Funding acquisition.